This article was downloaded by:
On: *21 January 2011*
Access details: *Access Details: Free Access*
Publisher *Taylor & Francis*
Informa Ltd Registered in England and Wales Registered Number: 1072954 Registered office: Mortimer House, 37-41 Mortimer Street, London W1T 3JH, UK

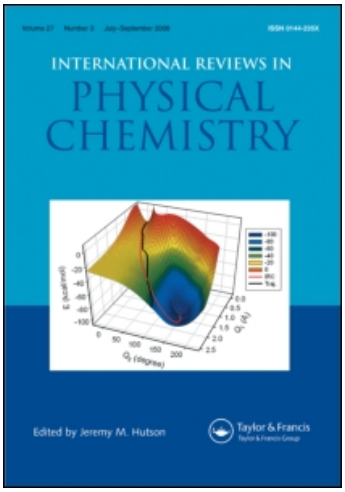

International Reviews in Physical Chemistry
Publication details, including instructions for authors and subscription information:
http://www.informaworld.com/smpp/title~content=t713724383

Photophysics of metal atoms in rare-gas complexes, clusters and matrices

C. Crepin-Gilbert; A. Tramer

Online publication date: 26 November 2010

To cite this Article Crepin-Gilbert, C. and Tramer, A.(1999) 'Photophysics of metal atoms in rare-gas complexes, clusters and matrices', International Reviews in Physical Chemistry, 18: 4, 485 — 556
To link to this Article: DOI: 10.1080/014423599229901
URL: http://dx.doi.org/10.1080/014423599229901

PLEASE SCROLL DOWN FOR ARTICLE

Full terms and conditions of use: http://www.informaworld.com/terms-and-conditions-of-access.pdf

This article may be used for research, teaching and private study purposes. Any substantial or systematic reproduction, re-distribution, re-selling, loan or sub-licensing, systematic supply or distribution in any form to anyone is expressly forbidden.

The publisher does not give any warranty express or implied or make any representation that the contents will be complete or accurate or up to date. The accuracy of any instructions, formulae and drug doses should be independently verified with primary sources. The publisher shall not be liable for any loss, actions, claims, proceedings, demand or costs or damages whatsoever or howsoever caused arising directly or indirectly in connection with or arising out of the use of this material.

INT. REVIEWS IN PHYSICAL CHEMISTRY, 1999, VOL. 18, NO. 4, 485–556

Photophysics of metal atoms in rare-gas complexes, clusters and matrices

C. CRÉPIN-GILBERT
Laboratoire de Photophysique Moléculaire CNRS, Université Paris-Sud, 91405-Orsay Cedex, France

and A. TRAMER
Mulleron, 91640-Janvry, France

Experimental studies of electronic spectra and dynamics of metal atoms M of groups I, II and III of the periodic system interacting with rare-gas atoms G in 1:1 MG complexes, MG_n clusters and M/G centres in matrices are reviewed. It is shown that the necessary condition for a good understanding of the properties of M/G solids is a detailed knowledge of the M–G interactions in diatomic MG molecules. In spite of their apparent simplicity, the electronic spectra of MG and M/G systems are complex because of a drastic difference between the M–G potentials in ground and excited states of M atoms.

Downloaded At: 16:53 21 January 2011

Contents

International Reviews in Physical Chemistry ISSN 0144-235X print/ISSN 1366-591X online © 1999 Taylor & Francis Ltd
http://www.tandf.co.uk/JNLS/rpc.htm http://www.taylorandfrancis.com/JNLS/rpc.htm

Downloaded At: 16:53 21 January 2011

1. Introduction

The scope of this paper is to present the actual level of understanding of the interactions in one of the simplest systems: one metal atom interacting with one or more rare-gas atoms. This definition covers a rather extended field going from one-to-one metal–rare-gas complexes to metals in rare-gas matrices through the aggregates involving a number of rare-gas atoms.

The diatomic metal–rare-gas complexes have been extensively studied and, in view of the simplicity of their spectra, their structure and dynamics are relatively well understood. Recent progresses in this field have been presented in review articles such as [1]. The properties of metal atoms embedded in rare-gas crystals are not so well known in spite of a large amount of work. For this reason we focus our attention on the rare-gas solids using the information deduced from gas-phase studies as a basis.

One of the challenges of modern physical chemistry is how to apply our detailed knowledge of energetics and dynamics of isolated atoms and molecules for a better understanding of chemical and physicochemical processes involving the same atoms (molecules) in condensed phases. In this paper, we are interested in the study of interactions in the simple systems composed of one metal atom M and one or more rare-gas atoms G which may be considered as a preliminary step in the investigation of chemical (photochemical) reactions in the systems involving the same metal atom

and small molecules. One can show that the experiments carried out in low-pressure gases, two-atom complexes and low-temperature matrices allow us to elucidate the mechanisms of such reactions.

Let us take as an example the photochemical process of insertion of metal atoms into X–H bonds (where X may be an aliphatic C_nH_{2n+1} or SiH_3 radical) with formation of molecules interesting as intermediates in organic syntheses [2–4]. The simplest reaction of this kind is the $M^* + H_2$ reaction, where M^* is the metal atom in the excited state [4]. Some 25 years ago, it was shown that in the $Hg^* + H_2$ gas-phase collisions, two processes compete:

$$Hg^*(^3P_1) + H_2 \rightarrow Hg(^1S_0) + H + H \text{ and } Hg^*(^3P_1) + H_2 \rightarrow HgH(X\,^1\Sigma^+) + H,$$

but the mechanism of this reaction was not known [5]. More recently, it has been shown that HgH is formed upon the excitation of the 'cold' $Hg \cdot H_2$ van der Waals complex to one of two electronic states correlated to the atomic $^3P_1$ state [6]. The energy distribution in the HgH product indicated that this reaction involves insertion of the Hg atom into the H–H bond with formation of the H–Hg–H# intermediate, the excess vibrational energy being so large that the molecules dissociates. This conclusion was confirmed by detection of stable H–Hg–H molecules formed upon the excitation of Hg atoms in H_2 or mixed H_2–Ar low-temperature matrices in which a rapid vibrational relaxation of the primary H–Hg–H product prevents its dissociation [7, 8a]. The same reaction was previously observed for $Mg(^1P_1)$ atoms in the H_2 matrix [8b].

Downloaded At: 16:53 21 January 2011

The transition from an isolated atom or molecule to liquid or solid solutions may be investigated in two different ways:

(*a*) by the study of collisional processes in M + G gaseous mixtures evolving with increasing pressure of the buffer (G) gas and decreasing temperature through supercritical phases to the liquid or

(*b*) by the study of cold ($T \rightarrow 0$ K) bound M + G systems going from 1:1 MG complexes through MG_n clusters (aggregates) to the mixed crystal which may be considered as a finite M/G centre, that is as an MG_n cluster embedded in the pure G crystal.

We shall concentrate on this latter way, introduced some 45 years ago by the development of the matrix isolation technique [9] and widened by the invention of supersonic nozzles, allowing the formation and study of weakly bound complexes and clusters [10]. The systems under study, namely isolated MG and MG_n 'molecules' as well as the M/G centres have well defined geometries with reduced vibrational amplitude (internal energy close to zero) and well resolved spectra. The closely related field of spectroscopy and dynamics of colliding M + G pairs will not be treated in this paper.

The well resolved electronic spectra of weakly bound MG complexes formed in supersonic expansions of the G carrier gas (or of the G + G´ gaseous mixture) seeded with M allow determination of essential parameters of the M–G interaction. The potential energy curves for ground and low excited states have been reported for a number of MG complexes and the relation between the M–G potential and the electronic structure of the M atom is relatively well understood [1].

When the backing pressure in the nozzle is increased, besides the MG diatomics, a mixture of MG_n clusters (with a pressure-dependent distribution of *n* values) is formed.

Rare-gas matrices are rare-gas crystals containing a small fraction (typically 10^{-4}–10^{-3}) of M. The concentration of M in the solid must be low to avoid formation of M_n molecules; since the M–M bond is significantly stronger than the M–G bond, 'solid solutions' of M atoms in G matrices are thermodynamically unstable. At higher temperatures ($T > 25$ K), when the diffusion of M atoms becomes possible, M_n aggregates are easily formed.

The matrix may be considered as an ensemble of non-interacting M/G centres composed of one M atom and of its G_n solvation shell. Because of their low concentration, their structures cannot be determined by X-ray diffraction but by indirect deduction from their optical and electron spin resonance (ESR) spectra. The calculations of the geometries have been also carried out using M–G and G–G potentials evaluated from experimental and computational studies of two-body systems.

The major part of metal atoms treated in this paper are those with ground S-states; atoms of group I (Li, Na, K, etc) and group IA (Cu, Ag and Au) have the $[X]^+ (ns)^1\ ^2S$ ground configuration and those of group II (Mg) and group IIA (Zn, Cd and Hg) the $[X]^{2+} (ns)^2\ ^1S$ ground state (where [X] indicates closed electron shells). We shall treat separately the atoms of group III (Al to Tl) with the $[X]^{3+} (ns)^2(np)^1\ ^2P$ ground states; other (Ni and Pd) will be mentioned only when their properties are of special interest.

Downloaded At: 16:53 21 January 2011

The M atoms with the $(ns)^1$ or $(ns)^2$ configurations have a spherical symmetry and their interaction with spherically symmetric rare-gas atoms is isotropic and due essentially to dispersion forces. As the strength of the M–G bond is close to that of the G–G bond, the M atom may replace one or a few G atoms without a strong distortion of the crystal lattice. The solid rare gases form fcc crystals in which the symmetry of the environment of each spherically symmetric G atom (its site symmetry) is octahedral (O_h). If the van der Waals radius r_{vdW} (M) of the M atom in the ^1S or ^2S state is close to the van der Waals radius r_{vdW} (G) of the rare-gas host, M may replace a single G atom and form a one-atom substitution site with conservation of the site symmetry. The M atom is surrounded by 12 equivalent nearest neighbours G and another six in the second shell with M–G distances of $2^{1/2}a$ and a respectively, where a is the lattice constant (figure 1). Otherwise, the 'large' (r_{vdW} (M) $\gg r_{vdW}$ (G)) M atom will occupy larger vacancies (multisubstitution sites) whereas in the r_{vdW} (M) $\ll r_{vdW}$ (G) case the 'small' M atom may slip in between the host atoms, forming an interstitial site. For several M + G pairs, the M atoms may occupy more than one type of site.

One of the essential features of all M + G systems is the dramatic change in strength of the M–G interaction upon excitation of the M atom in the $[X]^+ (ns)^1 \rightarrow [X]^+ (np)^1$ or $[X]^{2+} (ns)^2 \rightarrow [X]^{2+} (ns)^1(np)^1$ S → P transitions. The atoms in the ^{2S+1}P states are no longer spherically symmetric but show the axial ($C_{\infty v}$) symmetry and the M–G interaction is strongly anisotropic: attractive when the p electron occupies the $np\pi$ orbital perpendicular to the M–G axis and repulsive when the $np\sigma$ orbital directed along this axis is populated. In MG diatomics, the molecular states correlated to the P atomic state are a bound Π state and a dissociative Σ^+ state. The bonding energies D_e and equilibrium distances R_{M-G} in the ground and excited (bound) states may be determined from the study of their absorption (fluorescence excitation) and emission spectra.

The difference between the D_e and R_{M-G} parameters is much more pronounced in the case of metal–rare-gas complexes than in the case of large molecules (such as aromatic hydrocarbons and their derivatives A) forming 1:1 complexes with rare-gas

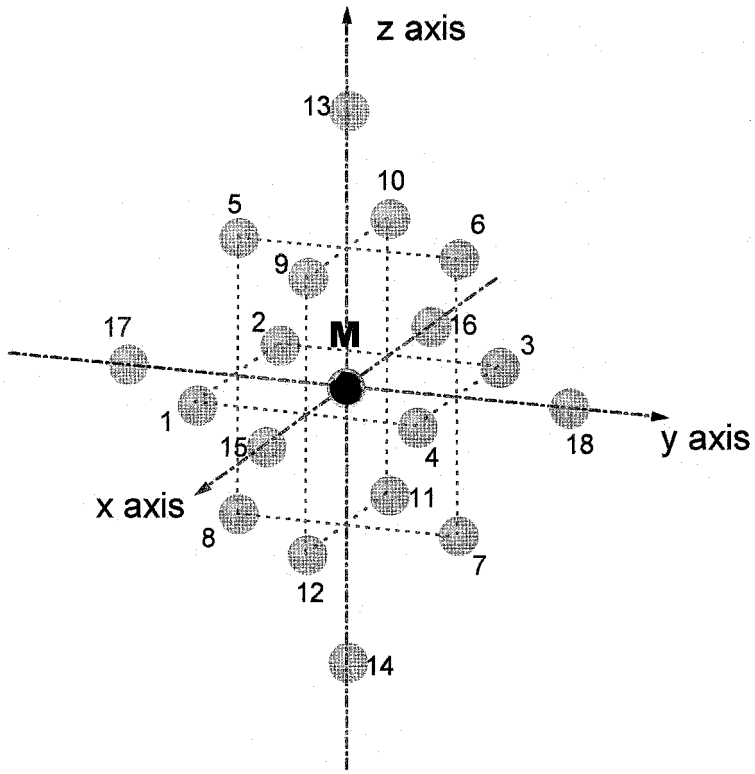

Figure 1. Schematic representation of an MG_{18} 'cluster' involving a central M atom, its 12 nearest neighbours G and six G atoms belonging to the second solvation shell.

Downloaded At: 16:53 21 January 2011

atoms. The A–G interaction is only slightly changed by a $\pi \rightarrow \pi^*$ or $n \rightarrow \pi^*$ electronic excitation. The $AG \rightarrow A^*G$ transition in a complex involving a molecule such as benzene and larger aromatic molecules [11] is only slightly (about 100 cm^{-1} or less) shifted with respect to the $A \rightarrow A^*$ transition in the free molecule. Since the equilibrium distances R_{A-G} and R_{A^*-G} are nearly the same, the only transitions allowed by the Franck–Condon rule are those in which the quantum numbers of intermolecular ν_{A-G} modes are unchanged ($\Delta v_{AG} = 0$). In contrast, the bonding energy of the MG complex is strongly changed so that the purely electronic ($v'' = 0 \rightarrow v' = 0$) transition shows a large ($\nu_M - \nu_{MG} = 300$–1500 cm^{-1}) frequency shift. Since the equilibrium distances R_{M-G} in both states are quite different, a long progression of the $v'' = 0 \rightarrow v'(v' = 0, 1, \ldots)$ vibronic bands is usually observed.

In an excited state of an MG_n cluster or M/G centre, the M* atom interacts with more than one G atom. The potential energy surface of such a multibody system cannot be determined by experiment. It may be approximated by assuming the additivity of individual $M^*–G_i (i = 1, 2, \ldots, n)$ terms, where each of them depends not only on the $M^*–G_i$ distance but also on the angle between the $M^*–G_i$ axis and that of the *n*p orbital. In a M/G centre with O_h symmetry, the promotion of the s electron to the *n*p orbital modifies the M–G interaction. The potential is no longer isotropic: attractive (π type) for G atoms in the nodal plane of the p orbital and repulsive (σ type) for the others. Such a 'σ–π interaction' will tend to deform the G_n shell surrounding the M atom or induce a shift of M out of its central position. In both cases, the

symmetry of the M/G centre is lowered so that the spatial degeneracy of the atomic P state is removed. This is a specific case of the general phenomenon known as the Jahn–Teller effect [12–14]: the intrinsic instability of electronically degenerate states. The spectroscopic signature of the Jahn–Teller effect in an $S \rightarrow P$ transition is the splitting of the absorption band resulting from the splitting of the upper (P) level and providing the origin to the 'triplets' in the spectra of a number of M/G centres.

The main features of the M/G spectra are due to a large difference between equilibrium configurations of their ground and excited state. One could expect that the absorption spectra of atoms in well defined sites will be composed of narrow, well resolved bands. This is not the case; their spectra composed of relatively broad (typically $\delta\nu \approx$ 50–250 cm^{-1}) bands are, apparently, similar to those of large molecules A. The origin of the bandwidths is, however, different, as may be shown by the fluorescence line narrowing (FLN) [15, 16] technique.

Upon narrow-band laser excitation (selective excitation of individual sites), the fluorescence spectrum of a molecular guest A is composed of narrow bands with the origin coinciding with the excitation frequency. This means that homogeneous widths are small and the observed bands are inhomogeneously broadened because of a wide continuous distribution of sites. On the other hand, in the case of atoms, the inhomogeneous broadening is not important, as shown by the weakness of the FLN effect; upon narrow-band excitation, the fluorescence spectra are composed of bands as large or larger than in absorption and strongly shifted with respect to the absorption. The bandwidths are essentially homogeneous.

Downloaded At: 16:53 21 January 2011

This difference between A/G and M/G centres may be explained in the same way as in the case of MG and AG diatomics. Since the A–G interaction is only slightly changed by excitation of the A molecule, the strongest band in the absorption spectrum of an individual site corresponds to purely electronic excitation of A, that is to the $\Delta v_i = 0$ transition where v_i are the quantum numbers of the phonon (lattice vibrational) modes. This narrow band (the zero-phonon line) is accompanied by a weaker broad band (phonon side band) corresponding to the simultaneous excitation of lattice phonons. In the M/G centre with significantly different potential energy surfaces of the ground and excited states, the electronic excitation implies simultaneous excitation of local phonons ($v_i'' = 0 \rightarrow v_i \neq 0$ phonon transitions). The 'lines' corresponding to these transitions (their widths are large because of the rapid relaxation times of phonon levels) overlap and give rise to a broad absorption band. The zero-phonon line is weak or absent. The same mechanism is responsible for the broadening of emission bands.

On the other hand, the inhomogeneous broadening is more pronounced in the case of molecules; their dimensions and shapes are quite different from those of the host atoms so that the molecules replace in the crystal lattice more than one host atom, creating a whole family of sites while the one-atom M/G substitution sites are quasi-identical.

This difference between atoms and molecules disappears in the case of Rydberg transitions. The guest–host interaction in M/G and A/G centres is drastically modified by the promotion of the valence electron of M or A to an extended Rydberg orbital strongly overlapping those of the G atoms of the first solvation shell. The repulsive interaction implies a large displacement of atomic or molecular Rydberg levels to higher energies and 'blue' shifts of absorption bands [17–20].

We shall not extend our discussion to the case of transition or rare-earth metal ions or the F centres in ionic crystals such as alkali halides, close analogues of G/M centres

in matrices. The guest–host interactions are in this case stronger than in van der Waals crystals so that the perturbation of their level structure is enhanced. For this reason, the spectra of G/M centres, conserving essential features of the spectrum of the free atom, are of interest for the study of the more strongly perturbed ionic analogues. On the other hand, the theoretical models [21, 22] and experimental techniques such as magnetic circular dichroism (MCD) spectroscopy using the analysis of data in terms of moments [23, 24] developed for the study of ionic crystals are widely used in the matrix studies.

Different points suggested here will be discussed in the following sections. The authors of this paper are experimentalists, specializing in the electronic spectroscopy of jet-cooled and matrix-embedded atomic and molecular species. Their experience in the field of quantum-chemical calculations and simulations as well in those of MCD and ESR is limited. For this reason, the absorption and emission spectra are discussed here in more detail while the supplementary information deduced from MCD and ESR spectra as well as the results of theoretical studies is reported without a detailed critical analysis.

In section 2, we review briefly experimental techniques applied to the studies of the M–G interaction in two-body systems (section 2.1), aggregates (section 2.2) and matrices (section 2.3).

Downloaded At: 16:53 21 January 2011

In section 3, we recall the basic properties of metal atoms included in the MG complex or M/G centre: the symmetry of orbital functions, the spin–orbit coupling strength and its dependence on the nature of G perturbers.

Electronic structures of MG diatomics are discussed in sections 4.1 and 4.2 with a discussion of specific properties of M*G Rydberg states. The MG_n clusters are treated in section 4.3.

Section 5 is devoted to M/G centres in matrices. The information concerning their structures is presented in section 5.1. On this basis, the essential features of absorption and fluorescence spectra are discussed in section 5.2.

In section 6, we discuss the radiative and non-radiative transitions in MG and M/G systems with a special interest for the mechanism of electronic relaxation of M*G and M*/G excited states.

In sections 3–6, we try to stress the essential properties of systems. A discussion of specific cases is delayed to section 7 where we treat also in a more detailed way the spectroscopy and dynamics of atomic Rydberg states.

2. Experiment—sources of information

In this section we shall review briefly the basic techniques yielding information about the properties of M + G systems in their ground and excited electronic states.

The electronic spectroscopy of jet-cooled species is the principal and almost the only way to study experimentally isolated (collision-free) MG diatomic complexes and MG_n aggregates. To our knowledge, no rotational (microwave) or vibrational (infrared) spectra of metal complexes have been reported and such measurements are hardly feasible because of the negligible electric moments of MG diatomics in their ground electronic states.

The ESR involving transitions between the levels of the same electronic state is one of the main sources of information about the ground states of the M/G centres in matrices. Other techniques such as extended X-ray absorption fine structure (EXAFS) [25] or Mössbauer (for example [26]) spectroscopy have not been widely used. The infrared spectra of transitions forbidden in the pure host crystal and induced in the

M/X centre (where X is a molecular host) have provided a large amount of information about the structure of the Hg/N_2 system [27, 28]. This technique may be applied to other M/X systems (where X is H_2, O_2, etc.) but not to atomic hosts.

A large amount of data has been collected by the electronic spectroscopy of metal guests in rare-gas matrices. Their absorption spectra have been extensively studied since the early days of the matrix isolation technique (for example [29]) but their interpretation is not self-evident. Progress in this field was attained by the study of emission spectra and lifetimes upon a selective excitation by laser and synchrotron radiation and by the study of MCD spectra.

2.1. *Isolated MG complexes*

MG complexes are very weakly bound in their ground electronic states so that an MG concentration large enough for spectroscopic measurements may be attained only upon an efficient cooling of the M + G mixture in supersonic expansions. As the vibrational temperature T_{vib} and rotational temperature T_{rot} are reduced to about 5 K, the complexes are 'cold', that is only a few rotational levels of the vibrationless ($v'' = 0$) state are efficiently populated. The electronically excited (but vibrationally 'cold') metastable states of the complex may be also populated if M* atoms in long-lived excited states are present in the expansion. For instance the $^3\Pi_0$ and $^3\Pi_2$ excited states of ZnAr are detected in presence of the Zn(^{3}P) atoms formed in the electric discharge [30] and the higher $^2\Pi_{3/2}$ sublevel of the ground $^2\Pi$ state of TlAr in presence of Tl($^2P_{3/2}$) [31].

The concentration of complexes is, nevertheless, too low for absorption measurements. The absorption spectra may thus be determined as follows.

(*a*) The excitation spectrum of luminescence can be recorded (the luminescence intensity as the function of the excitation frequency ν_1). The time- and/or energy-resolved emission spectra are recorded in the same experiment. If the excited M*G state is not luminescent but dissociates with formation of M atom in the excited radiant state M* or metastable M´ state, the 'action spectrum' is determined by measurements of the ν_1 dependence of the intensity of the spontaneous $M^* \rightarrow M + h\nu'$ emission or of the laser-induced $M' + h\nu_2 \rightarrow M^{**} \rightarrow M + h\nu'$ fluorescence [32, 33].

(*b*) The resonance enhanced multiphoton ionization (REMPI) technique [34] may be used. The state of interest is pumped by a laser with a variable frequency (ν_1); its population is detected by ionization using a second laser with a fixed frequency (ν_2). The resulting ion current is measured as a function of ν_1. If only ions with the e/m ratio corresponding to the MG^+ ion are counted (mass-selective resonance-enhanced multiphoton ionization (MSREMPI) technique) the MG spectrum may be separated from the features due to the MG_n clusters and M atoms present in the expansion.

The vibrational structure of excitation (or action) spectra is usually well resolved (figure 2) so that vibrational frequencies ω_e' and anharmonicity constants $\omega_e' x_e'$ of the excited state may be determined provided that the vibrational quantum numbers v' of the observed levels are known. This is not always the case since the transitions from the $v'' = 0$ level are allowed by the Franck–Condon rule only to a limited set of v' levels. If the $v' = 0 \leftarrow v'' = 0$ transition is not observed, this assignment is not obvious. The v' numbers may be determined by analysis of the band splitting due to different isotopic species of M or G [37] or from the dependence of the fluorescence spectrum on the

Downloaded At: 16:53 21 January 2011

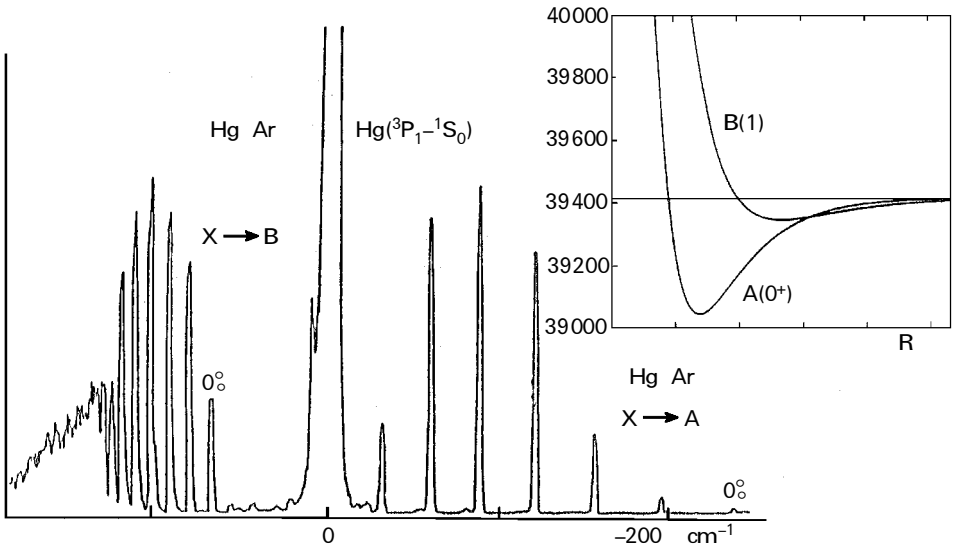

Figure 2. Fluorescence excitation spectrum of Hg atoms (saturated central line) and of the X → A transition at $\nu < \nu_{Hg}$ and X → B transition at $\nu > \nu_{Hg}$ of the HgAr complex. Note the dissociation continuum corresponding to transitions to the repulsive part of the potential curve of the B state. Potential energy curves of the strongly bound A state and weakly bound B state are as deduced from the excitation spectra. (From [35, 36].)

Downloaded At: 16:53 21 January 2011

excited v' level [38]. When the frequency ν_{00} of the $v' = 0 \leftarrow v'' = 0$ transition is known and the transitions to the dissociation limit are observed, the bonding energies D_0' and D_e' of the excited state are directly determined. Otherwise they may be estimated by extrapolation of the $\Delta G(v') = [E(v') - E(v'-1)]/hc$ series to $\Delta G = 0$ or by using the well known formulae

$$D_e' = \frac{\omega_e'^2}{4\omega_e' x_e'}, \; D_0' = \frac{\omega_0'^2}{4\omega_0' x_0'}, \tag{2.1}$$

which are valid when the absorption spectrum is well approximated by the Morse equation

$$V(R) = D_e\{1 - \exp[-\alpha(R - R_e)]\}^2. \tag{2.1 a}$$

The accuracy of these estimations is, however, limited because the deviations from the Morse formula are relatively important for weakly bound systems at large interatomic distances. Systematic errors may be also introduced when the frequencies of maxima of the unresolved vibronic bands are taken instead of band origins.

If the excited state MG* is fluorescent, the same information may be obtained for the ground electronic state by recording the fluorescence spectra. Since upon the excitation of different v' levels one can probe a large part of the ground-state potential energy curve including the energy minimum ($v'' = 0$ level) and dissociation limit, the bonding energy D_e'' of the ground state may be directly determined. If D_e', D_e'' and ν_{00} are obtained from independent measurements, the consistency of the data may be checked by the relation

$$D_e'' - D_e' + \nu_{00} = \nu_{M^*}, \tag{2.2}$$

where ν_{M^*} is the frequency of the M → M* transition in the free atom. The existence of large deviations from equation (2.2) indicates a particular form of the potential energy curve such as an energy barrier (see section 4.1.4).

In the case of complexes involving light M or G atoms, the rotational structure of different $v'' \leftrightarrow v'$ vibronic bands is resolved or, at least, the rotational constants B'_v and B''_v may be estimated by simulation of the band contours. The equilibrium distances R'_e and R''_e may be then determined by extrapolation of B'_v and B''_v to $v' = v'' = 0$. In the absence of these data, rough estimations of R''_e and R'_e or at least of the $R''_e - R'_e$ difference may be done on the basis of the intensity distribution within the vibrational structure by assuming the validity of the Franck–Condon approximation.

Precise or estimated values of the main parameters (D_e, R_e and α for the Morse equation) are actually available for bound ground and excited states of a number of MG complexes [1].

Theory predicts the existence of dissociative M*G states. The shapes of their potential energy curves are not directly accessible by experiment. In a few cases such as CdAr [39] their presence is indicated by the continuum in the excitation spectrum of Cd* atomic fluorescence resulting from the $Cd^*Ar \rightsquigarrow Cd^* + Ar$ dissociation of the repulsive state. Otherwise essential parameters of repulsive states may be obtained only by *ab initio* calculations (for example [40]).

In most cases, the excited M*G states decay radiatively with lifetimes not very different from those of the free M* atom. Measurements of long (microsecond or millisecond) decay times of metastable states are difficult because of the rapid escape of excited species from the detection region. In a few cases, M*G decays non-radiatively to the dissociative continuum of a lower excited M′G state with formation of M′ and G fragments occurring so rapidly that the M*G fluorescence is completely quenched. The relaxation rate may be then estimated from the widths of lines in the action spectrum of the M′ or M** emission [32, 33].

Downloaded At: 16:53 21 January 2011

2.2. MG_n clusters

These systems are of interest for us as intermediates between MG diatomics and M/G centres in matrices. They allow us to check the extent to which a many-body MG_n system may be described using two-body M–G and G–G potentials deduced from the study of MG and GG molecules. The next step consists in applying these potentials to an 'infinite cluster': an M atom embedded into a G crystal (i.e. an M/G centre).

The usual technique for the spectroscopic study of clusters is REMPI with subsequent mass selection (MSREMPI) which allows the separate recording of absorption spectra of individual MG_n^+ ions by scanning the pump laser. When corrected by eliminating features due to dissociation of heavier $MG_{n'}^+ (n' > n)$ ions this spectrum may be considered as that of the $MG_n^* \leftarrow MG_n$ transition for a known value of n. At the same time, ionization potentials of the selected MG_n species may be measured by scanning the second (ionizing) laser frequency. The clusters composed of an aromatic molecule and a number of rare-gas atoms have been extensively studied using that and related techniques [41–43] but the amount of reliable data for metal–rare-gas aggregates remains very limited.

2.3. M/G centres in matrices

The matrix–rare-gas G crystals containing a small fraction (typically 10^{-4}) of metal atoms M are obtained by deposition on a cold cryostat window ($T = 4$–20 K) of the gas saturated with metal vapours from an oven or a discharge or by laser evaporation. The concentration of the guest M must be small enough to avoid formation of M_2

molecules or M_n aggregates but high enough to allow the recording of absorption and luminescence spectra of M/G centres. Their spectra depend on the deposition conditions (the temperature of the sample holder) because M atoms may occupy different sites corresponding to substitution (replacement of one or more G atoms by one M atom) or interstitial positions. The sample deposition at relatively high T or annealing of the matrix allows the elimination of unstable sites.

We are essentially interested in electronically excited M*G centres but their properties may be understood only when the structures (symmetry, geometry, etc.) of ground M/G states are sufficiently well known. We shall thus begin with a short summary of the information deduced from the spectra of ESR and then treat the methods involving the electronic excitation: absorption and emission ultraviolet–visible spectroscopy with a special section on the spectroscopy in strong magnetic fields (MCD spectroscopy).

2.3.1. *Electronic spin resonance spectroscopy*

The ESR spectra correspond to transitions between spin sublevels of the ground electronic state of an M/G centre. Unfortunately, the application of the ESR spectroscopy is limited to paramagnetic species, that is in our case to doublet ($S = 1/2$) ground electronic states with the $(ns)^1$ (metals of groups I and IA) and $(ns)^2(np)^1$ (group III metals) configuration. It is possible to record the ESR spectra of metal atoms in long-lived excited electronic states with $S \neq 0$ (as was done for the triplet states of molecules [44]) but, to our knowledge, no experiments of this kind have been reported.

The ESR spectra have a simple structure composed of narrow lines. Their widths are determined by the spin–lattice relaxation times which are long in low-temperature matrices. ESR signals due to different M/G sites may be well separated and correlated with the bands in optical spectra corresponding to the same site by following the effects of annealing (suppression of characteristic features of unstable sites) [45, 46].

Downloaded At: 16:53 21 January 2011

In a magnetic field H the spin sublevels are eigenstates of the spin Hamiltonian which in the case of the axial symmetry of the M/G system with a single unpaired electron ($S = 1/2$), has the form

$$H_s = g_{\parallel}\beta S_z H_z + g_{\perp}\beta(S_x H_x + S_y H_y) + A S_z I_z + B(S_x I_x + S_y I_y), \tag{2.3}$$

where $g_{\parallel}$ and $g_{\perp}$ are components of the gyromagnetic tensor parallel and perpendicular respectively to the axis, $S_{i=x,y,z}$ and $I_{i=x,y,z}$ are the projections of the electron and of nuclear spin respectively of the M atom on the system axes, $H_{i=x,y,z}$ are the components of the magnetic field, A and B are hyperfine coupling constants and β is the Bohr magneton.

In the case of the ^{2}S ground state of the M atom in a cubic rare-gas crystal (figure 1) with spherical symmetry $g_{\parallel} = g_{\perp}$ and $B = A$ so that equation (2.3) is reduced to

$$H_s = g\beta SH + ASI. \tag{2.4}$$

The eigenstates of H_s correspond to the $m_s = +\frac{1}{2}$ and $-\frac{1}{2}$ and $m_I = -I, -I+1, \ldots, I$.

In view of the selection rules $\Delta m_s = 1$, $\Delta m_I = 0$, and $\Delta m_F = \pm 1$ (where $\vec{F} = \vec{S} + \vec{I}$), the ESR spectrum of each M/G site will be composed of $2I + 1$ lines with the centre of gravity given by g and the hyperfine splitting depending on A. Both g and A may be determined with a high accuracy. The difference Δg between the g value of the free electron and that observed in the matrix and the deviation ΔA of the coefficient A from that of the free M atom measure the strength of the M–G interaction. The theoretical

treatment of this problem was proposed by Adrian [47] and developed by Smith [48]. A slight variation in the g factor ($\Delta g < 0$) resulting from the mixing of the orbital of the unpaired electron of M with the orbitals of G atoms is proportional to the sum S_{MG} of overlap integrals. On the other hand, the major part of the electron spin–nuclear spin coupling ASI is due to the contact (Fermi) interaction, the strength of which is proportional to the density of the unpaired s electron at the nucleus. This density is increased by contraction of the M orbital induced by the repulsive M–G interaction resulting also from the M–G orbital overlap ($\Delta A > 0$) and is decreased when the M orbital is extended by the attractive van der Waals interaction or formation of M–G bonds ($\Delta A < 0$). The ΔA values will be thus higher in a tight site with reduced M–G distances than in a more 'comfortable' site with larger R_{M-G} values.

The electron spin of the M atom is also coupled to the non-zero nuclear spins I_G of the G atoms of the first solvation shell. In view of the reduced density of the M electron in the vicinity of the G atoms this coupling is weak but, if resolved, contains information about the number of equivalent G atoms in the first solvation shell of M [49].

The ESR spectra for atoms with the $(ns)^2(np)^1$ ^{2}P ground state studied, to our knowledge, only for Al/G and Ga/G systems [50] are completely different from those of the ^{2}S atoms. Because of the axial symmetry of the p orbitals, the M/G sites are strongly anisotropic with $g_\parallel - g_\perp$ values of the order of 0.05 for Al and 0.25 for Ga atoms and large differences between A and B. In the absence of any preferential orientation of M/G centres, the angle between the p-orbital axis and that of the magnetic fields can take all possible values. The intensity of the ESR absorption is thus strongly reduced but one can observe two systems of ESR lines corresponding to the axes close to the parallel and perpendicular orientations with respect to the field (the reason of this selection was discussed in detail in a similar case of triplet-state molecules [51]). The values of g in the 1.8–1.95 range (intermediate between $g = 2$ for a spin decoupled from the orbital moment and $g = \frac{2}{3}$ and $\frac{4}{3}$ for $^2P_{1/2}$ and $^2P_{3/2}$ atomic states respectively) indicate that the orbital moment of the p electron is only partially and not entirely quenched.

Downloaded At: 16:53 21 January 2011

2.3.2. *Electronic spectroscopy*

At guest concentrations of the order of 10^{-4}, absorption spectra of M/G centres can be recorded with a good signal-to-noise ratio. The emission spectra and lifetimes may be also determined upon a selective excitation of different sites. In the absence of impurity quenching in a rigid medium, even very weak emission from metastable states with lifetimes as long as about 1 s may be detected.

In spite of a different appearance, the spectra of M/G centres are closely related to those of free M atoms so that all bands of the matrix spectra may be unambiguously assigned to transitions appearing as narrow lines in the gas phase spectra. The specific features of matrix spectra (figure 3) are

(i) large frequency shifts $\Delta\nu_{abs}$ in absorption with respect to the gas-phase transitions,

(ii) large widths $\delta\nu_{abs}$ of absorption bands (of several tens to a few hundred reciprocal centimetres), similar or even larger widths $\delta\nu_{em}$ of emission bands shifted to lower frequencies with respect to absorption (the Stokes shift $\Delta\nu_{St} = \nu_{abs} - \nu_{em}$) whereas in the gas-phase absorption and emission lines corresponding to the same transitions are strictly resonant, and

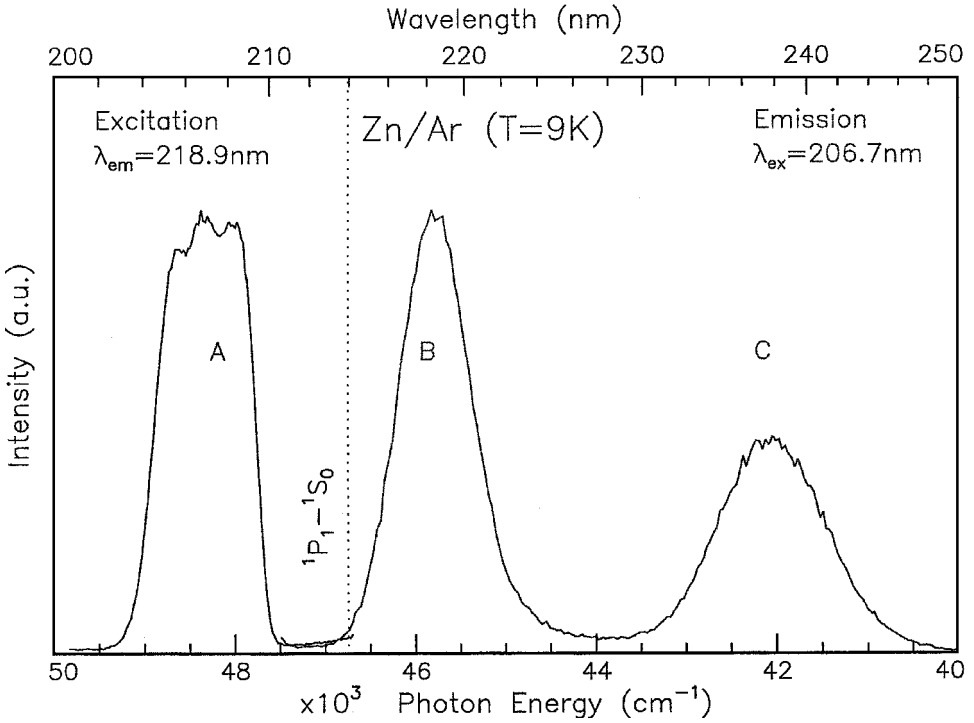

Figure 3. Absorption and fluorescence spectra of Zn atoms in the Ar matrix (a.u., arbitrary units). Note the 'triplet' structure of the absorption band and two emission bands strongly shifted to the red. (From [52].)

Downloaded At: 16:53 21 January 2011

(iii) splitting of the band corresponding to a single transition into several components (the 'multiplet structure' of transitions).

The reasons for these are as follows.

(i) In contrast with molecules in matrices showing usually small red shifts due to the stabilization of the polar molecule by the dielectric medium, the spectra of atoms are usually shifted to higher frequencies (a 'blue' shift which may attain a few thousand wavenumbers). This shift depends strongly on the host and is significantly different for different sites.

(ii) The origin of the widths of spectral bands may be determined by the FLN technique already described in section 1. A slight narrowing of emission bands upon narrow-band excitation indicates that the inhomogeneous broadening is not important. The residual widths observed under these conditions are homogeneous and are due to the unresolved phonon structure of the electronic transitions.

(iii) There are two independent reasons for the multiplet structure of absorption bands: the existence of multiple M/G sites and the splitting of degenerate atomic levels resulting from the low site symmetry (crystal-field effects) or from the static or dynamic Jahn–Teller effect. The separation of both effects is relatively easy; the intensity ratios of bands corresponding to different sites depend on the conditions of the matrix deposition [53–55] and are modified by annealing or irradiation. This is not the case for structures resulting from the

intrinsic level splitting. The fluorescence spectra are also a good indication; the spectrum of each site is different from the others whereas, within a level structure belonging to the same species, relaxation processes tend to establish the same final populations. Finally, the MCD spectra (see below) allow us to recognize whether the band structure is due to overlapping bands from different sites or to the level splitting effects.

A large fraction of excited M*/G centres decay by fluorescence with lifetimes modified, with respect to those of free atoms, only by the dielectric medium effects on the radiative rates. In several cases, the non-radiative relaxation is efficient and fluorescence is almost completely quenched. The relaxation may be monitored by detection of long-lived luminescence from lower metastable states with the decay times as long as 10^{-1}–1 s in the case of $^3P_0$ states of group II and IIA metals [52, 56–58]. Until now, no measurements of rates of the rapid (subnanosecond) relaxation have been reported. No information about decay rates can be deduced from line shapes because of large widths of absorption bands.

2.3.3. *Magnetic circular dichroism spectroscopy*

The information contained in the absorption spectrum may be refined by measurements of the circular dichroism spectra: $\Delta\varepsilon(\nu) = \varepsilon_+(\nu) - \varepsilon_-(\nu)$, where $\varepsilon_+(\nu)$ and $\varepsilon_-(\nu)$ indicate absorption of the right circularly polarized light σ^+ and left circularly polarized light σ^- corresponding to $\Delta m_z = +1$ and -1 transitions, where z is the light propagation axis. In the absence of external fields, $\varepsilon_+(\nu) \equiv \varepsilon_-(\nu)$ but in a longitudinal magnetic field H_z the absorption spectra of σ^+ and σ^- components are no longer equal and $\Delta\varepsilon(\nu) \neq 0$. The high sensitivity of polarization measurements allows the determination of a slight variation in $\Delta\varepsilon(\nu)/\varepsilon(\nu) \approx 10^{-4}$–$10^{-6}$ for absorption profiles with a width Γ exceeding by two or three orders of magnitude the Zeeman interaction energy $H' = \beta\langle i|gm_z H_z|i\rangle$ (of the order of 1 cm^{-1} in magnetic fields of 1 T).

A complete presentation of the theory of MCD developed by Stephens [24, 59] and applied to centres in different solids [60–64] is beyond the scope of this paper. We shall only define in a qualitative way the main mechanisms of the magnetic field effect on the absorption spectra and report a few relations important for spectroscopy of M/G centres.

We consider a case of transitions between two sets of quasicontinua of vibronic levels $\{|K,\kappa\rangle\}$ and $\{|L,\lambda\rangle\}$ belonging to $|K\rangle$ and $|L\rangle$ electronic states. In the semiclassical Franck–Condon approximation, the intensity and shape of the absorption band are given by

$$\varepsilon_\pm(\nu) = d_0 f(\nu), \tag{2.5}$$

where

$$d_0 = |\langle K|d_\pm|L\rangle|^2, \mathrm{f}(\nu) = \Sigma_{\kappa\lambda}|\langle\kappa|\lambda\rangle|^2\delta(\nu_{\kappa\lambda} - \nu) \tag{2.5 a}$$

and $d_\pm$ is the operator of the dipole moment for σ^+ and σ^- components.

The effect of the magnetic field may be represented in the first approximation by a sum of three independent effects.

(1) If at least one of the K and L states is paramagnetic, its levels are split in the magnetic field and the frequencies of the $\Delta m_z = +1$ and $\Delta m_z = -1$ transitions are displaced by

$$\Delta\nu_\pm = \frac{\beta H(g_K - g_L)}{hc}, \tag{2.6}$$

Downloaded At: 16:53 21 January 2011

where g_K and g_L are gyromagnetic factors in the K and L states respectively. If it is supposed that the contours of absorption bands are not modified, the spectra of σ^+ and σ^- components $f_\pm(\nu)$ will have different spectral distributions:

$$f_\pm(\nu) = f(\nu \pm \Delta\nu_\pm),$$

so that the shape of the MCD band $\Delta\varepsilon(\nu)$ equal to $f_+(\nu) - f_-(\nu)$ may be approximated by

$$\Delta\varepsilon(\nu) = d_0 \frac{\partial f(\nu)}{\partial \nu}. \tag{2.6 a}$$

(2) The transition moments $\langle K|d_\pm|L\rangle$ will be modified by the field-induced coupling of the $|K\rangle$ or $|L\rangle$ state to a state $|M\rangle$ in such a way that the strengths of $\Delta m_z = \pm 1$ and $\Delta m_z = -1$ transitions are no longer equal. This effect is weak except for the case of a quasiresonance between M and K or L states.

(3) If the ground (K) state is degenerate and its splitting in the H field is not negligible compared with kT, the equilibrium populations of its sublevels will be temperature dependent. The sign of effect depends on ordering of spin sublevels.

Downloaded At: 16:53 21 January 2011

By further treatment neglecting higher-order terms with respect to H we obtain for $\Delta\varepsilon(\nu)$

$$\Delta\varepsilon(\nu) = \gamma\left(-|a|_1 \frac{\partial f(\nu)}{\partial \nu} + (|b|_0 + |c|_0/kT) f(\nu)\right) \beta H_z, \tag{2.7}$$

expressed using the so-called Faraday parameters $|a|_1$, $|b|_0$ and $|c|_0$ corresponding to three previously described mechanisms [59].

These three terms reproduce the intensity and shape of the $\Delta\varepsilon(\nu)$ and $\varepsilon(\nu)$ spectra. It is important to note that the sign of MCD signals contains supplementary information, the asymmetry of the $\Delta\varepsilon(\nu)$ band is entirely due to the $|a|_1$ term, the MCD spectrum is temperature dependent through a term containing $|c|_0$, which is different from zero only when the ground state is paramagnetic. Also the $|b|_0$ parameter is the only parameter different from zero in the case of transitions between non-degenerate states but in a general case (i.e. when $|a|_1 \neq 0$ and $|c|_0 \neq 0$ and in absence of L–M quasidegeneracy) this term is smaller by one to two orders of magnitude than the other two terms.

The field effects are, however, so weak that it is usually impossible to deduce the exact form of the $|a|_1$, $|b|_0$ and $|c|_0$ functions from the $\varepsilon(\nu)$ and $\Delta\varepsilon(\nu)$ spectra. For this reason, instead of the direct analysis of band shapes it is more convenient to express them in terms of their spectroscopic moments [23]:

$$\langle\varepsilon\rangle_n = \int \varepsilon(\nu)(\nu - \nu_0)^n \partial\nu, \langle\Delta\varepsilon(\nu)\rangle_n = \int \Delta\varepsilon(\nu)(\nu - \nu_0)^n \partial\nu, \tag{2.8}$$

where the central frequency ν_0 is determined from

$$\int \varepsilon(\nu)(\nu - \nu_0)\partial\nu = 0. \tag{2.8 a}$$

$\langle\varepsilon\rangle_n$ and $\langle\Delta\varepsilon(\nu)\rangle_n$ are related in turn to the $|a|_n$, $|b|_n$ and $|c|_n$ moments of the Faraday parameters.

A few relations between $\langle\varepsilon\rangle_n$ or $\langle\Delta\varepsilon\rangle_n$ moments are currently used in the analysis of absorption and MCD spectra. An important advantage of this approach is that physical parameters are deduced not from the absolute values of $\langle\varepsilon\rangle_n$ or $\langle\Delta\varepsilon\rangle_n$ moments but from their ratios so that systematic errors are reduced.

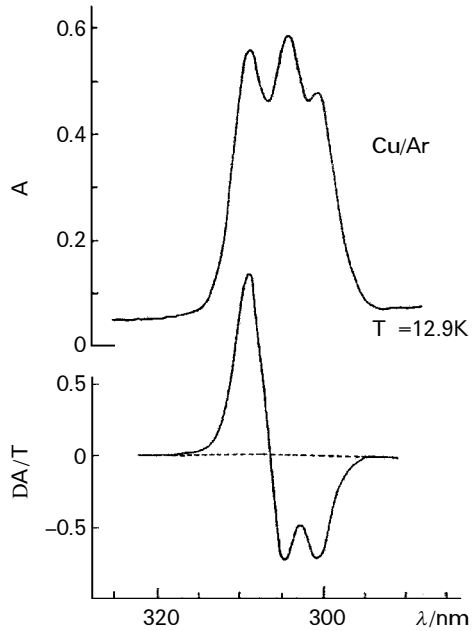

Figure 4. Absorption (top) and MCD (bottom) spectra of the $^2S \rightarrow {}^2P$ transition of Cu in the Ar matrix. (From [63].)

Downloaded At: 16:53 21 January 2011

The most important relations (for atoms with the ^{2s+1}S ground state and $\Delta S = 0$ transitions) are

$$\frac{\langle \Delta\varepsilon \rangle_1}{\langle \varepsilon \rangle_0} = 2\mu_B B\left(g_{orb} - \frac{a_s \zeta}{kT}\right), \tag{2.9}$$

$$\frac{\langle \Delta\varepsilon \rangle_2}{\langle \varepsilon \rangle_0} = \langle E^2 \rangle_c + \langle E^2 \rangle_{nc} + a_s \zeta^2, \tag{2.10}$$

$$\frac{\langle \Delta\varepsilon \rangle_3}{\langle \varepsilon \rangle_0} = 6\mu_B B\left(g_{orb} - \frac{a_s \zeta}{kT}\right)\left(\langle E^2 \rangle_c + \frac{\langle E^2 \rangle_{nc}}{2} + a_s \zeta^2\right), \tag{2.11}$$

where $a_s = -(kT/\mu_B B)[1/(2S+1)]\Sigma_{m_s} m_s \exp(-m_s \mu_B B/kT)$, g_{orb} is the orbital part of the gyromagnetic factor in $L \neq 0$ states, ζ is the spin–orbit coupling constant in the excited state, and $\langle E^2 \rangle_c$ and $\langle E^2 \rangle_{nc}$ are squares of the energies of cubic (totally symmetric) and non-cubic (non-totally symmetric) lattice modes respectively coupled to the electronic transition.

These relations allow the determination of the following important parameters characterizing the M/G centres.

(*a*) The observed value of g_{orb} is a measure of the quenching of the orbital momentum of the free atom embedded in the matrix.
(*b*) The modification of the spin–orbit coupling strength in matrices indicates the mixing of the M* orbital with those of the host atoms.
(*c*) The $\langle E^2 \rangle_{nc}/\langle E^2 \rangle_c$ ratio deduced from equations (2.10) and (2.11) indicates how the total energy of phonons created upon the electronic excitation of the M atom (which may be deduced from the width of the absorption band) is distributed between cubic and non-cubic local modes.

The non-zero MCD signal in the case of transitions between singlet states (e.g. $^1P_1 \leftarrow {}^1S_0$ transitions) [61] suggests that the orbital moment in the excited $^1P_1$ is not entirely quenched. The interference effects between transitions to three closely spaced levels indicate also that their structure is due to the Jahn–Teller splitting and not to multiple sites.

When the degeneracy of a spatially degenerate (P) state is removed, the projections of the magnetic moment on the crystal axes will be different. The signs of the MCD signals for three components of the $S \rightarrow P$ transition will be different. The absorption and MCD contours represented in figure 4 correspond to such a case and may be fitted by assuming the Jahn–Teller origin of the 'triplet' structure of the band.

3. Main features of M–G interactions

The M–G interaction in complexes, clusters and M/G centres is so weak that their electronic states may be considered, to a first approximation, as those of an isolated M atom slightly perturbed by its G partner(s) in the ground electronic state $^1S_0$. The electronic structure of the system is thus determined by that of the M atom and by the symmetry of the MG_n 'cluster'. From this point of view, we differentiate two cases of the M–G perturbation.

Downloaded At: 16:53 21 January 2011

(1) In a diatomic MG complex with $C_{\infty v}$ symmetry, the atom is subject to an axial field from its G partner along the M–G z axis.
(2) In a matrix, the symmetry of an M/G centre is not always known but for a large number of systems (see section 5.1), the M atom is surrounded 12 equivalent nearest neighbours G with the octahedral (O_h) symmetry of the MG_{12} cell. The present discussion will be limited to this case.

We shall deal in the following with the electronic states of diatomic and polyatomic systems correlated to:

(i) the atomic states with the spherical symmetry and $L = 0$ orbital moment: ground states of atoms of groups I, IA, II and IIA in the singlet $^1S_0$ $(ns)^2$ or doublet $^2S_{1/2}$ $(ns)^1$ configurations (the ions with a closed shell or with a single s electron out of the closed shell belong to the same ensemble);
(ii) the states with the $L = 1$ orbital moment and the $(np)^1$ or $(ns)^1(np)^1$ configuration: excited ^2P and $^{1,3}P$ states of these atoms as well as the ground $^2P(ns)^2(np)^1$ states of the atoms of group III;
(iii) the spherically symmetric Rydberg ^{2S+1}S states: $((n+1)s)^1$, $(ns)^1((n+1)s)^1$ or $(ns)^2((n+1)s)^1$;
(iv) the quasispherical excited $(nd)^9((n+1)s)^2\,{}^2D$ ($L = 2$) states of the atoms of group IA.

The symmetry species of the electronic states of MG and M/G systems may be deduced from the correlation between the $D(3)$ rotation–reflection group of the free atom and the $C_{\infty v}$ and O_h point groups (see table 1, in which are included the subgroups of O_h corresponding to a deformation of the cubic site).

In the spectral range in the study, the rare-gas atoms G are not electronically excited. The strength of the M–G interaction depends on the properties of their ground states: ionization potentials I, polarizabilities α and van der Waals radii r_{vdW}

Table 1. Correlation of the symmetry species in different symmetry groups.

$C_{\infty v}$	$D(3)$	O_h	D_{4h}	D_{2h}	C_{2v}
		^1S, ^1P and ^3P atomic states			
Σ^+ ←	$^1S_0$ →	A_{1g} →	A_{1g} →	A_{1g} →	A_1
$\Sigma^+(z)$ ↖		↗	$A_{2u}(z)$ →	$B_{1u}(z)$ →	A_1
	$^1P_1(x,y,z)$ →	$T_{1u}(x,y,z)$ →	$E_u(x,y)$ →	$B_{2u}(y)$ →	B_1
$\Pi(x,y)$ ↙			↘	$B_{3u}(x)$ →	B_2
0^- ←	$^3P_0$ →	A_{1u} →	A_{1u} →	A_u →	A_2
			$A_{2u}(z)$ →	$B_{1u}(z)$ →	A_1
$0^+(z)$ ←	$^3P_1(x,y,z)$ →	$T_{1u}(x,y,z)$ →	$E_u(x,y)$ →	$B_{2u}(y)$ →	B_1
$1(x,y)$ ↙			↘	$B_{3u}(x)$ →	B_2
		↗	B_{2u} →	B_{1u} →	A_1
0^- ↖		E_u →	A_{1u} →	A_u →	A_2
1 ←	$^3P_2$ ↗	↗	$E_u(x,y)$ →	B_{2u} →	B_1
2 ↙	↘	T_{2u}	↘	B_{3u} →	B_2
		↘	A_{1u} →	A_u →	A_2
	^2S and ^2P atomic states (in the strong spin–orbit coupling limit)				
$E_{1/2}$	← $^2S_{1/2}$ →	$E_{1/2}$ →	$E_{1/2}$ →	$E_{1/2}$	→ $E_{1/2}$
$E_{1/2}$	← $^2P_{1/2}(E_{1/2})$ →	$E_{1/2}$ →	$E_{1/2}$ →	$E_{1/2}$	→ $E_{1/2}$
$E_{1/2}$	↖	↗	$E_{1/2}$ →	$E_{1/2}$	→ $E_{1/2}$
	$^2P_{3/2}(G_{3/2})$ →	$G_{3/2}$			
$E_{3/2}$	↙	↘	$E_{3/2}$ →	$E_{1/2}$	→ $E_{1/2}$

Downloaded At: 16:53 21 January 2011

Table 2. Essential parameters of rare-gas atoms: ionization potentials I, frequencies ν_0 of the first transition in absorption, spin–orbit coupling constants ζ in the $(np)^5((n+1)s)^1$ configuration, polarizabilities α and van der Waals radii r_{vdW}.

Rare-gas atom	I (eV)	ν_0 (eV)	ζ (cm^{-1})	α (A^3)	r_{vdW} (A)
Ne	21.56	17.36	515	0.40	1.55
Ar	15.6	12.06	940	1.63	1.83
Kr	14.0	10.17	3480	2.47	2.0
Xe	12.13	8.37	6085	4.02	2.17

given in table 2. The increase in the dissociation energies of ground-state M–G diatomics in the Ne → Ar → Kr → Xe series is obviously due to the variation in I and α parameters (see section 4.1). The same dependence is observed for excited states of MG complexes and M/G centres.

3.1. *The orbital symmetry*

Let us treat first the electronic states of the M atom in which the spin–orbit (L–S) interaction is either totally absent as in the singlet ($S = 0$: ^1S, ^1P, ...) states and in $L = 0$ (^{2S+1}S) states or may be neglected (for systems involving only light M and G atoms).

In the ^{2S+1}S states, in view of the spherical symmetry of M and G atoms, the M–G interaction depends only on the interatomic distance R_{M-G}. The orbitally non-degenerate ^{2S+1}S states correlate to the $^{2S+1}\Sigma^+$ states of the MG diatomics. The M–G interaction is weak so that the polarization of the s orbitals (which may be described in terms of the s–p mixing) may be neglected. In the absence of the orbital moment, the spin states are degenerate. In the M/G centre with the O_h symmetry, the orbitally non-degenerate ^{2S+1}S state of the atom correlates with the $^{2S+1}A_{1g}$ state. The ground states

Table 3. $|J, m_J\rangle$ states as combinations of $|L_z, S_z\rangle$ states in the $L = 1$, $S = \frac{1}{2}$ (^{2}P) and $L = 1$, $S = 1$ (^{3}P) cases.

$^2P_{1/2}$	$(E_{1/2})$	$\left\|\frac{1}{2}, \pm\frac{1}{2}\right\rangle = \pm\left(\frac{2}{3}\right)^{1/2}\left\|\pm 1, \mp\frac{1}{2}\right\rangle \mp \frac{1}{3^{1/2}}\left\|0, \pm\frac{1}{2}\right\rangle$
$^2P_{3/2}$	$(E_{1/2})$	$\left\|\frac{3}{2}, \pm\frac{1}{2}\right\rangle = \left(\frac{2}{3}\right)^{1/2}\left\|0, \pm\frac{1}{2}\right\rangle + \frac{1}{3^{1/2}}\left\|\pm 1, \mp\frac{1}{2}\right\rangle$
	$(E_{3/2})$	$\left\|\frac{3}{2}, \pm\frac{3}{2}\right\rangle = \left\|\pm 1, \pm\frac{1}{2}\right\rangle$
$^3P_0$	(0^-)	$\|0,0\rangle = \frac{1}{3^{1/2}}[\|1,-1\rangle - \|0,0\rangle + \|-1,1\rangle]$
$^3P_1$	(0^+)	$\|1,0\rangle = \frac{1}{2^{1/2}}[\|1,-1\rangle - \|-1,1\rangle]$
	(1)	$\|1,\pm 1\rangle = \frac{1}{2^{1/2}}[\pm\|\pm 1,0\rangle \mp \|0,\pm 1\rangle]$
$^3P_2$	(0^-)	$\|2,0\rangle = \frac{1}{6^{1/2}}[\|1,-1\rangle + \|-1,1\rangle + 2\|0,0\rangle]$
	(1)	$\|2,\pm 1\rangle = \frac{1}{2^{1/2}}[\|\pm 1,0\rangle + \|0,\pm 1\rangle]$
	(2)	$\|2,\pm 2\rangle = \|\pm 1,\pm 1\rangle$

of atoms and ions of groups I and II as well as the S Rydberg states with the $(ns)^1((n+1)s)^1$ configuration belong to this class. The atoms with a spherically symmetric valence shell but incomplete internal shells (such as ^{2}D states with the $(nd)^9((n+1)s)^2$ configuration) are formally non-isotropic but in view of the efficient screening of the *n*d shell by the $(n+1)$s electrons the M–G interaction depends only slightly on the orientation of the M atom [65].

In the $^1P_1$ ($L = 1$, $S = 0$) state involving an unpaired *n*p electron, the Hamiltonian of the free atom is diagonal in the basis of equivalent np_x, np_y and np_z orbitals (or $L_z = 0, \pm 1$ states). In the MG complex with axial symmetry with respect to the M–G (z) axis, the triple degeneracy of the P state is removed and the energy depends on whether the p electron occupies the $np_z \equiv np\sigma$ ($L_z = 0$) or the $np\pi$ ($L_z = \pm 1$) orbital. The ^{1}P state thus gives rise to a pair of $^1\Sigma^+$ and $^1\Pi$ states degenerate at $R_{M-G} \to \infty$ but split at a finite M–G distance. As will be shown in section 4.1, the $^1\Sigma^+$ states are repulsive whereas the $^1\Pi$ states are bound so that the $^1\Sigma^+ - {}^1\Pi$ energy gap increases with decreasing R_{M-G} distance. This dependence of the bond strength on the angle between the M–G and p-orbital axes is essential for the dynamics of $M-G_n$ interactions in many-body systems.

The $^1P_1$ state correlates in an M/G site with O_h symmetry with a triply degenerate $^1T_{1u}$ state. Its degeneracy is, however, removed without any external perturbation because of intrinsic properties of the atom; the interaction of the p electron with its G neighbours is strongly anisotropic. As already mentioned (section 1), the M_n cage is deformed; if the p orbital is oriented along one of C_4 axes its site symmetry will be lowered to D_{4h} (D_{2h} or C_{2v}) and for the C_3 orientation of the orbital axis a D_{3d} site symmetry is expected. In any case, the $^1T_{1u}$ state splits into two (or three) components. This instability of the degenerate P state (Jahn–Teller effect) will be discussed in detail in section 5.

3.2. *The L–S coupling: weak- and strong-coupling limits*

In the free atom with non-zero spin and orbital moments ($S \neq 0$ and $L \neq 0$) the degeneracy of the $^{2S+1}$X state is removed by the spin–orbit coupling so that Hamiltonian is diagonal in the basis of $|J, m_J\rangle$ states whereas L (L_z) and S (S_z) are no longer good quantum numbers. Orbital wavefunctions corresponding to the $|J, m_J\rangle$ states are not individual np_i orbitals (L_z states) but their linear combinations with coefficients (Clebsch–Gordan coefficients), which may be deduced from general laws of coupling of kinetic moments [66] (table 3).

The nature of the electronic states of the MG molecule correlated to the $^{2S+1}$P state

Downloaded At: 16:53 21 January 2011

Table 4. Spin–orbit coupling constants ζ in the lowest $^{2S+1}$P states of atoms and bonding energies D_e of the corresponding $^{2S+1}\Pi$ states (stronger bound component).

	ζ (cm^{-1})	D_e(M–Ar) (cm^{-1})	D_e(M–Kr) (cm^{-1})
Li	0.34	800	1180
Na	17.2	568	760
Mg	40.8	316	—
Zn	385	487	—
Cd	1142	324	499
Hg	4265	376	629

of the M atom is determined by the relation between the spin–orbit coupling strength ζ and the energy gap $\Delta V(R)$ separating bound Π and repulsive Σ^+ states split by the M–G interaction. We shall use the terms of the weak and strong L–S coupling limits for limiting cases of $\Delta V \gg \zeta$ and $\zeta \gg \Delta V$, which are known in the spectroscopy of diatomic molecules as Hund's cases a and c [67, 68]. Since Π and Σ^+ are degenerate in the free atom, the $\zeta \gg \Delta V(R)$ condition is always fulfilled at a sufficiently large R_{M-G} distance and the molecular states tend to those of the atom for $R_{M-G} \to \infty$. The good quantum numbers are then J and $\Omega = |J_z|$ and $|J, \Omega\rangle$ states are linear combinations of Σ and Π states with the same coefficients as in the case of atoms.

If the $\zeta \gg \Delta V(R)$ condition is fulfilled in the whole R_{M-G} range including the equilibrium distance in the bound state (as in the case of Hg complexes (table 4)), it is convenient to treat the system in the basis of the (strong-coupling limit) $|J, \Omega\rangle$ states and to consider the M–G interaction as perturbation.

In contrast with this, for a large number of systems involving light M atoms, we have in the vicinity of the energy minimum $|V_{MG}(R_{eq})| = D_e \gg \zeta$ which corresponds to the weak L–S coupling limit. The Π states are only slightly split by the spin–orbit interaction and the Π–Σ mixing is negligible because of a large energy gap [68]. $\Lambda = |L_z|$, S and $\Sigma = |S_z|$ are then good quantum numbers characterizing electronic states $^{2S+1}$Y (where Y = Σ, Π, ...) split into $2S+1$ $^{2S+1}Y_\Omega$ (where $\Omega = \Lambda + S_z$) components.

The MG molecule may be thus treated within a limited range of R_{M-G} distances in the vicinity of R_{eq} in terms of the weak-coupling limit (Hund's case a) but with increasing R_{M-G} distance their energies and orbital functions must correlate with those of the strong-coupling limit (Hund's case c). This intermediate-coupling case is usually treated in the basis of $|\Lambda, \Sigma, \Omega\rangle$ functions of the weak-coupling limit split and mixed by the spin–orbit interaction (see section 4.2).

For a correct description of the excited states of M/G centres involving the ^{2}P or ^{3}P states of the M atom, the M–G interactions as well as the spin–orbit coupling must be taken into account. To our knowledge, the theory is not so well developed as in the case of diatomics. The experimental data suggest that, for the systems with the O_h symmetry, the atomic $|J, m_J\rangle$ states form the best basic set and that L is still a good quantum number as shown by the conservation of the $\Delta L = \pm 1$ selection rule for radiative transitions. In the case of heavy atoms such as Hg, Au or Tl, individual Ω components of the ^{3}P (^{2}P) multiplets behave as independent electronic states. The mixing of the $^3P_2$, $^3P_1$ and $^3P_0$ states of the Hg atom in rare-gas matrices is almost absent as evidenced by a dramatic difference of their radiative rates (see section 6). In contrast with this, no difference between the evolution of different spin sublevels of the excited states of light atoms (Li, Na and Cu) was reported, which suggests their

Downloaded At: 16:53 21 January 2011

Table 5. Spin–orbit coupling constants ζ for metal atoms M free (gas phase) and embedded in G matrices, deduced from MCD studies for the lowest ^{2}P states.

	ζ				
M	Gas	G = Ar	G = Kr	G = Xe	Reference
Li	0.23	− 16.3	− 70	− 147	[62]
Na	11.5	—	—	− 213	[69]
K	38.5		− 64	− 170	[69]
Cu	166	124	95	− 23	[60]
Ag	614	766 (783)	616 (638)	524 (583)[a]	[60]
Au	2543	2537 (3354)	2572 (3110)	2555 (2655)[a]	[60]

[a] Two different ways of estimating ζ.

Table 6. The observed splitting between spin–orbit states in absorption or emission for free atoms and matrices.

			Splitting				
M	Levels	Spectrum	Gas	Ar	Kr	Xe	Reference
Ag	$^2P_{1/2}$–$^2P_{3/2}$	Absorption	921	1130	900	800	[60]
Au	$^2P_{1/2}$–$^2P_{3/2}$	Absorption	3816	4470	4177	3614	[60]
Tl	$^2P_{1/2}$–$^2P_{3/2}$	Emission	7793	7995	7775	7450	[70]
Cd	$^3P_0$–$^3P_1$	Emission	542	486	—	—	[71]
Hg	$^3P_0$–$^3P_2$	Emission	6397	5900	5250		[58]

Downloaded At: 16:53 21 January 2011

efficient mixing by M–G interactions. The spectra and decay paths of Ag/G centres show a complex behaviour (see section 7.2) which may be related to the intermediate *L–S* coupling strength in the Ag atom.

3.3. *The heavy-atom effect*

We supposed that the spin–orbit coupling strength is entirely due to the electrons localized at the M atom in the ^{2}P or ^{3}P state. However, even in weakly interacting $M–G_n$ systems, the excitation is slightly delocalized at the M atom and, if the spin–orbit coupling is large in the lowest $(np)^5((n+1)s)^1$ state of G, a small admixture of the MG* in the M*G state may modify significantly the H_{so} term. This effect is relatively weak in MG complexes but it may explain the increase in the energy gap between $^2\Pi_{1/2}$ and $^2\Pi_{3/2}$ states of NaG with the mass of the G atom (see section 4.2.2 and table 11).

This effect is even more pronounced in matrices. The spin–orbit coupling constants deduced from MCD spectra (as discussed in section 2.3.3) and directly measured level splitting in absorption and emission are represented in tables 5 and 6. As can be seen, the ζ constants for alkali metals in Kr and Xe characterize the host rather than the guest. The effects are large even for heavy M atoms. The most surprising is that the ζ constant is increased in MG complexes and decreased (with a change in sign) in M/G centres.

The 'external heavy-atom effect' in fluid solvents and in matrices has been extensively studied for molecules since the early work of Kasha [72] but the interest was focused on its effect on the rates of the singlet–triplet radiative and non-radiative

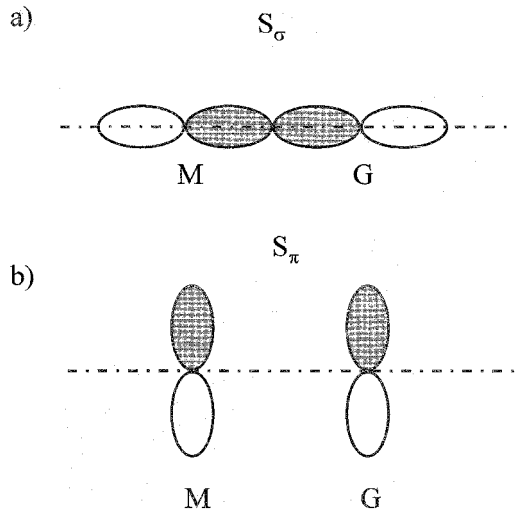

Figure 5. (*a*) σ- and (*b*) π-type overlaps of M and G orbitals for an M atom in the G matrix.

Downloaded At: 16:53 21 January 2011

transitions [44]. Less attention was paid to the environment effects on the level splitting induced by the spin–orbit coupling.

The theory of the heavy-atom effect for metal atoms in matrices was developed by Pellow and Vala [73] on the basis of the pioneering work of Ammeter and Schlosnagle [50]. In this model, the M/G centre is considered as an MG_{12} supermolecule, the excited states of which are linear superpositions of the M* locally excited state and delocalized Rydberg $[(np)^5,(n+1)p^1]$ state of the G_{12} 'solvation shell'. The M–G interaction depends on the values of overlap integrals S_σ and S_π between the *n*p orbital of M and $(n'+1)$p orbitals of G, where S_σ and S_π indicate the overlaps of orbitals with collinear (σ-type) and parallel (π-type) axes (figure 5). Another important parameter is the ratio of the spin–orbit coupling constants in the rare-gas and metal atoms: $Q = \zeta_G/\zeta_M$ (see tables 2 and 4). The diagonalization of the supermolecule spin–orbit operator H_{so} ($H_{so} = \zeta_M \mathbf{l}_M \cdot \mathbf{s} + \zeta_G \Sigma_{k=1}^{12} \mathbf{l}_k \cdot \mathbf{s}$) on the basis of the new excited states gives the expression of the effective spin–orbit constant ζ_{eff}. Calculations are applied to ^{2}P states of metal atoms. The ratio $k = \zeta_{eff}/\zeta_M$ depends on Q (k decreases with increasing Q) and on the values of S_σ and S_π. The above-cited workers reproduced different observed cases corresponding to $k > 1$ and $k < 1$ (including $k < 0$) by varying the values of Q, S_σ and S_π. $k > 1$ occurs when the spin–orbit coupling in the M atom is strong (i.e. when Q is small). In the case of light M atoms, the heavy-atom effect will reduce the value of ζ_{eff} and even change its sign (table 5). The important point is that the reduction in k is due to σ-type overlap integrals between the M and G orbitals of the same symmetry. The π-type overlap will enhance ζ_{eff}. The striking difference between M/G centres and MG diatomics may be explained in this way; the overlap integrals in the bound Π-states of MG molecules are always of the π type so that $k > 1$ and increases with increasing Q in the Ne → ··· → Xe series whereas in matrices the σ-type integrals are predominant.

The medium effect on the spin–orbit coupling in the M/G centre depends strongly on its symmetry and the Pellow model is strictly valid only for the sites with O_h symmetry. The conclusions may be very different for lower-symmetry sites. Since for a number of systems the fluorescence is emitted from such deformed sites, it is not evident whether this model may be directly applied to emission spectra.

4. Spectroscopy of isolated MG and MG_n systems

The electronic spectra of collision-free jet-cooled MG complexes are the main source of information about M–G potentials and their relation to the electronic structure of the M atom. These data may be then applied to the study of MG_n clusters and M/G centres in matrices. We shall try to present in the simplest way the main features of M–G interactions in three distinct cases involving different structures of the M atom or M^+ ion (where [X] indicates the closed-shell ion core):

(1) spherically symmetric (and quasisymmetric) ionic $[X]^+$ or $[X]^{2+}$ $(ns)^1$ and neutral $[X]^+$ $(ns)^1$ or $[X]^{2+}$ $(ns)^2$ ground states;
(2) ^{2S+1}P $[X]^+$ $(np)^1$ and $[X]^{2+}$ $(ns)^1(np)^1$ states;
(3) Rydberg states.

4.1. *M–G bonds in complexes involving M atoms and M^+ ions*

4.1.1. *S states of atoms and ions*

The common feature of the ionic M^+G and neutral MG $^{2S+1}\Sigma^+$ states correlated to ^{2S+1}S states of the M atom (ion) is the isotropy of the MG potentials which depend only on the M–G distances. The nature of the bonding is, however, different, as shown by the difference of their bonding energies between 20 and 200 cm^{-1} for neutrals and between 1000 and 5000 cm^{-1} for ions [1].

In the case of M^+G ions, the leading term in the M^+–G interaction is the interaction of the M^+ ion charge with dipole moment induced in the G atom:

$$V(R) = \frac{k(\varepsilon_{M+})^2 \alpha_G}{R_{M-G}^4}, \tag{4.1}$$

where ε_{M+} is the effective charge of the M^+ ion, α_G is the polarizability of G and R_{M-G} is the M–G distance. The observed variation in the dissociation energies D_e of the ground states of M^+G ions (table 7) is close to that predicted by equation (4.1).

In view of the extreme simplicity of the model, such good agreement is surprising.

In the case of a strongly interacting M^+–G pair the model may be improved by taking into account a term describing the $G \rightarrow M^+$ charge transfer due to the overlap of the empty M^+ ns_M orbital with the $np\sigma_G$ orbital containing an electron pair. The total wavefunction will be

$$\Psi = a_1\varphi_1(M^+G) + a_2\varphi_2(M{-}G^+) \tag{4.2}$$

The a_2^2/a_1^2 ratio, that is the relative weight of the MG^+ structure, $(n'p_G)^5$ $[X]^+$ $(ns_M)^1$, which may be represented by the $(n'p_G)^4(n'p_G + ns_M)^2$ $[X]^+$ configuration involving the M–G^+ covalent bond, depends on the energy difference $\Delta E = E(M{-}G^+) - E(M^+G)$. If the difference between charge-induced dipole terms of M^+G and MG^+ is neglected, ΔE may be approximated by

$$\Delta E = I_G - I_M - D_e(M{-}G^+),$$

where I_G and I_M are the ionization potentials and $D_e(M{-}G^+)$ is the dissociation energy of the covalent bond supposed equal to that of an isoelectronic neutral molecule (e.g. NaCl in the case of $NaAr^+$). It may be easily shown that, for Na^+Ar and Mg^+Ar complexes, ΔE is of the order of 6 eV so that the amount of the $G \rightarrow M^+$ charge transfer is negligible. In contrast, for Be^+Ar and Hg^+Xe, $\Delta E = 0.6$ and 0.95 eV respectively, which may explain their large dissociation energies of 4100 cm^{-1} in the former [74] and of 6300 cm^{-1} in the latter [75] case. For the H^+Ar system, $\Delta E =$

Downloaded At: 16:53 21 January 2011

Table 7. The $D_e(G)/D_e(Ar)$ ratios for MG neutrals and M^+G ions from experiment [1] and (in parentheses) obtained from equation (4.1) for ions and from equation (4.3) for neutrals.

	$D_e(G)/D_e(Ar)$			
M	G = Ne	G = Ar	G = Kr	G = Xe
Li^+	0.45 (0.475)	1 (1)	1.45 (1.43)	1.95 (2.1)
Na^+	0.42 (0.37)	1 (1)	1.42 (1.25)	1.66 (1.8)
Mg^+	—	1 (1)	7.5 (6.3)	
Na	0.19 (0.22)	1 (1)	1.62 (1.67)	2.78 (2.48)
Mg	0.33 (0.30)	1 (1)	—	—
Zn	—	1 (1)	1.5 (1.4)	2.16 (1.63)
Cd	0.365 (0.37)	1 (1)	1.21	1.71
Hg	0.325 (0.33)	1 (1)	1.25 (1.3)	1.79 (1.53)

− 2.2 eV, which corresponds to the stable H–Ar^+ configuration. In fact, the bonding energy of this molecule ion is of 33 650 cm^{-1} [76], close to that of the isoelectronic HCl molecule (35 150 cm^{-1}).

In the presence of *n*s valence electrons, the core charge is screened with an efficiency close to unity so that properties of the group II ions with the $[X]^{2+}$ $(ns)^1$ electronic structures are not significantly different from those group I $[X]^+$ ions.

For neutral atoms in S ground states the screening is so efficient that the ground states of MG complexes may be well described by universal formulae involving the dispersion forces between two neutrals:

$$V(R) = \frac{\alpha_G\, \alpha_M [I_M\, I_G/(I_M + I_G)]}{R^6_{M-G}}, \tag{4.3}$$

as shown in table 7. They do not differ from other van der Waals complexes and most of the M–G 'bonds' are slightly weaker than those of G–G rare gas dimers [77].

The repulsive terms in the M–G potential resulting from the overlap of the $M(^2S^{+1}S)$ atom *n*s orbitals with the closed electron shells of the G atom are small compared with the case of the M atom in the $^2S^{+1}P$ state (see below). The ns_M–$n'p_G$ orbital overlap is relatively weak because of a large extension of the s orbital and isotropic distribution of the electron density.

4.1.2. ^2D states of atoms of group IA

The only diatomic system involving a ^2D atom with the $(nd)^9((n+1)s)^2$ configuration observed up to now is the jet-cooled AgAr complex [65]. Its spectra (consistent with the data obtained for Cu, Ag and Au in matrices [78–81]) show that the a $^2\Pi_{3/2}$ state issued from the $^2D_{5/2}$ $(4d)^9(5s)^2$ state of the atom is as weakly bound (D_e = 100 cm^{-1}) as the ground X $^2\Sigma_{1/2}$ state corresponding to the ground $^2S_{1/2}$ $(4d)^{10}(5s)^1$ configuration. Obviously, the screening of the ionic core of Ag is not strongly modified by promotion of one electron from the *n*d to the $(n+1)$s orbital.

4.1.3. ^{2S+1}P atomic states

The specific properties of these states are due to a pronounced anisotropy of p orbitals. The simplest case is the $[X]^+$ $(ns)^1 \rightarrow [X]^+$ $(np)^1$ excitation of a light alkali atom (Li and Na) in which the spin–orbit coupling effects may be neglected. As previously

Downloaded At: 16:53 21 January 2011

mentioned (section 3.1), in the axial field of a rare-gas atom the ^{2}P state gives rise to two states which differ by the projections of the orbital momentum L on the quantization axis z: the doubly degenerate Π ($L_z = 1$) state with an ns electron promoted to the npπ orbital (linear combination of $n\mathrm{p}_x$ and $n\mathrm{p}_y$ orbitals perpendicular to the M–G axis) and the Σ^+ ($L_z = 0$) state with an electron at the $n\mathrm{p}_z\sigma$ orbital oriented along the M–X axis.

The essential terms of the M–G interaction (screening of the charge of the $[X]^+$ ionic core, repulsion resulting from overlap of complete electronic orbitals and charge transfer effects) are significantly different in the Σ^+ and Π states.

As an example of this difference, the main parameters of the $^2\Pi$ and $^2\Sigma^+$ states of NaG complexes are given in table 8. The A $^2\Pi$ state is much more strongly bound than the ground state of the complex (but not as strongly as the ionic state) while the B $^2\Sigma^+$ state is repulsive (an extremely shallow minimum has been observed uniquely in the case of the NaNe complex [82, 83] while for others the $X \rightarrow B$ absorption was not detected).

The reasons for this difference are obvious (figure 6).

(*a*) In the $^2\Sigma^+$ state, the screening of the ionic core by an electron at the p_z (σ) orbital is more efficient than in the case of an ns electron because the electron density is concentrated in the vicinity of the M–G axis. The repulsion due to the overlap of the p_z (σ) orbital with the complete electron shell of the G atom is also enhanced.

(*b*) In the Π state, the promotion of the s electron to the π orbital implies a reduction in the screening, the electron density in the vicinity of the G atom being reduced. The overlap of G orbitals with those of M is also weaker because of the perpendicular orientation of pπ orbitals. Finally, the $G \rightarrow M$ charge transfer (less efficient than in the case of M^+G ion) is possible because of the overlap of the empty σ (ns) orbitals of M with the p_z orbital of G occupied by an electron pair. This transfer is compensated by the $M \rightarrow G$ delocalization of the valence electron (such a double electron transfer effect involving the back donation proposed by Duval *et al.* [35] and Duval [87] in the case of more stable MG complexes may be applied here). The excited Π state may thus be described by a superposition of states:

$$|\Psi\rangle = a_1|\varphi(\mathrm{M}^*\ldots\mathrm{G})\rangle + a_2|\varphi(\mathrm{M}^+\ldots\mathrm{G}^-)\rangle + a_3|\varphi(\mathrm{M}^-\!-\!\mathrm{G}^+)\rangle, \tag{4.4}$$

where

$$|\varphi(\mathrm{M}^*\ldots\mathrm{G})\rangle = [\mathrm{X}]^+ (n\mathrm{p}\pi_\mathrm{M})^1 (n'\mathrm{p}_\mathrm{G})^6,$$
$$|\varphi(\mathrm{M}^+\ldots\mathrm{G}^-)\rangle = [\mathrm{X}]^+ (n'\mathrm{p}_\mathrm{G})^6 ((n'+1)\mathrm{p}_\mathrm{G})^1,$$
$$|\varphi(\mathrm{M}^-\!-\!\mathrm{G}^+)\rangle = [\mathrm{X}]^+ (n\mathrm{p}\pi_\mathrm{M})^1 (n'\mathrm{p}_\mathrm{G} + n\mathrm{s}_\mathrm{M})^2 (n'\mathrm{p}_\mathrm{G})^4$$

and

$$a_1 \gg a_2, a_3$$

To the best of our knowledge, the earliest theoretical treatment of this problem was performed by Baylis [88] at the time when no experimental data for excited states of alkali–rare-gas complexes were available. He developed a simple model accounting for the core–core repulsion by using pseudopotentials while the electrostatic interaction of the valence electron with the X^+ core was corrected for repulsive terms resulting from orbital overlap. Baylis's calculations gave a correct prediction of the main characteristics of the ground and excited $^2\Pi$ and $^2\Sigma^+$ states of NaG complexes

Downloaded At: 16:53 21 January 2011

Table 8. Bonding energies D_e and equilibrium distances R_{eq} for NaG complexes in the states correlated to the ground (3s), lowest excited (3p) and ionic Na^+ states.

	X(3s) $^2\Sigma^+$		A(3p) $^2\Pi_{3/2}$		B(3p) $^2\Sigma^+$		Na^+ ion		
	D_e (cm^{-1})	R_{eq} (Å)	D_e (cm^{-1})	R_{eq} (Å)	D_e (cm^{-1})	R_{eq} (Å)	D_e (cm^{-1})	R_{eq} (Å)	Reference
NaNe	8.0	5.3	144	2.3	4.5	7.9	520	2.41	[82]
NaAr	42	5.01	568	2.91	≈ 0	—	≈ 1200	2.75	[38, 84]
NaKr	68	4.92	760	3.05	≈ 0	—	1775	2.91	[85]
NaXe	117	4.95	1120	3.22	≈ 0	—	2080	3.0	[86]

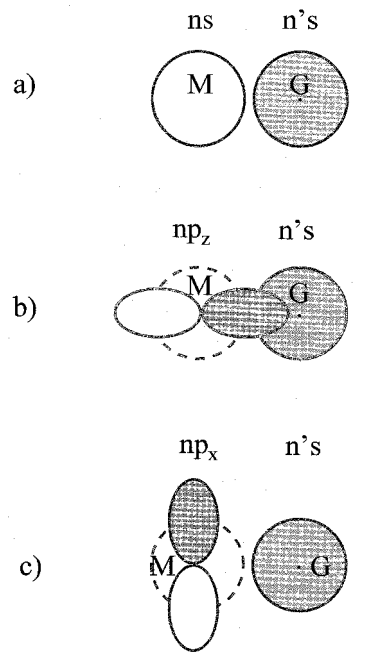

Figure 6. Filled or half-filled (——) and empty (– – –) orbitals of an alkali–rare gas complex in the $^2\Sigma$ (*n*s), $^2\Sigma$ (*n*pσ) and $^2\Pi$ (*n*pπ) states of the M atom.

and Na^+G ions. This simple model underestimates the depths of the energy wells in the $^2\Pi$ states especially for the light rare-gas atoms. Further refinements by the pseudopotential method [89] resulted in an excellent agreement in the case of the Na–Ne system, while for Na–Ar the *ab initio* calculations [90] give also the results close to the experimental data (table 9). The existence of a non-negligible M^-–G^+ dipole moment, expected in the case of significant $G \rightarrow M$ electron transfer, was also confirmed by *ab initio* calculations [90].

The same rules are valid for the complexes of alkaline earth (Mg, Ca, Sr and Ba) and group IIA metals (Zn, Cd and Hg) in their singlet $D\,^1\Sigma_0^+$ and $C\,^1\Pi_1$ states correlated to the $^1P_1$ atomic state. The $D\,^1\Sigma_0^+$ states are repulsive while the $C\,^1\Pi_1$ states are strongly bound [32, 91–94] (see table 20 and section 7.3). The difference between the M–G potential in the ground $X^1\,\Sigma_0^+\,(ns)^2$ and excited $C\,^1\Pi_1\,(ns)^1(np)^1$ state of these atoms is not as drastic as in the case of alkali metals because the screening of the M^+ core is not so strongly modified; in the $^1P_1\,(ns)^1(np)^1$ configuration of group II (IIA)

Downloaded At: 16:53 21 January 2011

Table 9. Experimental and calculated parameters D_e and R_e for NaNe and NaAr complexes.

	X(3s) $^2\Sigma^+$		A(3p) $^2\Pi$		B(3p) $^2\Sigma^+$	
	D_e (cm^{-1})	R_e (Å)	D_e (cm^{-1})	R_e (Å)	D_e (cm^{-1})	R_e (Å)
			NaNe			
Experimental	8.0	5.3	144	2.3	4.5	7.9
Calculated [88]	1.35	6.9	10.8	4.52	0.4	10.3
Calculated [89]	7.8	5.3	132	2.65		
			NaAr			
Experimental	42	4.99	568	2.91	≈ 0	—
Calculated [88]	30.9	5.03	327	3.19	7.3	7.82
Calculated [90]	55	5.01	492	3.04	32	6.8

Downloaded At: 16:53 21 January 2011

metals we still have one *n*s electron screening the ion core while, in the $^2P_{1/2}$ $(np)^1$ state of alkalis, the ionic core is naked. The ionic Mg^+G complexes isoelectronic with NaG neutrals show a slightly smaller difference between bond energies in their ground $^2\Sigma^+$ and excited $^2\Pi$ states: 117 ± 50 and 1804 cm^{-1} respectively for the Ne complex and 1280 and 5550 cm^{-1} for the Ar complex [95, 96]. The importance of the screening of the core charge by the s electrons may be illustrated by the interesting case of the Mg**Ar complex involving the Mg atom in a doubly excited $[X]^{2+}$ $(3p\pi)^2$ configuration [97, 98]. This state, in spite of the presence of two valence electrons, is much more strongly bound ($D_e = 2960$ cm^{-1} and $R_e = 2.39$ Å) than the Mg^+Ar ionic complex with the $[X]^{2+}$ $(3s)^1$ configuration ($D_e = 1280$ cm^{-1} and $R_e = 2.89$ Å) [1]. The core is better screened by one s electron than by two pπ electrons!

4.1.4. *Rydberg states*

The experimental information about the Rydberg states of MG complexes is limited to the lowest state involving an $(n+1)$s orbital (where n is the principal quantum number of the valence shell). The AlAr and AlKr complexes are the only ones for which the transitions to higher Rydberg states have been reported [99].

The specific properties of Rydberg states result from the diffuse and extended form of the spherical Rydberg $(n+1)$s orbital. An important step towards the understanding of the MG interaction in Rydberg states was made by Duval *et al.* [100] who reported the unusual shape of the potential energy curve of the HgAr $E\,^3\Sigma^+$ Rydberg state involving the $Hg^3S((6s)^1(7s)^1)$ atom; the existence of a deep ($D_e = 1430$ cm^{-1}) minimum at a short ($R_e = 2.81$ Å) distance separated by a 120 cm^{-1} barrier from a shallow ($D_e = 38 \pm 7$ cm^{-1}) minimum at a very large distance of 6.95 Å. The first minimum, with its equilibrium distance much shorter than the radius of the 7s Hg orbital, corresponds to the penetration of Ar atom inside the Rydberg electron orbit. Such a system, with D_e and R_e close to those of the Hg^+Ar ion ($D_e = 1630$ cm^{-1} and $R_0 = 2.87$ Å) [101] may be considered as the Rydberg state of a molecule with a $(HgAr)^+$ ionic core. The secondary minimum of the Hg*–Ar complex at a large M–G distance is due to dispersion forces the weakness of which is due to a large extension of the $(n+1)$s orbital. The energy barrier at about 5 Å corresponds to the maximum

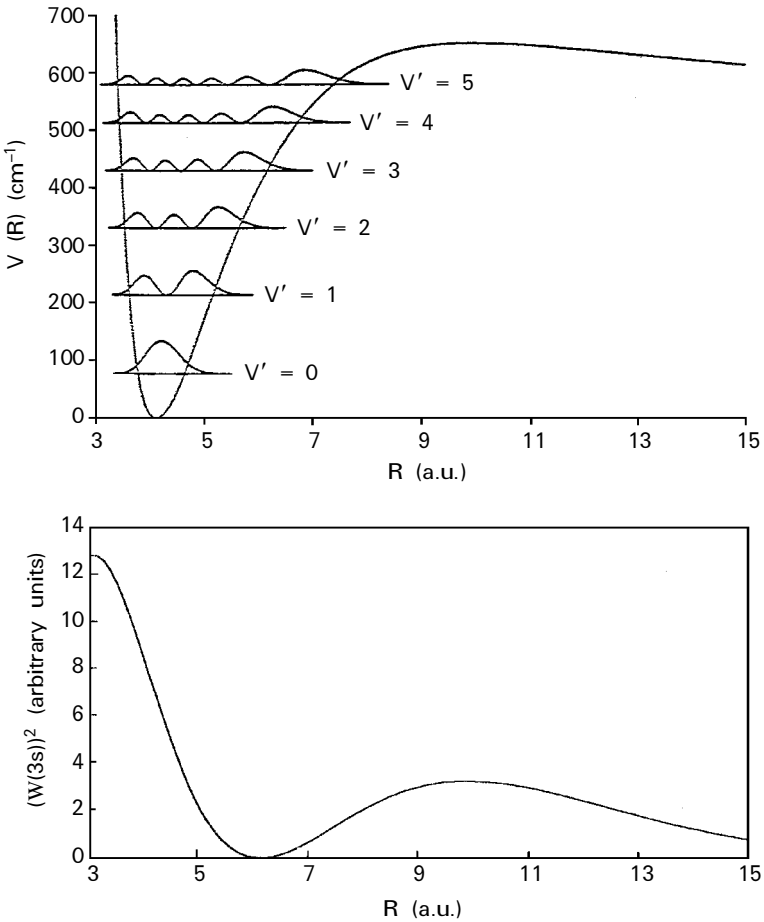

Downloaded At: 16:53 21 January 2011

Figure 7. Potential energy curve of the $^2\Sigma$ (3s) Rydberg state of the LiNe complex (from [102]) compared with the electron density distribution $[\psi(3s)]^2$ of the Li 3s orbital (a.u., arbitrary units).

repulsion resulting from the maximum overlap of the Rydberg Hg* orbital with the closed $(np)^6$ electron shell of the rare-gas atom.

A similar shape of the potential energy curve with a barrier of at least 60 cm^{-1} was observed for the Li(3s)Ne $^2\Sigma^+$ state [102]. This curve is represented in figure 7 together with that of the electron density distribution of the Li (3s) state approximated by a H-like function assuming the effective core charge of 1.155 corresponding to the 0.4 quantum defect. Note that positions of $V(R)$ and $|\psi|^2$ maxima coincide.

A determination of an extended part of the potential curve was realized in these two cases by the two-photon excitation of the Rydberg state using as an intermediate different vibrational levels of the lower states: the $A(0^+)$ and B(1) $Hg((6s)^1(6p)^1)$ states in the case of HgAr and the Li $(2p)^2\Pi$ state in the case of LiNe. For other systems, for which the level pattern is less favourable, only a part of the curve corresponding to small intermolecular distances could be explored. They confirm the essential conclusion from HgAr and LiNe studies: the existence of a deep energy minimum at an R_{MG} distance short compared with the radius of the Rydberg orbital. For example, the M–Ar bond in the Rydberg $E\,^3\Sigma^+$ $(ns)^1((n+1)s)^1$ states of MgAr, ZnAr and CdAr

complexes is almost as strong as in M^+Ar ions and significantly stronger than in excited valence (ns)(np) states [103, 104]. The screening of the ionic core by a Rydberg electron is obviously much weaker than by an npπ electron.

The existence of an energy barrier in the Rydberg state of complexes other than HgAr and LiNe was never directly evidenced but indirect indications (such as an overestimation of the dissociation limit deduced from the vibrational level pattern, and broadening of higher vibronic levels) have been found for several complexes of the group III atoms [31, 105, 106].

The experimental data seem to be well described by a simple electrostatic model of the penetration of the rare-gas atom inside the Rydberg orbital of the metal atom. Curiously, no energy minimum at the short interatomic distance could be found in the *ab initio* calculations carried out at the self-consistent field level for BAr and GaAr complexes [106, 107]. Such a minimum appears only in calculations carried out at the configuration interaction level. This suggests a more complex interaction involving more than one electronic configuration [106]. Such potential curves displaying two minima separated by an energy barrier have been deduced from high-level *ab initio* calculations of the Rydberg states of H–rare-gas and Li–rare-gas complexes [108].

Downloaded At: 16:53 21 January 2011

4.2. *Role of the spin–orbit interaction*

4.2.1. *Weak and strong L–S coupling limits*

The previous treatment, neglecting the electron spin, is valid when the spin–orbit coupling is much weaker than the M–G interaction. As previously indicated, in the weak L–S coupling limit the $|\Lambda\,\Sigma\rangle$ states are only weakly perturbed.

When the spin–orbit coupling is stronger than the M–G interaction (doublet and triplet states of heavy atoms such as Au, Hg or T1), we use as a basis the $|J,\Omega\rangle$ molecular states correlated to $|J,m_J\rangle$ states of the isolated M atom. These states are linear combinations of molecular orbitals involving atomic npσ and npπ wavefunctions with $\alpha(R_{M-G})$ and $\beta(R_{M-G})$ coefficients. As long as the spin–orbit coupling strength is not seriously modified by the M–G interaction (i.e. for large M–G distances), one can consider that the α and β coefficients are identical with the atomic Clebsch–Gordan coefficients (table 3). One can also tentatively assume that the potential energy curve $V_X(R_{MG})$ of an X state involving the 'mixed' orbital of the M atom,

$$\phi_X = \alpha_X(n\mathrm{p}\sigma) + \beta_X(n\mathrm{p}\pi),$$

will be

$$V_X(R_{MG}) = \alpha_X^2\, V_\sigma(R_{MG}) + \beta_X^2\, V_\pi(R_{MG}), \tag{4.5}$$

where $V_\sigma(R_{MG})$ and $V_\pi(R_{MG})$ are potential energy functions in the 'pure' σ and π states.

The validity of these relations was checked for a group of states of the HgAr complex correlated to the ^{3}P states of the Hg atom [35, 36, 87, 100, 109]. The $V_A(R)$ and $V_B(R)$ potentials of the A(0^+) and B(1) states corresponding to Hg($^3P_1$) were determined from the study of excitation spectra and since the mixing coefficients α_A, α_B, β_A, and β_B (see table 3) are known, the interatomic potentials: $V_\Pi(R)$ and $V_\Sigma(R)$ of 'pure' $^3\Pi$ and $^3\Sigma$ states may be deduced from equation (4.5). Hence

$$V_A(R) = V_\Pi(R),\ V_B(R) = \frac{V_\Pi(R) + V_\Sigma(R)}{2} \tag{4.6}$$

One can predict in this way the essential parameters of the potential of other excited states correlated to $^3P_0$ and $^3P_2$ for which Clebsch–Gordan coefficients are

Downloaded At: 16:53 21 January 2011

Table 10. Properties of the a–c states of HgAr estimated from the experimental data for the A and B states and Clebsch–Gordan coefficients compared to experimental values for a and b states.

	$A(0^+)\,P_1$ with coefficients 1, 0	$B(1)\,P_1$ with coefficients $\frac{1}{2}, \frac{1}{2}$	$a(0^-)\,P_0$ with coefficients $\frac{2}{3}, \frac{1}{3}$		$b(2)P_2$ with coefficients 1, 0		$c(1)P_2$ with coefficients $\frac{1}{2}, \frac{1}{2}$		$d(0^-)P_2$ with coefficients $\frac{1}{3}, \frac{2}{3}$	
	Observed	Observed	Calculated	Observed	Calculated	Observed	Calculated	Observed	Calculated	Observed
R_{eq} (Å)	3.38	4.66	4.21	4.33	3.38	3.31	4.66	—	4.95	—
D_e (cm^{-1})	369	67	101	110	369	437	67	—	59	—

known. As can be seen in table 10, these predictions are close to the experimental values of D_e and R_{eq} of a(0^-) and b(2) states. The experimental data for the c(1) and d(0^-) states are still not available.

Note that in this case the shape of the potential energy curves of the 'pure' repulsive $^3\Sigma$ state may be estimated experimentally whereas that of the $^1\Sigma$ state is not accessible by experiment.

4.2.2. *Intermediate L–S coupling case*

The majority of MG systems correspond to a transition from Hund's pure case c for $R_{MG} \to \infty$ and/or $V_{MG} \to 0$ towards Hund's case a for $R_{MG} \approx R_{eq}$ and $V_{MG} \approx D_e$. This transition is described in terms of the R dependence of energies: $E_i(R)$ and wavefunctions Ψ_i of molecular states expressed in terms of the spin–orbit Hamiltonian H_{so}.

In a free atom the level splitting is

$$\Delta E_{at} = \tfrac{\zeta}{2}(\mathbf{J}^2 - \mathbf{L}^2 - \mathbf{S}^2) = \tfrac{\zeta}{2}[J(J+1) - L(L+1) - S(S+1)], \tag{4.7}$$

which gives, for ^{2}P atomic states $\Delta E_{3/2,\,1/2} = 3\zeta/2$ and, for ^{3}P, $\Delta E_{2,\,1} = 2\zeta$ and $\Delta E_{1,\,0} = \zeta$. These values of ΔE are conserved (to a first approximation) for molecules in Hund's case c. In Hund's case a, it is convenient to treat separately the terms of H_{so} diagonal and off-diagonal in the $|\Lambda, \Sigma, \Omega\rangle$ basis.

The diagonal part $\zeta L_z S_z$ of H_{so} induces the splitting of the energy levels:

$$\Delta E_{mol} = \zeta \Lambda \Sigma, \tag{4.8}$$

yielding, for the $^2\Pi$ state, $\Delta E_{3/2,\,1/2} = \zeta$ and, for the $^3\Pi$ state, $\Delta E_{2,\,1} = \Delta E_{1,\,0} = \zeta$ [67]. If it is supposed that the spin–orbit coupling in the M–G complex is entirely determined by the spin–orbit coupling constant of the M atom, we would expect the splitting of energy levels to increase with increasing vibrational energy (i.e. with increasing average value of the R_{MG} distance) from ζ for $v = 0$ to its atomic ΔE_{at} value in the vicinity of the dissociation limit.

On the other hand, the off-diagonal terms $(\zeta/2)(L_+S_- + L_-S_+)$ of H_{so} induce a coupling between the $|\Lambda, \Sigma, \Omega\rangle$ and $|\Lambda \pm 1, \Sigma \mp 1, \Omega\rangle$ states described by the ϕ_1 and ϕ_2 functions such as the $^2S^{+1}\Sigma_\Omega$ and $^2S^{+1}\Pi_\Omega$ states. In the approximation of the two-level system, the resulting wavefunctions ψ_1 and ψ_2 are given by

$$\psi_1 = \alpha\phi_1 + \beta\phi_2, \psi_2 = -\beta\phi_1 + \alpha\phi_2 \tag{4.9}$$

where

$$\alpha = \cos(\tfrac{\theta}{2}), \beta = \sin(\tfrac{\theta}{2}), \tan\theta = \frac{2H_{so}}{|E_1 - E_2|}.$$

In the case of $^2\Sigma^+$ and $^2\Pi$ states correlated to the ^{2}P state of an atom, as the $^2\Pi$ state is split into $^2\Pi_{1/2}$ and $^2\Pi_{3/2}$ by the diagonal part of H_{so}, the $^2\Pi_{1/2}$ and $^2\Sigma^+_{1/2}$ states are coupled and mixed by the off-diagonal H_{so} terms while the $^2\Pi_{3/2}$ state remains uncoupled. The efficiency of the coupling (the α and β coefficients in equation (4.9)) depends not only on H_{so} but also on the energy gap between the vibronic levels, so that in the vicinity of the dissociation limit the $^2\Pi_{1/2}$ and $^2\Sigma^+_{1/2}$ states are completely mixed, giving rise to the $|\frac{1}{2}, \frac{1}{2}\rangle$ and $|\frac{3}{2}, \frac{1}{2}\rangle$ states of Hund's case c (the α and β coefficients become identical with Clebsch–Gordan coefficients) while the $^2\Pi_{3/2}$ correlates to $|\frac{3}{2}, \frac{3}{2}\rangle$. In the other limit, for $v = 0$ and $\langle R_{MG}\rangle \approx R_{eq}$ the energy gap is large so that $\alpha \to 1$ and $\beta \to 0$ and the stationary states are nearly pure $^2\Pi_{1/2,\,3/2}$ and $^2\Sigma^+_{1/2}$ states. One can establish

Downloaded At: 16:53 21 January 2011

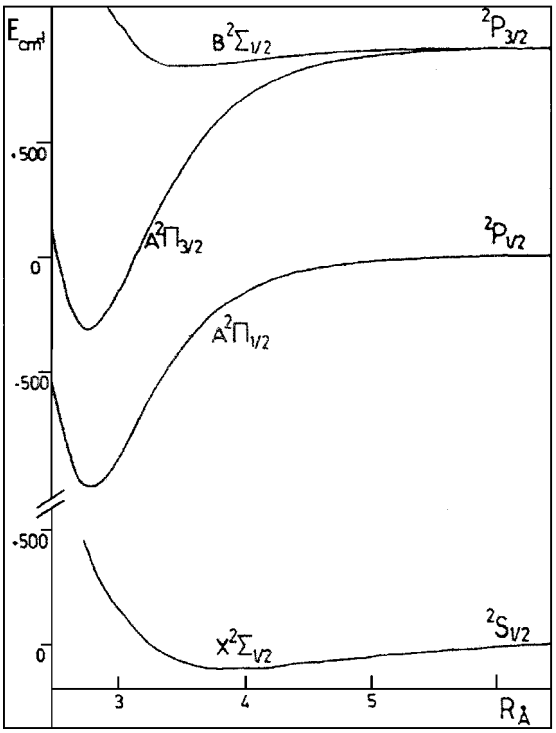

Figure 8. Potential energy curves of the AgAr complex illustrating transition between Hund's case c (degeneracy of the $A|\frac{3}{2},\frac{3}{2}\rangle$ and $B|\frac{3}{2},\frac{1}{2}\rangle$ states at large R values) and Hund's case a. (From [65].)

Downloaded At: 16:53 21 January 2011

in this way a correlation between the states corresponding to Hund's case a and Hund's case c limits (figure 8) by linear combinations of the $\{\phi_k\}$ basis set: $\Psi_i = \Sigma a_{ik}(R)\phi_k$ where $\{\phi_k\}$ are the pure Λ states $(\Sigma, \Pi, \ldots)$.

The observable are the v dependence of the energy gap between $^2\Pi_{1/2}$ and $^2\Pi_{3/2}$ states and that of the transition moment from the ground to the $^2\Pi$ state. Since the $X\,^2\Sigma^+_{1/2} \rightarrow {}^2\Sigma^+_{1/2}$ and $X\,^2\Sigma^+_{1/2} \rightarrow {}^2\Pi$ transition moments are different, the oscillator strength of the transition to the $\Omega = \frac{1}{2}$ states will depend on their α/β ratio varying the vibrational quantum number.

Let us take as the characteristic parameter the splitting of the $^2\Pi$ state $\Delta E_\pi(R_{M\text{–}G}) = E_{^2\Pi_{3/2}}(R_{M\text{–}G}) - E_{^2\Pi_{1/2}}(R_{M\text{–}G})$. Its value will be modified when R_{MG} decreases from $R_{MG} \approx \infty$ to R_{eq} by three previously discussed mechanisms.

(i) ΔE_π is reduced from $3\zeta/2$ to ζ corresponding to the transition from Hund's case c to Hund's case a.

(ii) The ζ constant varies owing to the increasing overlap of M and G orbitals. If the spin–orbit coupling constant is larger in G than in M atoms, this effect will tend to increase ΔE_π.

(iii) Π–Σ mixing occurs. Since the $^2\Pi_{1/2}$ state is mixed with the repulsive $^2\Sigma^+_{1/2}$ state, its bonding energy is reduced while that of the $^2\Pi_{3/2}$ component remains unchanged. Since the ^{2}P multiplets of group I and IA atoms are normal $(E_{3/2} > E_{1/2})$, this interaction tends to reduce ΔE_π. Its dependence on R_{MG} is complex because the amount of mixing depends not only on the ζ constant but also on the $^2\Pi_{1/2}$–$^2\Sigma^+_{1/2}$ energy gap which tends to zero for $R_{M\text{–}G} \rightarrow \infty$ and may be large for $R_{M\text{–}G} \approx R_{eq}$.

Table 11. Splitting of observed vibrational levels $V_{min}, \ldots, V_{max}$ and its extrapolation to $v = 0$ for $^2\Pi_{1/2}$–$^2\Pi_{3/2}$ states of Na–G complexes (ΔE(Na) = 17.196 cm^{-1}; A_0 = 11.464 cm^{-1}).

G	V_{max}	$\Delta E(V_{max})$ (cm^{-1})	V_{min}	$\Delta E(V_{min})$ (cm^{-1})	$\Delta E(v = 0)$ (cm^{-1})	Reference
Ne	6	15.09	3	12.118	—	[82]
Ar	10	13.48	7	14.79	—	[84]
Kr	14	20.51	7	32.8	49.6	[85]
Xe	16	44.8	10	68.27	116.7	[86]

The most detailed data on the $^2\Pi_{1/2}$–$^2\Pi_{3/2}$ level splitting are available for Na–G complexes and show a clear dependence of ΔE_π on the rare gas and on the vibrational quantum number [82–86] (table 11), suggesting a competition between the mechanisms (i) and (ii). Only in the case of the Ne complex do we have $\zeta < \Delta E_\pi < 3\zeta/2$ and ΔE_π which tends to ζ for $v \to 0$, as expected for the simple transition from Hund's case c to Hund's case a. In all other systems the $\Delta E_\pi = f(v)$ dependence is inverted and ΔE_π increases in the Ne → Ar → Kr → Xe series so that for Na–Kr and Na–Xe complexes we obtain by extrapolation $\Delta E_\pi(v = 0) \gg \zeta$. Such a dependence must be due to the 'borrowing' of the spin–orbit coupling strength from the rare-gas atom ('heavy-atom effect'). Note that $\zeta_{Na} \ll \zeta_G$ for all rare gases (see tables 2 and 4).

On the other hand, the role of this mechanism seems to be negligible in the case of the $^2\Pi$ state of the AgAr complex in which the splitting of the $v = 0$ levels of the $^2\Pi_{1/2}$ and $^2\Pi_{3/2}$ states is about 740 cm^{-1} while ^{2}P state of Ag is split by $3\zeta/2 = 92$l cm^{-1} (hence $\zeta = 614$ cm^{-1}) so that $\zeta < \Delta E_\pi(R_{eq}) < 3\zeta/2$ [65]. Note that in this case $\zeta_{Ag} \approx \zeta_{Ar}$. The role of mechanism (iii) is probably important for ground states of metals of the group III (see section 7.4).

4.3. *MG_n clusters*

It seems obvious that, by adding, one by one, the rare-gas atoms to the M atom, one can build an MG_n cluster with geometry analogue to that of the first solvation layer of an M/G centre. This procedure, applied to the systems involving aromatic molecules and rare-gas atoms was successful [41–43]. Unfortunately, in the case of metal–rare-gas systems the results are disappointing. All these systems have a common feature: a relative weakness of the M–G bond weaker than the G–G bond (60 and 100 cm^{-1} for Na–Ar and Ar–Ar respectively [110]). This implies that the structures in which the G–G bonds are broken by formation of the M–G bonds (i.e. with the M atom inside the cluster) are unstable. The energy of an M atom within the G_n cluster is even higher than that of the non-interacting M + G_n system. In the matrix, the metal atoms are 'forced' to remain within the volume while, in the finite rare-gas clusters, they escape from the inside and occupy the surface states. Such a behaviour was observed for Ba atoms in large Ar_n ($n \approx 1000$) clusters [111]; two absorption bands shifted by -120 and $+460$ cm^{-1} with respect to the free atom transition correspond to the $^1S_0 \to {}^1P_1$ excitation of the Ba atoms with the p orbitals parallel and perpendicular to the surface. This assignment is consistent with the spectrum and polarization of the $^1P_1 \to {}^1S_0$ fluorescence. In the case of $AlAr_n$ clusters [112], the Al absorption shows, in large ($n \approx 40$) clusters, a frequency shift with respect to the free atom much smaller (about 1000 cm^{-1}) than in an Ar matrix (4300 cm^{-1}). Such a large difference suggests that Al atom is placed at the surface and not embedded in the Ar_n cluster. The only exception from this 'non-wetting' rule are mixed rare-gas clusters such as $XeAr_n$ which will be discussed in section 7.5.

Downloaded At: 16:53 21 January 2011

Calculations at different refinement levels (pseudopotentials, *ab initio*, Monte Carlo, etc.) of the stable structures of MG_n clusters carried out for alkali–rare-gas (mainly $NaAr_n$) systems [113–119] confirm the instability of the structures with an Na atom in the centre of the cluster. These calculations are relatively easy in view of the isotropy of M–G potentials which may be considered as additive. They predict stable structures for small ($n = 3$–4) clusters: pyramids with a Na atom at the top and an Ar_3 or Ar_4 basis [117]. For larger $NaAr_n$ systems up to 'infinite' Ar surfaces, the stable structures correspond to Na atoms adsorbed at the surface [115, 116]. Calculations carried out for the Ba + Ar system confirm the stability of surface states in good agreement with experiment [120].

The only observable is the electronic spectrum of an individual MG_n species. In order to check the validity of calculations, it is necessary to determine the potential energy surface of the excited electronic state in the vicinity of the ground-state energy minima and then to simulate the MG_n absorption. This problem is much more complex than the evaluation of the ground-state structures because of the anisotropy of M*–G potentials and the doubts concerning their additivity.

The M–G potential depends (as discussed in section 4.1) on the angle θ between the axis of the np orbital of M on the M–G vector. In diatomic systems, because of their symmetry, the angle θ may take only the values 0 or $\pi/2$ corresponding to the σ and π configurations. A polyatomic MG_n is characterized by an ensemble of $M–G_i$ ($i = 1, 2, \ldots, n$) vectors and θ_i angles different from 0 and $\pi/2$.

In the absence of more elaborate models, one can tentatively express the dependence of the M–G potential on the angle θ for $0 \leqslant \theta \leqslant \pi/2$ by

$$V_\theta(R) = \cos^2\theta\, V_\Sigma(R) + \sin^2\theta\, V_\Pi(R) \tag{4.10}$$

and assume that the total potential energy of the system is a simple sum

$$V_{\text{tot}} = \sum_i V_i(R_{M-G_i}) + \sum_{i,j \neq i} V_{ij}(R_{G_i-G_j}). \tag{4.11}$$

Such calculations carried out for Na–Ar systems with the Na atom at the cluster surface predict the splitting of the $^2S \rightarrow {}^2P$ absorption into two bands: a narrow band only slightly shifted from the free atom frequency and a broad band with a stronger blue shift. They are assigned to the π and σ configurations of the system in which the 3p orbital of Na is either parallel or perpendicular to the surface plant [117, 118]. No data for $NaAr_n$ clusters are available but the results of calculations are consistent with observed spectra of Ba atoms on Ar_n ($n \approx 1000$) clusters so large that their surface may be considered as a plane [111, 120]. The blue shifts predicted for unstable configurations of $NaAr_{24}$ clusters with Na atom in the centre ($\Delta\nu = 2800$–$3600\ \text{cm}^{-1}$) [116] are larger than those observed for the Na in Ar matrices (about $1400\ \text{cm}^{-1}$) and are probably overestimated.

The only systems for which the validity of this model was checked are small $HgAr_n$ ($n \leqslant 4$) clusters the spectra of which have been determined by fluorescence excitation and mass-selected two-photon ionization (MSREMPI) spectroscopy [121–124]. It has been shown that, in the simplest case of $HgAr_2$ molecule [121, 122], deviations from additivity are not important. The equilibrium geometries and electronic spectra of $HgAr_n$ ($n = 1$–4) clusters have been calculated and compared with MSREMPI spectra, showing reasonably good agreement. For larger systems, the calculated frequency shift for $HgAr_{12}$ cluster ($+930\ \text{cm}^{-1}$ from that of the free atom [123])

Downloaded At: 16:53 21 January 2011

represents about 75% of the shift observed for Hg in the Ar matrix (+ 1230 cm^{-1} [57]). Since the matrix shift is due not only to 12 nearest Ar neighbours but also to the further solvation shells, this agreement may be considered as satisfactory.

Recently, a similar model was used to predict the crossing or non-crossing of the potential energy surfaces of states correlated to the $^1P_1$ and ^3P_J atomic states in small MG_n clusters ($n = 2, 3$) [125, 126]. As before, the calculations are based on the assumption of additivity of potentials deduced from experiment or from *ab initio* calculations for MG diatomics. Their validity cannot be checked as long as the experimental data for $^1P_1 \rightsquigarrow {}^3P_J$ relaxation rates in clusters are missing.

The accuracy is limited by deviations from the additivity of two-body potentials which are probably more important in the systems with a stronger M–G interaction because of a 'quasichemical' interaction involving the M↔G charge transfer. The assumption of additivity must be thus considered as a zero-order approximation which breaks down when the M–G interaction strength increases.

5. Spectroscopy of M/G centres

5.1. *Structure and M–G interactions in M/G centres*

An M atom may occupy in a rare-gas matrix either a substitution site (corresponding to a vacancy created by elimination of one or more host atoms) or an interstitial site. The information about their symmetries and structures is deduced from optical (absorption and MCD) spectra and more directly from the ESR spectra but their assignments are often uncertain. In a large number of systems, more than one type of site is populated. Their relative stabilities may be checked by recording the effect of annealing (or irradiation) of the matrix on the relative intensities of spectral bands assigned to each type of centre.

Downloaded At: 16:53 21 January 2011

It is often admitted that the necessary condition for a stable one-atom substitution site is that the van der Waals radius of the guest is smaller than or equal to the host atom radius: $r_{vdW}(M) \leqslant r_{vdW}(G)$. Unfortunately, if the reliable values of van der Waals radii deduced from the nearest-neighbour distances in crystals and collisional cross-sections are available for rare gases, those of neutral metal atoms are uncertain. Their values estimated in different ways differ drastically, as shown in table 13 where crystal radii reported in [128] are compared with those of [129]. For this reason, it seems to us more reliable to take as a criterion the relation between the equilibrium distance in the ground electronic state of an MG complex and the nearest-neighbour guest–host distances calculated for the one-atom substitution sites and interstitial sites in the G-crystal.

The data in tables 12 and 13 suggest that none of the listed atoms can occupy an interstitial site but most of them may substitute a single Kr or Xe atom. In the Ar lattice the place 'reserved' for a guest atom seems rather uncomfortable while in Ne it is clearly insufficient for an M atom with the possible exception for smallest atoms such as B, Al and Pd.

We shall discuss separately the simple case of atoms with $(ns)^1$ and $(ns)^2$ non-degenerate, spherically symmetric ground-state configuration, that is of metals of groups I, IA, II and IIA. The more complex case of group III metal atoms with spatially degenerate $(ns)^2(np)^1$ ^2P ground-state configurations will be treated together with that of the excited ^{2s+1}P states.

Table 12. Nearest neighbour distances for different sites in rare-gas matrices. (From [127].)

R_{G-G}	G = Ne	G = Ar	G = Kr	G = Xe
Substitutional	3.21	3.83	4.05	4.41
Octahedral interstitial	2.27	2.71	2.87	3.12
Tetrahedral interstitial	1.96	2.35	2.48	2.7

Table 13. vdW radii r_{vdW} from [128] and (in parentheses) [129] and interatomic distances R_{M-G} in the ground states of MG complexes. (From [1].)

		R_g(M–G) (Å)			
M	r_{vdW} (Å)	G = Ne	G = Ar	G = Kr	G = Xe
Na ($(ns)^1$)	1.8 (3.07)	5.3	5.01	4.92	4.95
Ag	1.6		~4.0		
Mg	1.5 (2.75)	4.4	4.49	—	4.56
Zn ($(ns)^2$)	1.35	—	4.18	4.2	4.4
Cd	1.55	4.26	4.31		
Hg	1.5	3.90	3.99	≈ 4.07	≈ 4.25
B	0.85 (1.78)	—	3.57	—	—
Al ($(ns)^2(np)^1$)	1.25 (2.3)		3.79	3.84	
In	1.55		4.13		

Downloaded At: 16:53 21 January 2011

5.1.1. *Atoms with ground* $^1S_0$ *and* $^2S_{1/2}$ *states*

A tentative assignment of the site type is based on its optical spectrum (the host dependence of the gas-to-matrix frequency shift) and ESR spectrum (isotropy or anisotropy, hyperfine splitting, and interactions with the host nuclei). Computer simulations of the site geometry and energy are also useful.

5.1.1.1. *The gas-to-matrix shift.* The origin of the shift of the absorption band of an M/G centre with respect to a free M atom ($\Delta\nu_{abs} = \nu_{abs} - \nu_{gas}$) will be discussed in the next few sections. This shift is related to the strength of the short-range M–G repulsive interaction in the excited state and strongly depends on the size of the vacancy (i.e. of the average M–G distance). One can thus expect a decrease in $\Delta\nu_{abs}$ in the series Ne → Ar → Kr → Xe for the same type of site.

In fact, $\Delta\nu_{abs}$ varies in a regular way for Ar, Kr and Xe but, in the Ne matrix, $\Delta\nu_{matr}$ is either larger (Mg, Cd, and Pd) or smaller than in the Ar crystal (table 14). A reduced blue shift in the Ne case suggests that the structure of the M/Ne site is different from that of other M/G sites; the one-atom substitution in the case of heavier gases and a multi-atom vacancy in that of neon. The M–Ne distance is larger than it would be in one-atom sites so that the repulsion is reduced. Note the anomalous behaviour of the Pd atom; it shows a larger blue shift in the Ne than in the Ar matrix and an unusually large shift in Xe. This anomaly was tentatively explained by a very small orbital radius of Pd resulting from its unusual $(4d)^{10}$ electronic configuration with an empty 5s orbital. The Pd atom may thus occupy a one-atom vacancy in Ne and enter into the 'crowded' interstitial site in Xe which is otherwise inaccessible for larger atoms [127].

The different nature of the M/Ne sites from the M/Ar and M/Kr sites was clearly evidenced in the case of the Ni atoms [139–141]. The absorption spectra of Ni/Ne sites and of the unstable Ni/Ar and Ni/Kr sites indicate that the $(3d)^8(4s)^2\ ^3F_4$ state (the ground state of the isolated Ni atom) remains its ground state in the solid. In contrast,

Table 14. Frequency shifts of absorption maxima (or centres of gravity of multiplets) with respect to the gas-phase frequencies: $\Delta\nu_{abs} = \nu_{abs} - \nu_{gas}$.

		$\Delta\nu_{abs}$ (cm^{-1})				
		Ne	Ar	Kr	Xe	References
Li	$^2P_{1/2,3/2} \leftarrow {}^2S_{1/2}$	723	1070	375	70	[53, 130]
Na	$^2P_{1/2,3/2} \leftarrow {}^2S_{1/2}$	—	1395	665	835	[54, 62, 131]
Cu	$^2P_{1/2,3/2} \leftarrow {}^2S_{1/2}$	1870	2415	1490	300	[131–133]
Ag	$^2P_{1/2} \leftarrow {}^2S_{1/2}$	—	2150	1430	310	
	$^2P_{3/2} \leftarrow {}^2S_{1/2}$	—	2650	1620	350	[59, 134, 135]
Au	$^2P_{1/2} \leftarrow {}^2S_{1/2}$	—	1535	765	−715	
	$^2P_{3/2} \leftarrow {}^2S_{1/2}$	—	2480	1370	−680	[59]
Mg	$^1P_1 \leftarrow {}^1S_0$	1365	455	210	−1055	[56, 136]
Zn	$^1P_1 \leftarrow {}^1S_0$	—	1610	320	−1280	[52]
Cd	$^1P_1 \leftarrow {}^1S_0$	1880	1670	450	−1135	[71]
Hg	$^1P_1 \leftarrow {}^1S_0$	—	2050	450	−1600	[137]
	$^3P_1 \leftarrow {}^1S_0$	940	1250	750	50	[57, 138]
Pd	$^3D_1 + {}^1P_1 \leftarrow {}^1S_0$	6850	6050	5650	8050	[127]

Downloaded At: 16:53 21 January 2011

the spectra of stable Ni/Ar and Ni/Kr sites are completely different and correspond to absorption from the $(3d)^9(4s)^1\,{}^3D_3$ state which in the gas phase has an energy 200 cm^{-1} higher than that of the $(3d)^8(4s)^2\,{}^3F_4$ level. This indicates that the perturbation of the guest atom is weaker in Ne (and in the unstable Ar and Kr sites) than in the stable Ni/Ar and Ni/Kr sites, that is that the cavity is larger in the first group of sites (perhaps indicating a multi-atom vacancy). This result is consistent with the smaller frequency shifts in unstable Ar, Kr and Xe sites (1600, 240 and −1360 cm^{-1} respectively) than in the stable sites (about 2200, about 1400 and about 400 cm^{-1} respectively).

5.1.1.2. *Electron spin resonance*. The narrow-line ESR spectra allow the separation of signals corresponding to different sites better than the broad-band optical spectra do. The ESR spectra of alkali atoms [45, 46, 142] confirm the existence of multiple sites and separate even the spectral features due to slightly different environments; in the case of Na/Ar and K/Ar 'blue sites', a few closely spaced lines are assigned to individual members of a 'family of sites' with identical structures of the first solvation shell but with different imperfections in the further shells [45, 142]. The annealing technique allows the correlation of the ESR and optical spectral features corresponding to the same type of site.

An important parameter, deduced from the ESR spectrum is the value of the hyperfine structure (HFS) constant A characterizing the coupling of the electron spin with that of the M-atom nucleus. As mentioned in section 2.3.1, the $\Delta A/A$ ratio (where A is the HFS constant of the free atom) increases with contraction of the ns orbital owing to its overlap with those of host atoms [47]. In the ESR spectra of Li in Ar and Kr matrices, the signal corresponding to the more stable ('blue') site shows a significant increase in A with respect to the free atom ($\Delta A/A = 0.025$) while, for the less stable ('red') site, $\Delta A/A = -0.01$ [46]. The stable site seems thus to be more 'crowded' than the unstable site, which suggests a one-atom substitution in the stable site and a larger many-atom vacancy in the less stable site. Similar results have been obtained for K and Rb atoms [45, 143] and are consistent with the conclusion deduced from the frequency shifts in optical spectra that the more 'crowded' one-atom

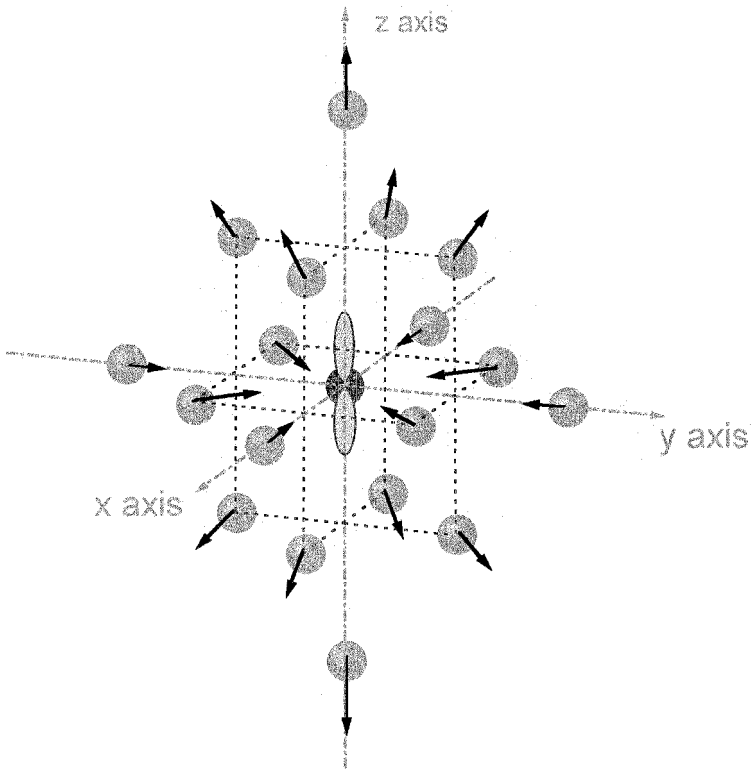

Figure 9. Displacements of G atoms in the MG_{18} corresponding to the $O_h \rightarrow D_{4h}$ deformation of the centre induced by the 'σ–π interaction'.

Downloaded At: 16:53 21 January 2011

substitution sites are stable. The isotropy of ESR spectra indicates that both 'blue' and 'red' sites conserve the cubic symmetry but does not allow a differentiation of the four-atom vacancies with the T_d symmetry from the O_h symmetry of the one-atom substitution site.

The ESR spectra of Cu, Ag and Au in Ar, Kr and Xe matrices [49] are isotropic and consist of single systems of narrow lines. Such a spectrum corresponds to guest atoms which occupy only one type of site having a cubic symmetry. Moreover, the ESR spectra of Cu and Ag in the Xe matrix show a hyperfine structure composed of closely spaced lines which have been explained by the coupling of the electron spin of the guest with the nuclear spins of the Xe atoms. It may be fitted by assuming the presence of 12 equidistant Xe atoms, which implies an unperturbed O_h substitution site. It is, to our knowledge, the only case in which the site structure is established in such a detailed way. On the other hand, in Ne matrices, several sites coexist; the site giving rise to broad lines seems to correspond to the amorphous Ne solid while other sites display sharp lines and show a pronounced anisotropy. Obviously, the metal atoms occupy the sites of lower (non-cubic) symmetry with axes preferentially oriented perpendicular to the sapphire support. Such sites may correspond to a two-atom substitution with an axial symmetry.

5.1.1.3. *Computer simulations.* The computer simulations using molecular dynamics, Monte Carlo and simulated annealing techniques and two-body M–G and G–G potentials have been performed for different alkali–rare-gas systems [113–118, 130,

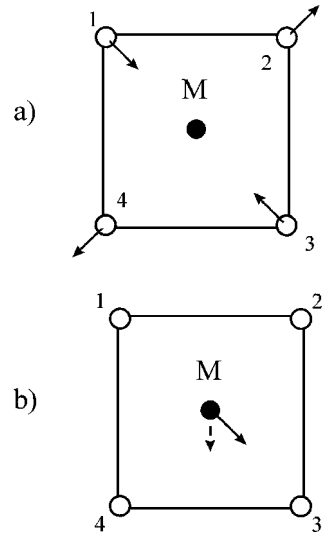

Figure 10. Deformation of the MG_4 ($z = 0$) structure corresponding to (*a*) $D_{4h} \rightarrow D_{2h}$ and (*b*) $D_{4h} \rightarrow C_{2v}$ symmetry lowering.

Downloaded At: 16:53 21 January 2011

144–147]. In spite of some discrepancies the results suggest 'competition' between two types of site: single atom vacancies with the octahedral O_h symmetry and four-atom vacancies belonging to the tetrahedral T_d symmetry group. Their relative stability depends on the relation between the van der Waals radii: r_{vdW} (M)/r_{vdW} (G). The stable structure of the Na/Ar centre is probably a single-atom O_h vacancy [118] (the unstable Na/Ar ('red') sites might well correspond to a four-atom substitution). The stable site of Li/Ne is probably also a four-atom vacancy [144]. To our knowledge, no simulations of this type have been performed for M/G systems involving metal atoms of the groups IA or II.

5.1.1.4. *Conclusion*. In view of this abundant although incomplete information, we may assume that for the majority of systems involving the atoms of groups I, IA, II and IIA in Ar, Kr and Xe hosts the structures of M/G sites correspond to one-atom substitution sites with the O_h symmetry (in Ne, typical sites seem to be multi-atom vacancies). Such a one-atom site may be represented in the first approximation as an MG_{18} 'cluster' involving a central M atom in the origin (000) position (figure 1). Its 12 nearest neighbours G $a/2^{1/2}$ distant occupy four by four the $z = 0$ and $z = \pm\frac{1}{2}$ planes. Six other G atoms at a distance a from M are placed in the equivalent $(\pm 1, 0, 0)$, $(0, \pm 1, 0)$ and $(0, 0, \pm 1)$ positions, where a is the lattice constant. This 'cluster' is embedded in the G solid which may be approximated by a dielectric continuum. The propensity towards 'crowded' sites, unexpected at the first sight, may be probably explained by the weaker perturbation of the crystal lattice than in the case of more extended vacancies.

5.1.2. ^{2s+1}P *states of M/G centres*

Here, we shall focus our attention on the M–G interaction resulting from the $ns \rightarrow np$ (S $\rightarrow$ P) excitation of an M/G site with an initial O_h symmetry. The case of the ^{2}P ground states of group III metals will be also mentioned.

The properties of ^{1}P, ^{2}P and ^{3}P states are essentially determined by those of the np orbital, the symmetry of which in the O_h point group is t_{1u}. The simplest case is that

of excited $^1P_1$ states, in which the spin–orbit effects are absent and the 'pure' np_x, np_y, np_z orbitals form a good basis. The T_{1u} state is unstable in the O_h symmetry and its degeneracy is removed by deformation of MG_{18} 'cluster'; this behaviour is a specific case of the instability of degenerate electronic states of polyatomic systems (Jahn–Teller effect) [12–14]. It may be easily shown that the shape of the potential energy surface of the M*(P)/G centre is different from that of the ground M(S)/G state.

Let us consider the M atom in its $^1P_1$ state prepared by radiation polarized along the z (001) crystal axis, that is with the p electron on the p_z orbital (this choice is arbitrary but in view of the spherical symmetry of the site all orientations are equivalent). We shall consider that the interaction with its G neighbours depends on the θ angle between the z-orbital axis and the M–G radius vector (see section 4.3 and equation (4.10)). This interaction will be different for three groups of G atoms (figures 1 and 9).

(1) For four G_i ($i = 1$–4) atoms distant by $a/2^{1/2}$ and four others ($i = 15$–18) distant by a, all of them placed in the ($z = 0$) plane (the nodal plane of the p_z orbital ($\theta = \pi/2$)) this interaction is attractive as in the case of the π orbital of the M–R complex.
(2) For eight ($i = 5$–12) host atoms in the ($z = \pm a/2$) planes and at the $a/2^{1/2}$ distance ($\theta = \pi/4$) the interaction is strongly repulsive as it would be for an orbital with a pronounced σ character.
(3) It is also repulsive for two G_i ($i = 13$ and 14) atoms in the (0, 0, $\pm$ 1) positions ($\theta = 0$; $R_{MG} = a$).

This 'σ–π interaction' [50] tends to deform the cavity containing the M atom; the minimum of the energy corresponds to the cluster expanded in the z direction and constrained in the (x, y) plane so that for $i = 1$–4 the equilibrium M–G distances are reduced while those of $i \equiv 5$–12 and $i \equiv 13$ and 14 are increased. The symmetry of the site is then reduced from O_h to D_{4h} inducing a partial splitting of the degenerate T_{1u} state into its A_{2u} and E_u components. It is important to note that identical energy minima (corresponding to expansion of the MG_{18} cluster along the x and y axes) result from excitation of the ns electron to np_x and np_y states. The same general conclusions will be deduced from an analysis of an M*/G centre with the np orbital oriented along one of the C_3 axes.

A further deformation of the cluster may take place when the energy minimum does not correspond to the central position of the M atom interacting with equidistant $i = 1$–4 G_i atoms but rather to a reduced distance between M and one or two G atoms. This may be realized either by such displacements of G_1 and G_3 atoms that the square composed of $i = 1$–4 G atoms is transformed into a rhombus or by a displacement of the M atom from its central position [57] (figure 10). The symmetry of the centre is then reduced to D_{2h} in the former and to C_{2v} in the latter case inducing a complete removal of the degeneracy of the T_{1u} state. The symmetry will be also lowered if the M atom is displaced along the z axis [52, 147].

The multidimensional potential energy surface $V_{exc}(Q)$ of the excited P state is usually represented in a one-dimensional scheme as a double-minimum curve with the minima at $Q_{exc} = Q_0 \pm \Delta Q$ (where ΔQ represents the displacement from the ground-state equilibrium configuration: $Q_g = Q_0$) and a central energy barrier (figure 11 (b)). With such a surface, the vibrationless level of the T_{1u} state is split by the tunnel effect into a set of levels. Moreover, the Q_0 configuration of the excited state does not

Downloaded At: 16:53 21 January 2011

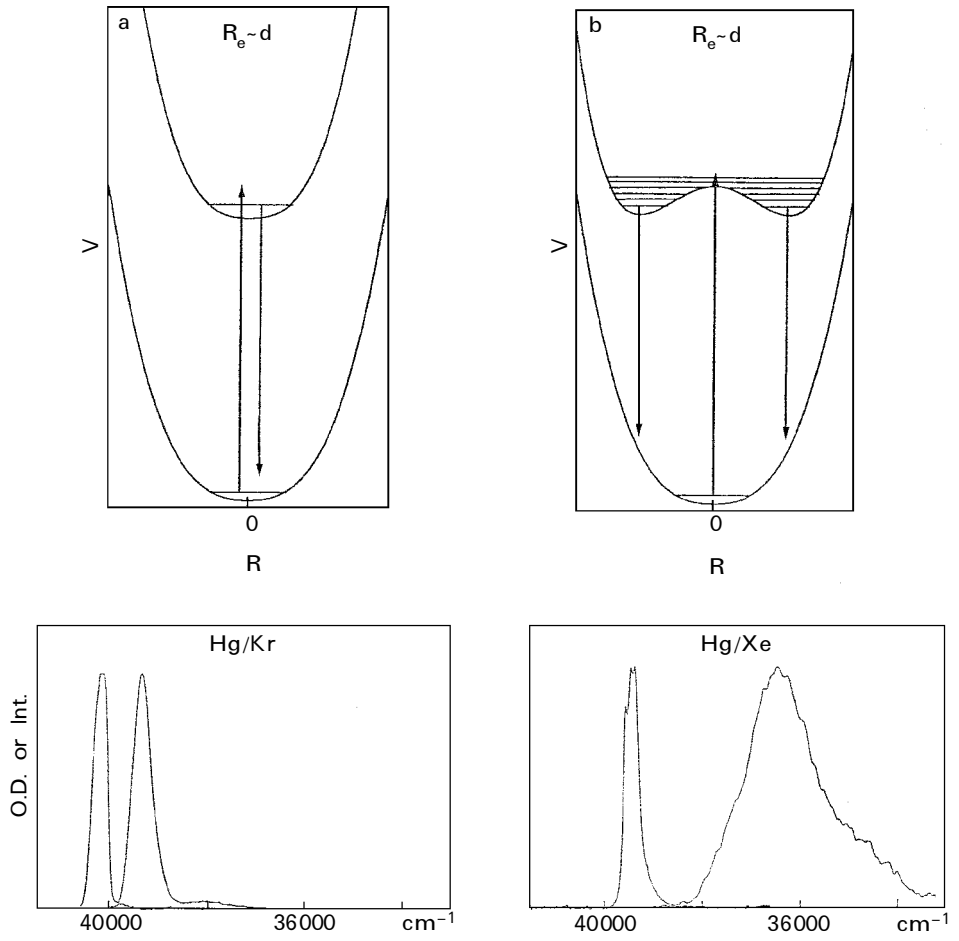

Downloaded At: 16:53 21 January 2011

Figure 11. Scheme of absorption and emission transitions between the ground-state (single minimum) surface of an M/G centre and its excited single-minimum (left) and double-minimum (right) surface. The absorption and fluorescence spectra of Hg in Kr and Xe matrices correspond to these schemes (note the 'triplet' structure and the large Stokes shift in the latter case).

correspond to an energy minimum so that a 'vertical' excitation of the ground $^1S_0$ state at $Q = Q_0$ prepares the P state with the vibrational energy excess $\Delta E_{vib} \approx V_{exc}(Q_0) - V_{exc}(Q_{exc})$, that is with the simultaneous excitation of phonon modes including the non-totally symmetric e_g and t_{2g} modes. The fluorescence is emitted after thermal equilibration of the excited M*/G centre from the Q_{exc} configuration(s) to excited vibrational (phonon) levels of the ground state which implies a red shift in emission. Since the symmetry of the Q_{exc} configuration is lowered, one can expect the breakdown of the selection rules which are valid in the higher-symmetry Q_0 configuration.

It is important to note that in the initial O_h symmetry the orbital moment of the M atom is not completely quenched as evidenced by the g_{orb} values deduced from the MCD spectra [148] and by a partial conservation of the $\Delta L = \pm 1$ selection rule (see section 6.1).

This picture, neglecting the spin–orbit interaction, corresponds to the weak L–S

coupling limit. In the strong-coupling limit, the $^3P_0$, $^3P_1$ and $^3P_2$ components of the ^3P state (the $^3P_2$ splits into T_{2u} and E_u in the O_h point group) and the $^2P_{1/2}$ and $^2P_{3/2}$ components of ^2P may be considered as individual states (see section 3.2). Large differences between $\Delta\nu_{abs}$ gas-to-matrix shifts in the $^2S_{1/2} \rightarrow {}^2P_{1/2}$ and $^2S_{1/2} \rightarrow {}^2P_{3/2}$ of Ag and Au may be related to the different shapes of their orbitals resulting from different pσ–pπ mixing (Clebsch–Gordan) coefficients. The same is true for the $^3P_0$ and $^3P_1$ states of Hg atoms; the $^3P_0$ state is nearly isotropic as shown by its projections on the np states whereas the $m_J = 0$ component of the $^3P_1$ state is strongly anisotropic. The M–G interactions in the $^3P_0$ state are much weaker than in the $^3P_1$ state as evidenced by their sensitivity to the host; the differences between the emission frequencies (the strongly forbidden $^1S_0 \rightarrow {}^3P_0$ absorption is not observed) of Hg atoms in Kr and Xe are 600 cm^{-1} for $^3P_0$ and 3000 cm^{-1} for $^3P_1$. The $^3P_0$–$^3P_1$ mixing induced by the M–G interaction is negligible as shown by a dramatic difference in their radiative properties [57].

A more efficient mixing of excited states is expected in the intermediate L–S coupling case. The decay processes of Ag/G centres (see section 7.2) correspond probably to this case but the interpretation of complicated relaxation paths in these systems is still uncertain.

The only study of M(P)/G centres by ESR spectroscopy was carried out for ground-state (^2P) Al and Ga atoms in Ne, Ar, Kr and Xe matrices [50]. Their spectra were analysed using the theory of the Jahn–Teller effect in ESR previously developed by Ham [149]. The spectra are completely different from those of atoms in the $^2S_{1/2}$ states; they show a pronounced anisotropy, which indicates a breakdown of the spherical symmetry of the M/G centres and its axial symmetry. The values of the gyromagnetic parameter g are intermediate between those expected for the free atom in the $L = 1$ state and the free electron; the orbital moments are thus partially but not completely quenched. The hyperfine structure of the Al/Kr spectrum assigned to the coupling with the ^{83}Kr nuclei may be fitted by assuming the existence of 5 ± 1 nearest neighbours. All these results indicate a large deformation of the MG_{18} 'cluster' due to the anisotropy of M–G interactions.

Downloaded At: 16:53 21 January 2011

5.1.3. *^2D states of M/G centres*

The ^2D excited states of Cu, Ag and Au atoms with $((n-1)d)^9(ns)^2$ configurations deviate from the spherical symmetry of their ground $((n-1)d)^{10}(ns)^1\,{}^2S_{1/2}$ states. The screening of the hole in the nd shell by the ns electrons is, however, so efficient that the interaction of the M atom with its environment is almost isotropic and its strength is entirely determined by the ns electrons as in the case of MG diatomics (section 4.1.2). In fact, the matrix shifts are nearly the same for ^2D and ^2S levels so that the spectra of $^2D \rightarrow {}^2S$ transitions are much less sensitive to the host than those of $^2P \rightarrow {}^2S$ ones (sections 5.2.2 and 7.2).

5.2. *Electronic spectra of M/G centres*

The spectra of metal atoms of groups I and II corresponding to the $ns \rightarrow np$ electron promotion have many common features and may be presented all together. Similar features are observed also in the case of the $(n-1)d \rightarrow np$ excitation, for example in that of the $((n-1)d)^{10}(ns)^1\,{}^2S_{1/2} \rightarrow ((n-1)d)^9(ns)^1(np)^1\,{}^2P_J$ excitation in atoms of group IA. In both cases, we are dealing with the transitions between a configuration with a spherical (or quasispherical) symmetry and that involving an anisotropic p orbital.

5.2.1. *Essential parameters of absorption spectra*

The spectral data for a few selected M/G systems are given in tables 14 and 15. As already mentioned (sections 2.3.2 and 5.1.1) their absorption spectra are characterized by

(i) a more or less resolved multiplet ('triplet' in most cases) structure,
(ii) large widths ($\delta\nu_{abs} \approx 100$–$400\ cm^{-1}$) of absorption bands and
(iii) large frequency shifts with respect to the positions of the lines in the free (gas-phase) atoms with a pronounced dependence on the G host.

We shall now discuss these in more detail.

(i) The structure of the absorption band due to intrinsic effects must be separated from the effects resulting from the presence of multiple sites. This may be realized either by suppression of less stable sites by annealing or by recording excitation spectra of individual fluorescence bands (for example [52]).

In a number of M/G systems the bands corresponding to a single free-atom transition are split in one site into a few (usually three) component bands separated by an interval Δ_i. This structure is either completely resolved as in the case of the Li/Xe and Na/Xe (figure 14, later) centres whereas for Li/Ar the individual transitions appear as shoulders of a single broad band [62, 63]. In several systems (such as Mg/Ne [56] and Hg/Ar [57]), only one band is observed, the splitting probably being smaller than the widths of component bands.

This structure is induced by the dynamic Jahn–Teller effect. The splitting is observed for M/G centres with the O_h symmetry in the ground electronic states (Na/Xe [146], Cu/Xe and Ag/Xe [49] centres) as evidenced by their ESR. The absence of the level splitting in the ground electronic state is a proof that this effect cannot be explained by the static crystal field. Still stronger arguments in favour of the dynamic effects are deduced from the MCD spectra with the signs and intensity ratios which cannot be fitted by the models assuming either multiple sites or crystal-field effects and are consistent with the Jahn–Teller mechanism [60–64, 136, 150].

The splitting mechanisms are, to our best knowledge, not completely elucidated. Such a splitting is expected for potential energy surfaces with multiple minima but we would also expect its strong dependence on the properties of M/G centres (strength of the M–G interaction). As can be seen in table 15, the Δ_i intervals vary little and in an erratic way. The absence of a clear dependence of Δ_i on the nature of the guest (^1P, ^2P and ^3P states; different van der Waals radii) and of the host is surprising. There is for example no significant difference between the band splitting for the Zn/Ar, Mg/Ar and Sr/Ar [136, 148] in spite of a large difference in their van der Waals radii equal to 1.35, 1.5 and 2.0 Å respectively [128]. We observe some tendency for a decrease in the average splitting in the Ar → Kr → Xe series for Zn and Cd but this rule does not hold for alkalis. Such constant values of Δ_i are still more surprising in view of the large variation in the widths of absorption bands in the same class of systems (see below).

(ii) It may be easily shown by the FLN technique (see section 2.3.2) that the width of the absorption bands is essentially homogeneous and due to the excitation of local phonons simultaneously with the electronic excitation of the M atom (phonon side band). Since the frequencies of lattice modes are a few or a few tens of reciprocal centimetres, the phonon levels form at $E_{vib} \approx V_{exc}(Q_0) - V_{exc}(Q_{exc})$ a dense quasicontinuum. The level widths of excited phonon states (determined by

Downloaded At: 16:53 21 January 2011

Table 15. Total absorption bandwidths $\delta\nu_{abs}$, total emission bandwidths $\delta\nu_{em}$ bands, partial widths $\delta\nu_{part}$ of absorption components, widths Δ_c due to cubic modes, widths Δ_{nc} due to non-cubic modes, splitting Δ_1 and Δ_2 of the absorption 'triplets' and Stokes shifts $\Delta\nu_{St}$ in a few selected systems.

M/G	$\delta\nu_{abs}$ [a]	$\delta\nu_{part}$ [b]	Δ_c	Δ_{nc}	Δ_1	Δ_2	$\delta\nu_{em}$	$\Delta\nu_{St}$	References
Li/Ar	880[a]	> 500	330	180	320	300	1050[a]	3650	[50, 60]
Li/Kr	700[a]	150–300	180	310	300	300	1030[a]	4400	[175]
Li/Xe	600[a]	50–100	180	210	340	250	1150[a]	5600	[127, 175]
Mg($^1P_1$)/Ar	815	350	380	450	205	210	485	1880	[56, 136]
Zn($^1P_1$)/Ar	1120[a]	350	$\Delta_c \ll \Delta_{nc}$		280	350	1155	2700	[52, 148]
							1640	6350	
Zn($^1P_1$)/Kr	700[a]	250	$\Delta_c \ll \Delta_{nc}$		200	240	1150	5330	[52, 148]
							1500	8470	
Zn($^1P_1$)/Xe	650[a]	200	—		175	165	NF[c]		[52]
Hg($^3P_1$)/Ar	430	NR[d]	—		NR[d]		400	710	[57]
Hg($^3P_1$)/Kr	340	NR[d]	—		NR[d]		420	800	[57]
Hg($^3P_1$)/Xe	330	≈ 100	—		100	80	1200	2950	[57]

[a] Estimated from figures in publications.
[b] Very rough estimations from unresolved band contours.
[c] NF, non-fluorescent.
[d] NR, non-resolved bands.

Downloaded At: 16:53 21 January 2011

their rapid relaxation times) are also of the order of 10 cm^{-1} so that the structure of the phonon bands cannot be resolved. The main parameters of the band are its width $\delta\nu_{abs}$ (the width $\delta\nu_{part}$ of an individual component band in the case of multiplets) and the shift with respect to the purely electronic transition: $\nu_{abs} - (\nu_{00})_{matr}$ corresponding to the average energy transferred to phonons, that is $\langle\nu_{ph}\rangle$. Both $\delta\nu_{abs}$ and $\langle\nu_{ph}\rangle$ indicate the strength of the electron–phonon coupling. ν_{abs} and $\delta\nu_{abs}$ may be directly measured but in order to determine $\langle\nu_{ph}\rangle$ we must know $(\nu_{00})_{matr}$, the frequency of purely electronic transition of the M atom in the matrix. It corresponds to the frequency of the zero-phonon line but this line is usually missing in the spectra of M/G centres.

In the absence of the zero-phonon line, this frequency may be only estimated in specific cases of the so-called mirror-image symmetry of absorption and emission bands [151]. If both bands have roughly the same contours and the Stokes shift $\delta\nu_{St} = \nu_{abs} - \nu_{em}$ is of the same order of magnitude as their widths, one can suppose that absorption and emission take place without a major change in the configuration of the centre ($Q_{exc} \approx Q_g$). In this case, the average energy transferred to phonons is the same in absorption as in emission: $\langle\nu_{ph}\rangle_{abs} = \langle\nu_{ph}\rangle_{em}$. Since $\nu_{abs} = (\nu_{00})_{matr} + \langle\nu_{ph}\rangle_{abs}$ and $\nu_{em} = (\nu_{00})_{matr} - \langle\nu_{ph}\rangle_{em}$, one can consider that the frequency of the 0–0 transition is

$$(\nu_{00})_{matr} \approx \frac{(\nu_{abs} + \nu_{em})}{2}. \tag{5.1}$$

In the absence of mirror-image symmetry the estimations of $(\nu_{00})_{matr}$ are uncertain and it seems better to use $\delta\nu_{abs}$ for the analysis of the band shapes assuming that $\langle\nu_{ph}\rangle_{abs}$ is of the same order of magnitude as $\delta\nu_{abs}$.

If the multiplets ('triplets') in absorption spectra are considered as partly overlapping but not interacting transitions to different levels of the excited state,

only the widths $\delta\nu_{part}$ of individual components have a physical meaning. They may be considered as a measure of the degree of deformation of the M/G site induced by excitation of the M atom. Unfortunately, the published absorption spectra do not contain any quantitative analysis of band contours so that our rough estimations of partial and overall bandwidths given in tables 15, 17 and 21 are deduced from published spectra in a more or less intuitive way. They show, nevertheless, a strong dependence of $\delta\nu_{abs}$ on the G host: a decrease in the bandwidth in the Ar → Kr → Xe series which may be related to a decrease in the electron–phonon coupling (σ–π effect) with increasing cavity size and initial M–G distance.

In view of the diffuse unresolved contour of the phonon band, it is not possible to learn from absorption spectrum which lattice modes are active. This information may be, however, deduced from the spectroscopic moments of absorption and MCD spectra through the Δ_c^2 and Δ_{nc}^2 parameters which represent the squares of the average values of energy transferred to cubic (totally symmetric a_{1g}) and non-cubic phonon modes (see section 2.3.3, equations (2.10) and (2.11)). The sum $\Delta_c + \Delta_{nc}$ is not always equal to $\delta\nu_{abs}$ because of the limited accuracy of measurements but we are interested rather in the Δ_c/Δ_{nc} ratio than in their absolute values. The energy of the totally symmetric modes indicates the amount of isotropic expansion or contraction of the G_n solvation shell conserving its O_h symmetry, whereas that of the non-cubic (e_g and t_{2g}) modes indicates the degree of deformation of the cell. In the case of an $ns \rightarrow np$ electron promotion we expect an anisotropic deformation of the cell resulting from the 'σ–π interaction', which is more pronounced than its isotropic expansion (contraction). In fact, the non-cubic modes contain an important (predominant in the case of Zn/G centres) part of the phonon energy.

(iii) We are interested in the medium dependence of the frequency ν_{00} of the purely electronic (0–0) transition but, as previously indicated, the observed frequency in absorption ν_{abs} is a sum: $\nu_{abs} = (\nu_{00})_{matr} + \langle\nu_{ph}\rangle$ in which the $\langle\nu_{ph}\rangle$ term which is usually not known. We are thus obliged to use $\Delta\nu_{abs} = \nu_{abs} - \nu_{gas}$ instead of $\Delta\nu_{00}$ but, since $\langle\nu_{ph}\rangle \approx \delta\nu_{abs}$ and $\delta\nu_{abs}$ varies within narrow limits, the $\Delta\nu_{abs} - \Delta\nu_{00}$ difference is not very large and nearly constant.

The dependence of $\Delta\nu_{abs}$ on the matrix is given for several selected transitions in table 14. $\Delta\nu_{abs}$ decreases systematically in the Ar → Kr → Xe series (as already discussed in section 5.1.1) but all attempts to represent this dependence by simple functions of matrix parameters were rather unsuccessful; the linear dependence of $\Delta\nu_{abs}$ on the polarizability α of the host [152] or on α/r_{vdW} (M) (where r_{vdW} (M) is the van der Waals radius of the guest) [148] is observed only for limited number of M atoms. In any case, such a dependence on a single parameter cannot be expected because the $\Delta\nu_{abs}$ frequency shift is a sum of two independent effects:

(*a*) the short range repulsive interaction which decreases when the vacancy radius increases and

(*b*) the long range attractive interaction which increases with increasing host polarizability.

The addition of both effects implies a better stabilization of the excited atom in the heavy gas so that for a number of M atoms we have $\Delta\nu_{abs} > 0$ for Ar and Kr matrices and $\Delta\nu_{abs} < 0$ in xenon.

Downloaded At: 16:53 21 January 2011

The dependence of $\Delta\nu_{abs}$ on the properties of the excited state of the M atom appears also in the data of the tables 14 and 15. The values of $\Delta\nu_{abs}$ and their host dependence are similar for $^1P_1 \leftarrow {}^1S_0$ transitions in Zn, Cd and Hg whereas this effect is reduced for the $Hg(^3P_1) \leftarrow Hg(^1S_0)$ transition. As previously discussed, the anisotropy of the excited atom is stronger in the $^1P_1$ than in the $^3P_1$ state so that the difference between equilibrium configurations of the ground and excited states is more pronounced in the former than in latter case.

The difference between $^2P_{3/2}$ and $^2P_{1/2}$ states of Ag and Au atoms is also related to the difference in the shape of the mixed $\sigma + \pi$ orbitals of the $\Omega = \frac{1}{2}$ and $\Omega = \frac{3}{2}$ states.

5.2.2. *Fluorescence spectra and lattice relaxation effects*

The fluorescence spectra are reported only for a limited number of systems (table 15). Several M/G centres are not fluorescent because of a rapid non-radiative relaxation (see section 6).

The essential parameters characterizing the evolution of the excited M*/G centre during its lifetime is the fluorescence-to-absorption shift (the Stokes shift $\Delta\nu_{St} = \nu_{abs} - \nu_{em}$) and the width $\delta\nu_{em}$ of the emission band (figure 11). As previously discussed, the 'vertical' transition in absorption prepares the excited centre in the Franck–Condon ($Q = Q_g$) configuration which may not correspond to its energy minimum Q_{exc} so that $\nu_{abs} = (\nu_{00})_{matr} + \langle\nu_{ph}\rangle_{abs}$. The relaxation of the cage takes place on a picosecond time scale so that the fluorescence is emitted from the thermally equilibrated centre with the $Q = Q_{exc} \neq Q_g$ configuration towards higher vibrational (phonon) levels of the ground-state surface. As in absorption, a part of the energy $\langle\nu_{ph}\rangle_{em}$ is transferred to phonons so that the emission frequency is $\nu_{em} = \nu_{00} - \langle\nu_{ph}\rangle_{em}$. The Stokes shift

$$\Delta\nu_{St} = \nu_{abs} - \nu_{em} = \langle\nu_{ph}\rangle_{abs} + \langle\nu_{ph}\rangle_{em}$$

is thus equal to the sum of energies transferred to phonons in absorption and emission transitions. $\langle\nu_{ph}\rangle_{em}$ increases with increasing difference between the shapes of the ground and excited surfaces and the width $\delta\nu_{em}$ of the emission band, which is roughly proportional to the slope of the ground surface at $Q \approx Q_{exc}$, has a similar behaviour. If the ground-state energy surface may be approximated by a parabola (or paraboloid), $\langle\nu_{ph}\rangle_{em} = V_g(Q_{exc}) - V_g(Q_g) \approx (Q_{exc} - Q_g)^2$ and $\delta\nu_{em} = (\partial V_g/\partial Q)_{Q_g} \approx (Q_{exc} - Q_g)$ are correlated in a simple way.

In the spectra of large molecules in fluid or solid solutions with unresolved vibrational structures, we observe, as already mentioned, the so-called mirror-image symmetry of absorption and emission spectra: similar shapes and widths of bands ($\delta\nu_{em} \approx \delta\nu_{abs}$) and a 'normal' Stokes shift $\Delta\nu_{St}$ of the same order of magnitude as $\delta\nu_{abs}$ [151]. Such a behaviour, which indicates that the equilibrium configuration of the A/X centre is nearly the same in the ground and excited state, is typical for molecules weakly interacting with their medium. An 'anomalously large' Stokes shift is observed for molecules showing a drastic change in the dipole moment or the proton transfer in the excited state.

In contrast with molecules, the mirror-image symmetry and 'normal' Stokes shifts are rather an exception in the case of M/G centres. Very narrow emission bands correspond to transitions between electronic states in which the M–G interaction and the configuration of the centre are nearly the same. As already mentioned, the M–G interactions in ^2S, namely $(n\mathrm{d})^{10}((n+1),\mathrm{s})^1$, and in ^2D, namely $(n\mathrm{d})^9((n+1)\mathrm{s})^2$ states of group IA atoms, are similar. In fact, the bands assigned to the $^2D \rightarrow {}^2S$ forbidden

Downloaded At: 16:53 21 January 2011

transition in Cu/G and Au/G centres are significantly narrower ($\delta\nu \approx 90$ cm^{-1}) [81] than those of the $^2P \rightarrow {}^2S$ emission ($\delta\nu \approx 1000$ cm^{-1}) of Ag/Ar [74, 135] and Cu/Ne [79]. The narrowest band observed for metal atom in matrices ($\delta\nu \approx 30$ cm^{-1}) is that of the forbidden intramultiplet $^2D_{3/2} \rightarrow {}^2D_{5/2}$ transition in Au/G centres involving two nearly identical configurations [81]. The Stokes shift is also anomalously small in the case of the $^2D \leftrightarrow {}^2S$ transitions in Ag/Ar: ν_{abs} (determined by a two-photon fluorescence excitation) amounts to 30 815 cm^{-1} while $\nu_{em} = 30\,675$ cm^{-1} and hence $\Delta\nu_{St} = 140$ cm^{-1} [153]. Absorption frequencies of forbidden $^2S \rightarrow {}^2D$ transitions of Cu/G and Au/G centres are not known so that the values of the Stokes shift cannot be determined but the gas-to-matrix shifts of emission bands are exceptionally small ($\Delta\nu_{em}$ is in the 30–250 cm^{-1} range).

The $\delta\nu_{em} \approx \delta\nu_{abs}$ and $\Delta\nu_{St} \approx \delta\nu_{abs}$ relations are respected only in the Hg($^3P_1$)/Ar and Hg($^3P_1$)/Kr cases [57] and, to some extent, in those of Zn($^1P_1$)/Ar [52] and Cd($^1P_1$)/Ne [71] centres. The 'normal' Stokes shift in these systems indicates that the Q_g and Q_{exc} configurations are not very different (figure 11(*a*)) but already for Zn($^1P_1$)/Kr and Hg($^3P_1$)/Xe we have $\Delta\nu_{St} \gg \delta\nu_{abs} + \delta\nu_{em}$ and $\delta\nu_{abs} \ll \delta\nu_{em}$.

The 'anomalously large' Stokes shift observed for the majority of M/G centres is a signature of a large difference between equilibrium configurations of the ground and excited states (Q_g) and (Q_{exc}) but it does not contain any direct information about the $V_{exc}(Q_g) - V_{exc}(Q_{exc})$ energy difference (figure 11(*b*)). Also it does not contain any information about the geometry of the equilibrium configuration in the excited state of the M/G centre. One can guess from what we know about the 'σ–π interactions' that the symmetry of the MG_{18} 'cluster' is lowered so that one can expect a breakdown (or softening) of the selection rules for emission from the Q_{exc} configuration. However, no data showing a difference between oscillator strengths in absorption and emission are available.

In several cases, the emission spectrum is composed of two well resolved bands (figure 3). Such a behaviour was observed for the first time for Na in different matrices [131] and then for Ag/G [78, 79] (this case will be treated in section 7), Hg($^1P_1$)/Ar and Hg($^1P_1$)/Kr [137]. It was shown in the latter case that the intensity ratio of two emission components depends on the way the $^1P_1$ level was populated: by direct excitation or by recombination $Hg^+ + e$. The origin of this doublet was elucidated in the Zn($^1P_1$)/G case [52, 154]; two emission bands correspond to two different potential energy minima populated at the sub-nanosecond time scale from the initially prepared Franck–Condon configuration. It has been shown that the intensity ratio of the 'red' to 'blue' emission component increases in a reversible way with temperature and that the emission of the 'red' form builds up with a delay suggesting that this state is populated by two channels: a direct (Franck–Condon) $\rightsquigarrow$ 'red' and indirect (Franck–Condon) $\rightsquigarrow$ 'blue' $\rightsquigarrow$ 'red' relaxation. The data have been fitted by a model of the 'blue' $\rightsquigarrow$ 'red' transition through a potential energy barrier of 40 cm^{-1} for Zn/Kr and 130 cm^{-1} for Zn/Ar with a temperature-dependent rate. The barrier height of 380 cm^{-1} calculated using the cluster model (see below) is too high but of a good order of magnitude.

In the absence of information about the equilibrium configurations of excited M/G centres, computer simulation based on good knowledge of M*–G potentials and taking into account all coordinates of the system would be of the greatest interest. Such a programme has not been undertaken up to now and it would probably necessitate more refined potentials; the model assuming the additivity of two-body terms seems to be too crude for reliable calculations.

Downloaded At: 16:53 21 January 2011

Several attempts have been made in order to describe the behaviour of observed systems by simple models taking into account a limited number of coordinates. The present authors in one of their early papers [57] treated the case of Hg/G (G = Ar, Kr or Xe) centres. The validity of two-body potentials was assumed and only the Hg atom was allowed to move within the rigid G_{18} frame. It has been shown that in the system in which the equilibrium distance in the excited Π state of the HgG complex is shorter than the Hg–G distance in the Hg/G centre, the energy minimum corresponds to the Hg atom approaching closely one of G atoms. Similar results may be obtained by deformation of the $G_1 \ldots G_4$ square to a rhombus with a decrease of two M–G distances and an increase in the two other distances. Such deformations imply a breakdown of the fourfold symmetry of the site: the $D_{4h} \rightarrow C_{2v}$ transition in the former and $D_{4h} \rightarrow D_{2h}$ transition in the latter case. Among the Hg/G centres, this condition is fulfilled only for Hg/Xe and Hg/CH_4 [155]. Calculations of the same type lead to the same conclusions in the case of the Na/Ar system [145].

A more refined model was recently proposed for the $Zn(^1P_1)/G$ systems taking into account two possible deformations: symmetric contraction of the G_4 shell (called by the authors 'waist vibrational mode') and displacement of the M atom along the *n*p orbital axis ('body mode') [52, 147, 156]. The scope of this treatment was to explain the presence of two well separated bands in the fluorescence spectra of $Zn(^1P_1)/Ar$ and $Zn(^1P_1)/Kr$. On the basis of calculations carried out for a finite $ZnAr_n$ cluster, two minima were assigned respectively to the configuration with the compressed G_4 shell (the 'blue' form) and to the Zn atom displaced to the interstitial site with a simultaneous displacement of one Ar atom (the 'red' form).

A more complete treatment has been applied to the study of the 'lattice' relaxation in a large mixed rare-gas cluster $XeAr_n$ following excitation of the Xe atom to the Rydberg state [157, 158] (see section 7.5) but this case is simpler, the M*–G potential being isotropic for the M atom in the Rydberg state.

It seems possible to undertake now calculations of equilibrium configurations of excited M*/G centres (and of their M^*G_n models) followed by the study of lattice relaxation processes using molecular dynamics techniques. The best object for such studies would be the system involving the M atom with a simple electronic structure and weakly polarizable host such as the Li/Ne centre and $LiNe_n$ cluster.

Downloaded At: 16:53 21 January 2011

6. Radiative and non-radiative transitions

6.1. *General remarks*

We are interested here in the effects of the M–G interactions on the radiative and non-radiative transitions in a metal atom involved in an MG complex or in an M/G centre. The $\Delta L = \pm 1$, $\Delta J = 0, \pm 1$ ($J = 0 \leftarrow|\rightarrow J = 0$), $\Delta S = 0$ selection rules for radiative transitions that are valid in the central field of a free or only slightly perturbed (Hund's case c) M atom will be modified in a diatomic MG complex of axial ($C_{\infty v}$) symmetry. In Hund's case a only $\Lambda = |L_z|$ and $\Omega = |J_z|$ are good quantum numbers so that selection rules are $\Delta\Lambda = 0, \pm 1$, $\Delta\Omega = 0, \pm 1$. In the intermediate case, the degree of conservation of the atomic selection rules indicates the strength of the M–G perturbation.

In a highly symmetric (O_h) ground state of an M/G centre, J is still a good quantum number and even the orbital moment is not completely quenched (see sections 5.1 and 5.2). One can expect $\Delta J = 0, \pm 1$ and even the $\Delta L = \pm 1$ rule to be valid in absorption. However, if the emission takes place from a configuration of lower

symmetry, the rigidity of atomic selection rules may be attenuated. This effect may be described in terms of the mixing of states allowing the 'intensity borrowing' from allowed transitions.

The rate of the non-radiative relaxation between different excited and ground states of molecular systems, when allowed by symmetry, is determined to a large extent by interstate energy gaps ΔE. A common feature of MG and M/G systems is that their bonding energies are small compared with the energy gaps. As a rule, the energy of the $v = 0$ level of the second excited state (M**G) is higher than the dissociation threshold of the first excited (M*G) state. The M**G–M*G coupling is weak because of a small overlap between vibrational functions of the bound M**G state and the M* + G dissociation continuum and rapidly decreases with increasing ΔE. In the same way, the energy minimum of the M**/G state in the matrix is isoenergetic with a dense continuum of high M*/G levels. According to the energy gap law [159], the coupling strengths and relaxation rates decrease exponentially with the number of phonons necessary to fill the M**/G–M*G gap. In view of the low frequencies of accepting phonon modes ($\nu_{ph} \approx 20$–50 cm^{-1}), the relaxation rate becomes negligibly low for large ΔE values.

In fact, the non-radiative relaxation rates of excited M**G and M**/G states are often so low that their decay times are close to the radiative lifetimes of free M atoms (corrected in the case of matrices for the refractive index of the medium). A rapid electronic M** $\rightsquigarrow$ M* relaxation may be expected only in the case of an intersection (or quasi-intersection) of their potential energy surfaces. One can also expect an acceleration of the M** $\rightsquigarrow$ M* process in presence of intermediate M´ levels ($E_{M^{**}} > E_{M'} > E_{M^*}$) so that the energy gap in each (M** $\rightsquigarrow$ M´ and M´ $\rightsquigarrow$ M*) step is smaller than in the M**–M* step. This pathway may be more efficient than the direct pathway even when the M** $\leftrightarrow$ M´ and M´ $\leftrightarrow$ M* coupling is weak.

We shall apply this point of view to the analysis of actually available and still fragmentary data concerning:

(*a*) forbidden transitions in absorption (fluorescence–excitation) spectra of Ag [65] and Al [99] in jet-cooled complexes and of Ag [78, 132, 135], Pd [127] and Ca [160] in rare-gas matrices,
(*b*) the singlet–triplet (^{1}P $\rightsquigarrow$ ^{3}P) relaxation of group II and IIA atoms (Mg, Zn, Cd and Hg) in complexes [32, 33, 39, 56, 91, 93] and matrices [58, 70, 71, 137, 147, 154] investigated also by theoretical methods [40, 125, 126, 161],
(*c*) radiative and non-radiative transitions between ^{2}P, ^{2}D and ^{2}S states of Cu, Ag and Au atoms in rare-gas matrices [78–81, 135, 153, 162] and
(*d*) the intramultiplet relaxation within the ^{3}P state of Hg in complexes [37, 163] (see [161] for theory) and matrices [57] and the $^2D_{3/2} \rightarrow {}^2D_{5/2}$ and $^2P_{3/2} \rightarrow {}^2P_{1/2}$ transitions of Au [81] and Tl [70].

6.2. *Forbidden transitions in absorption*

The mixing of *n*p (*ungerade*) with *n*s and *n*d (*gerade*) orbital functions, strictly forbidden in free atoms, may occur when the inversion symmetry of the M atom is broken by the M–G interaction. This effect was observed for Rydberg transitions in the AlAr and AlKr jet-cooled complexes [99], in which several lines are assigned to 4f $\leftarrow$ 3p, 5f $\leftarrow$ 3p and 6p $\leftarrow$ 3p transitions induced by the contamination of 3p or *n*f atomic orbitals by corresponding d orbitals. The redistribution of the oscillator strength of allowed transitions among a number of forbidden transitions was also

Downloaded At: 16:53 21 January 2011

observed for Pd [127] and Cu [132] atoms in matrices. In the same way, the absorption and MCD spectra of Cu and Ag in Ar, Kr and Xe matrices corresponding to the $4p \leftarrow 3d$ transitions in the $\nu = 40000$–$56000\ cm^{-1}$ range contain several features absent in the spectra of free atoms [79, 162]. The spectra may be correlated with those of free atoms [164] by assuming an extended mixing of states differing by their L, S and even J quantum numbers [132].

The mixing of states is obviously more efficient in the case of densely spaced levels but the assignments of such complicated spectra with overlapping bands are not always unambiguous. Detection of forbidden transitions in simple, well resolved spectra is therefore of special interest.

Such a transition forbidden by the $\Delta L = \pm 1$ rule was found in the excitation spectrum of the $Ca(^3P) \rightarrow Ca(^1S)$ phosphorescence in Ar matrices [160]. It contains, besides a strong $23698\ cm^{-1}$ band of the $^1P \leftarrow {}^1S$ transition ($23652\ cm^{-1}$ in the gas phase), a weaker narrow line at $22188\ cm^{-1}$ assigned to the $^1D \leftarrow {}^1S$ transition expected in the free atom at $21849\ cm^{-1}$. Its oscillator strength is obviously due to the $^1P \leftrightarrow {}^1D$ mixing favoured by a small energy gap between the two levels. The structure of the Ca/Ar site is not known but it seems plausible to assume a multisubstitution site with a symmetry lower than O_h. The intensity ratio of the forbidden to the allowed transitions is not known and the radiative lifetime of the ^1D level could not be determined because of its rapid non-radiative relaxation.

The perturbation of the allowed $^2\Pi_{3/2} \leftarrow {}^2\Sigma_{1/2}$ transition (correlated to the atomic $^2P_{3/2} \leftarrow {}^2S_{1/2}$) in the fluorescence excitation spectrum of the jet-cooled AgAr complex is due to the coupling of the $^2\Pi_{3/2}(^2P_{3/2})$ state to a state correlated to the atomic $^2D_{5/2}$ state (probably a $^2\Pi_{3/2}$ state). From the shift of the perturbed levels, the electronic coupling matrix element may be estimated as $V_{el} = 20 \pm 5\ cm^{-1}$, indicating the breakdown of the symmetry of the Ag atom in the AgAr complex [65]. This result is of interest in view of the role of the D states in the decay of $^2P_{1/2,3/2}$ states of Ag in matrices (section 7.2).

Downloaded At: 16:53 21 January 2011

6.3 *Singlet–triplet relaxation*

The dependence of the $^1P_1 \rightsquigarrow {}^3P_J$ intersystem crossing rates k_{ST} of MG complexes and M/G centres (where M = Mg, Zn, Cd or Hg) on the nature of the G partner illustrates more general rules concerning relaxation mechanisms of weakly bound systems. The $^1P_1$ states of unperturbed M- atoms decay by the $^1P_1 \rightarrow {}^1S_0$ radiative transition with a rate of the order of $10^9\ s^{-1}$. This implies that an MG (M/G) system excited to the $^1P_1$ state will show a strong fluorescence provided that the intersystem crossing rate k_{ST} does not exceed $10^9\ s^{-1}$. In contrast with this, the fluorescence is completely quenched for $k_{ST} \gg 10^9\ s^{-1}$. Note that the relative populations of final ^3P_J levels may be determined in the case of MG complexes by the laser-induced fluorescence from the metastable ^3P_J atoms and in that of the matrix, by recording the long-lived $^3P_J \rightarrow {}^1S_0$ emission.

In the MG complexes the decay of the $C\ ^1\Pi_1$ state correlated to the $^1P_1$ state of the atom is purely radiative with a negligible yield of the ^3P_J atoms in the case of MgAr, MgXe [92, 93], ZnAr [91], CdNe, CdAr and CdKr [39] complexes. HgNe, HgAr, HgKr and HgXe complexes are strongly fluorescent and the yield of Hg ^3P_J atoms is weak if any [94]. On the other hand, the ZnXe and CdXe complexes are not fluorescent (the lifetime of the $C\ ^1\Pi_1$ state being of the order of a few picoseconds). The predissociation of the excited complex yields metal atoms in metastable ^3P_J states, uniquely in the $^3P_2$ state in the case of Cd while for Zn the concentration ratio $[^3P_2]/[^3P_1]$ is of the order of 10 [32, 33].

The M($^1P_1$)/G centres in matrices (where M = Mg, Zn, Cd or Hg) show a similar dependence on the rare gas host [52, 56, 58, 71, 137, 147]; in Ar matrices all M/G centres decay by the prompt $^1P_1 \rightarrow {}^1S_0$ fluorescence which indicates that $k_{ST} \ll 10^9\ s^{-1}$. In Kr matrices, besides the singlet state emission ($\tau \approx 1$ ns), the emission from the ^3P_J state with a long decay time of 9 ms is observed for Mg/Kr [56]. The long-lived phosphorescence (lifetime longer than 1 μs) was observed also for Zn/Kr [52] and Cd/Kr [71]. The rate of the $^1P_1 \rightsquigarrow {}^3P_J$ relaxation is low because no significant shortening of the $^1P_1$ decay time is observed. In the Hg/Kr system, the relaxation is as selective as in the CdXe complex and populates uniquely the $^3P_2$ level decaying by the long-lived $^3P_2 \rightarrow {}^1S_0$ emission [58]. In all M/Xe centres, the $^1P_1 \rightarrow {}^1S_0$ fluorescence is entirely quenched and only the $^3P_J \rightarrow {}^1S_0$ emission is observed. In the case of Hg the $^3P_2$ and $^3P_1$ levels are populated but the decay time of the $^3P_1 \rightarrow {}^1S_0$ emission, much longer than the intrinsic lifetime of the $^3P_1$ level, indicates that the relaxation corresponds to a sequential process: $^1P_1 \rightsquigarrow {}^3P_2 \rightsquigarrow {}^3P_1$ with a rapid $^1P_1 \rightsquigarrow {}^3P_2$ and slow $^3P_2 \rightsquigarrow {}^3P_1$ step so that the $^3P_2 \rightarrow {}^1S_0$ emission is still observed [58].

It is surprising that the relaxation rate depends so strongly on the rare gas while it is almost independent of metal atom in spite of drastically different values of the spin–orbit coupling constant (from 40 cm^{-1} for Mg to 4265 cm^{-1} for Hg). It is, therefore, impossible to correlate the observed differences with the values of the electronic singlet–triplet coupling constants V_{ST}. On the other hand, the difference between the $^1P_1$–$^3P_2$ and $^1P_1$–$^3P_1$ energy gaps are not large enough for Cd or Hg to explain the selective population of the $^3P_2$ states.

An alternative explanation was proposed in an early work by Breckenridge and Malmin [165] and developed in further studies by Breckenridge and co-workers [40, 93, 125, 126]. In view of a strong dependence of the intersystem crossing rate on the energy difference between potential energy surfaces predicted by the energy gap law (see above), the singlet–triplet relaxation should be efficient only in the case of a crossing of the singlet surface with that of one of the triplet states issued from the ^3P_J states (figure 12). The analysis of the potential curves of MG complexes suggests as the most probable event a crossing of the curve of the strongly bound C $^1\Pi_1$ state with the $^3\Sigma_1$ repulsive state correlated to the $^3P_2$ atomic state. In order to be efficient for the $^1P_1 \rightsquigarrow {}^3P_2$ transition, the crossing must occur below the dissociation limit of the C $^1\Pi_1$ state and in the energy range accessible in a 'vertical' transition from the ground state. The probability of the crossing increases in the Ne → ... → Xe series since the strength of the M*–G bond (the depth of the energy minimum) in the C $^1\Pi_1$ state increases whereas the shape of the repulsive curve of the $^3\Sigma_1$ (calculated by *ab initio* methods or estimated from experimental data) become more repulsive. This model is consistent with experimental data obtained for 1:1 complexes and explains well the reasons for the selective population of the $^3P_2$ state by deactivation of the $^1P_1$ level in ZnXe and CdXe complexes. It explains also qualitatively the relaxation of Hg/Kr and Hg/Xe centres in matrices and may be extended to other types of relaxation process (see below).

More recently, this model was applied to small MG_n clusters [125] and to larger clusters and matrices [126]. It has been shown that the main trends of processes occurring in matrices may be reproduced but the results of computations were extremely sensitive to the details of the M*–G potential. Unfortunately, the accuracy of computed repulsive M*–G potential energy curves (non-accessible to any experiment) is difficult to appreciate. No experimental data for small clusters, allowing a direct comparison with calculations, are actually available.

Downloaded At: 16:53 21 January 2011

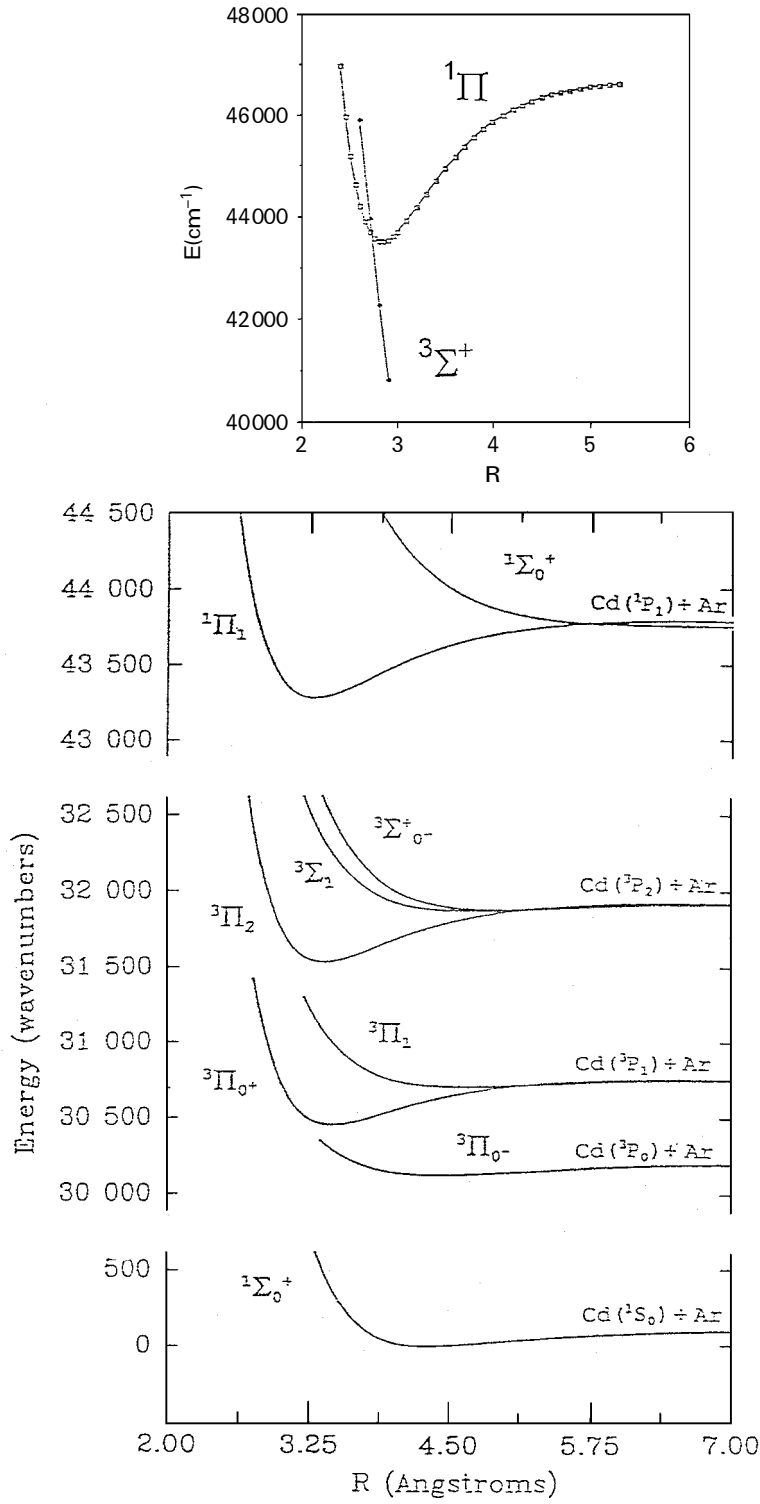

Figure 12. For legend see opposite.

Downloaded At: 16:53 21 January 2011

Table 16. Energies of the lowest excited states of the free metal atoms of group IA.

Atom	Energy (cm^{-1})			
	$^2P_{1/2}$	$^2P_{3/2}$	$^2D_{5/2}$	$^2D_{3/2}$
Cu	30535	30784	11202	13245
Ag	29552	30472	30242	34714
Au	37358	41174	9161	21435

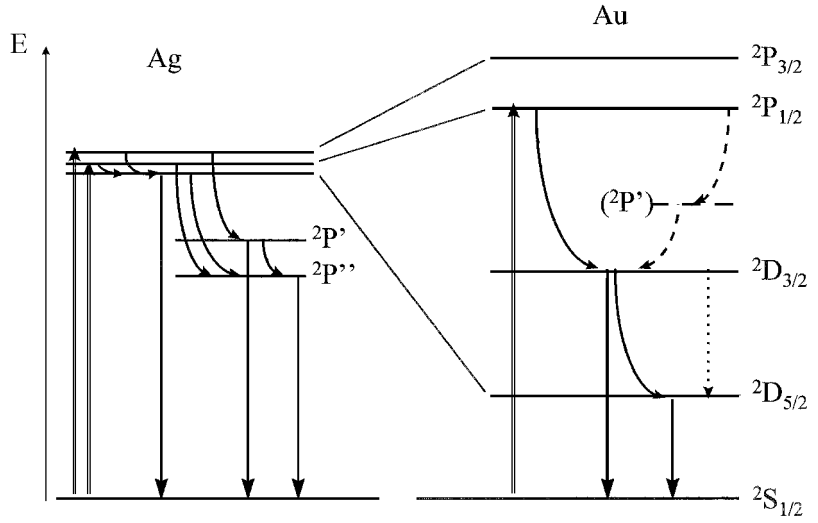

Figure 13. Scheme of radiative and non-radiative transitions between ^2P, ^2D and $^2P'$ (I, II and III) levels of Ag/G and Au/G centres.

6.4. $^2P \leftrightarrow {}^2D$ *coupling effects*

Specific properties of the Cu/G, Ag/G and Au/G systems are due to the presence of the $^2D_{5/2}$ and $^2D_{3/2}$ atomic states below (in Cu and Au) or in a quasiresonance (in Ag) with $^2P_{1/2}$ and $^2P_{3/2}$ states involved in the resonance $^2P_{1/2,3/2} \leftrightarrow {}^2S_{1/2}$ ($np \leftrightarrow ns$) transitions. The different behaviour of Cu and Au as compared with Ag is related to this difference between their ^2P–^2D energy gaps (table 16 and figure 13).

The fluorescence of Au atoms excited to the $^2P_{1/2}$ state is completely quenched in all rare-gas matrices. The observed emission spectrum corresponds to the $^2D_{3/2} \rightarrow {}^2S_{1/2}$ and $^2D_{5/2} \rightarrow {}^2S_{1/2}$ forbidden transitions slightly shifted with respect to their gas-phase frequencies with the lifetimes of about 0.25 and 1.5 ms respectively (the $^2D_{3/2} \rightarrow {}^2D_{5/2}$ intramultiplet transition is also observed) [80, 81]. The absence of the allowed, short lived $^2P \rightarrow {}^2S$ fluorescence shows that the $^2P \rightsquigarrow {}^2D$ relaxation is rapid ($k_{rel} > 10^{10}$ s^{-1}) in spite of the large gap between the ^2P and ^2D levels.

A similar behaviour was observed for Cu atoms in Ar, Kr and Xe matrices yielding the narrow-band emission spectra, $^2D_{3/2} \rightarrow {}^2S_{1/2}$ and $^2D_{5/2} \rightarrow {}^2S_{1/2}$ with small gas-to-

Figure 12. Scheme of molecular states correlated to the $^1P_1$ and $^3P_1$ levels of the atoms of group II metals (bottom) and (top) calculated shapes of C $^1\Pi_1$ and $^3\Sigma_1$ potential energy curves of CdAr showing their crossing in the vicinity of the minimum of the C $^1\Pi$ state. (From [40].)

Downloaded At: 16:53 21 January 2011

matrix shifts and non-exponential decay curves containing 1–20 ms components [81]. On the other hand, in the Ne matrix the emission spectrum contains, besides the $^2D_{3/2} \rightarrow {}^2S_{1/2}$ and $^2D_{5/2} \rightarrow {}^2S_{1/2}$ bands (almost unshifted from the gas phase: $\Delta\nu_{m-g} = +8$ and $-15\ cm^{-1}$ respectively) a broad ($\delta\nu \approx 1800\ cm^{-1}$) band shifted by about $3400\ cm^{-1}$ with respect to the $^2P_{1/2} \leftarrow {}^2S_{1/2}$ absorption band [79]. Its decay time of 6.9 ns, nearly the same as that of the Cu atom $^2P_{1/2}$ state in the gas phase, $\tau = 7.3$ ns, indicates that the $^2P \rightsquigarrow {}^2D$ relaxation rate does not exceed $1.5 \times 10^7\ s^{-1}$.

It is known from the spectrum of AgAr complex (see above section 6.2 [65]) that the coupling between the $^2\Pi_{3/2}$ states correlated to $^2P_{3/2}$ and $^2D_{5/2}$ states of the Ag atom is strong. One can thus suppose that the P–D coupling in Cu and Au is also very strong. Nevertheless, a relaxation rate as rapid as $k_{rel} > 10^{10}\ s^{-1}$ is surprising in view of the large energy gap between ^2P and ^2D states. It may be tentatively explained by assuming a deep energy minimum in the ^2P state (even more pronounced than in the case of Ag), inducing a crossing with the shallow ^2D surfaces. The reduction of the relaxation rate for Cu in Ne is consistent with this explanation and with the model of Breckenridge and co-workers (the depth of minimum in the ^2P states is smaller in Ne than in other hosts).

It is interesting to note that upon the excitation of higher levels of the Cu/Ne centre in the $46800\ cm^{-1}$ range corresponding to the $(3d)^9(4s)^1(4p)^1 \leftarrow (3d)^{10}(4s)^1(^2P \leftarrow {}^2S)$ transitions, the same $^2P \rightarrow {}^2S$ emission spectrum is observed but with an approximately 8 ns rise time and an apparent decay time of 50 ns. The 8 ns time is obviously that of decay while the 50 ns component indicates that the ^2P emitting level is populated by an indirect relaxation path from the initially excited $(3d)^9(4s)^1(4p)^1$ to the emitting $(3d)^{10}(4p)^1$ level involving a long-lived intermediate state. This state may be tentatively identified as one of higher D levels with the $(3d)^9(4s)^1(4p)^1$ configuration [79, 132].

A detailed discussion of complicated relaxation paths of Ag/G centres is delayed to section 7.2. We shall stress only the role of transitions between the $^2P_{3/2}$, $2P_{1/2}$ and $^2D_{5/2}$ quasiresonant states [78, 79, 135, 153]. Each of them may be selectively excited by one-photon ($^2P \leftarrow {}^2S$) or two-photon ($^2D \leftarrow {}^2S$) absorption. Upon the excitation of the highest ($^2P_{3/2}$) level, the fluorescence spectrum is composed of a prompt, strongly red-shifted $^2P \rightarrow {}^2S$ fluorescence and of a narrow-band $^2D_{5/2} \rightarrow {}^2S_{1/2}$ emission with a 1.8 μs lifetime. This lifetime, shorter by one order of magnitude than that of the $^2D_{5/2}$ levels of Cu and Au, indicates a further non-radiative relaxation of the $^2D_{5/2}$ level with a rate of the order of $5 \times 10^5\ s^{-1}$. The presence of a long ($\tau \gg 200$ ns) component in the decay of the ^2P fluorescence shows that low levels of the ^2P state are populated through this channel. Such a 'reversible' $^2P \rightsquigarrow {}^2D \rightsquigarrow {}^2P$ relaxation path is surprising.

6.5. *Intramultiplet relaxation*

The radiative transitions between different components of a multiplet are strictly forbidden in the electric dipole approximation in atoms and molecules. The experiment shows that non-radiative processes are also inefficient in MG complexes and M/G centres.

The $^2D_{3/2}$ level of Cu atoms in rare-gas matrices has a decay time of the order of 1 ms in spite of a small $^2D_{3/2}$–$^2D_{5/2}$ energy gap of about $2000\ cm^{-1}$. For Au atoms, with a larger gap of about $12000\ cm^{-1}$, the relaxation is so inefficient that the weak line corresponding to the $^2D_{3/2} \rightarrow {}^2D_{5/2}$ radiative transition with the 0.25 ms decay time is observed in all rare-gas hosts [81]. The radiative transitions are observed also between the $^2P_{3/2}$ and $^2P_{1/2}$ (X1 and X2) components of the ground state of T1 atom in Ar, Kr and Xe matrices when the X2 state is populated from the Rydberg $^2S_{1/2}$ state (the decay

Downloaded At: 16:53 21 January 2011

time of this emission and the lifetime of the X2 state have not been reported) [160]. Note that the $^2P_{3/2} \rightarrow {}^2P_{1/2}$ radiative transition may borrow its intensity from the allowed $^2P_{3/2} \rightarrow {}^2S_{1/2}$ in view of the $^2P_{1/2}$–$^2S_{1/2}$ mixing allowed by the reduced symmetry of the site. The $^2D_{3/2}$–$^2P_{3/2}$ mixing in the Au case is much less efficient.

The problems of the intramultiplet relaxation between the states correlated to the ^3P_J atomic states have been studied in a detailed way for Hg in complexes and matrices. A better understanding of its mechanism was attained by extending the list of complex partners and hosts to small molecules such as CH_4, CF_4 and N_2.

In HgG complexes [36, 109] and Hg/G centres [57] (G = Ne, Ar, Kr or Xe) the rate of the non-radiative $^3P_1 \rightsquigarrow {}^3P_0$ relaxation is so low that the decay time of the $^3P_1 \rightarrow {}^1S_0$ fluorescence is the same as the radiative lifetime of the free atom (corrected in matrices for the refractive index of the medium). The intensity of the $^3P_0 \rightarrow {}^1S_0$ emission induced in matrices by the $^3P_1 \rightsquigarrow {}^3P_0$ relaxation is negligible. The $^3P_2 \rightsquigarrow {}^3P_1$ relaxation is also extremely inefficient in Kr matrices so that the $^3P_2$ state decays by the forbidden $^3P_2 \rightarrow {}^1S_0$ emission with 220 ms decay time. This process is accelerated but still very slow in the Xe matrix [58].

The rates of the intramultiplet transitions are strongly enhanced when the symmetry of the complex is lowered by interaction with a molecule of a lower symmetry. The key experiment was a study of the fluorescence excitation spectrum of the linear $Hg \cdot N_2$ complex, conserving the $C_{\infty v}$ symmetry of a diatomic in its vibrationless level [36, 37, 161, 163]. When the complex is excited to the vibrationless level of the 0^+ state or to vibronic levels involving only the Hg–N_2 stretching mode, its fluorescence lifetime remains equal to that of the Hg atom. On the other hand, upon the excitation of the bending mode which implies a deviation from the linear configuration, the complex lifetime is reduced by the $^3P_1 \rightsquigarrow {}^3P_0$ ($0^+ \rightsquigarrow 0^-$) relaxation followed by dissociation of the weakly bound 0^- state. In this system, the non-radiative rates do not exceed 10^8 s^{-1} but in Hg complexes with molecules of lower symmetry such as the H_2O the nonradiative process is so rapid that the fluorescence is entirely quenched [166]. The $^3P_1 \leftarrow | \rightarrow {}^3P_0$ selection rule is related to the symmetry of the system as shown by the analysis of the coupling patterns within the ^3P multiplet [161]. The same scheme may be applied to Hg atoms in matrices; the lifetime of the $^3P_1$ level of Hg is reduced from 60 to 5 ns in a CF_4 matrix (non-cubic monoclinic lattice) with the appearance of a strong $^3P_0 \rightarrow {}^1S_0$ emission [167]. In N_2 matrices with the S_6 site symmetry, the $^3P_1 \rightsquigarrow {}^3P_0$ relaxation takes place on the subnanosecond time scale so that the emission from the $^3P_1$ state is entirely quenched. The relaxation on the subnanosecond time scale is observed also in mixed Kr–N_2 matrices for Hg atoms having at least one nitrogen molecule as the nearest neighbour [168–171]. The rapid relaxation is observed also for $Hg \cdot H_2O$ and $Hg \cdot NH_3$ pairs in rare-gas matrices doped with small quantities of water or ammonia [172].

The available data concerning the intramultiplet non-radiative transitions between $^2P_{1/2}$ and $^2P_{3/2}$ or $^2D_{3/2}$ and $^2D_{5/2}$ states of the metal atoms of group IA and III are fragmentary. More data and a general theory of environment-induced transitions between sublevels of atomic multiplets in MG and M/G systems would be of the greatest interest.

7. Selected M–G systems

In the sections 3–6 we focused our attention on the general properties of the systems involving metal and rare-gas atoms. In this section we discuss briefly individual features of four groups of atoms. We include also a discussion of the Rydberg states of MG and M/G systems.

Downloaded At: 16:53 21 January 2011

Table 17. Main parameters of absorption and emission spectra of Li and Na atoms in rare-gas matrices: absorption frequencies ν_{abs} (gravity centres of 'triplets'), emission frequencies ν_{em}, the Stokes shift $\Delta\nu_{St}$, splitting Δ_1 and Δ_2 of 'triplet' bands in absorption, absorption bandwidths $\delta\nu_{abs}$ and emission bandwidths $\delta\nu_{em}$.

M/G	$\Delta\nu_{abs}$ (cm^{-1})	Δ_1 (cm^{-1})	Δ_2 (cm^{-1})	$\delta\nu_{abs}$ (cm^{-1})	$\delta\nu_{part}$ (cm^{-1})	$\Delta\nu_{St}$ (cm^{-1})	$\delta\nu_{em}$ (cm^{-1})	References
Li/Ar	+ 5	305	285	880[a]	> 500	3650	1050[a]	[62, 176]
Li/Kr	− 90	360	260	700[a]	150–300	4400	1030[a]	[176]
Li/Xe	− 210	380	375	600[a]	50–100	5600	1150[a]	[62, 176]
Na/Ar violet	+ 2535	310	380	1000[a]	—[b]	NO[c]	NO[c]	[54, 131]
Na/Ar blue	+ 1385	320	310	—[b]	—[b]	3650	950[a]	
						5100	1200[a]	[54, 131]
Na/Ar red	+ 35	370	245	—[b]	—[b]	2700	≈ 1000[a]	
						4000	≈ 1000[a]	
Na/Kr blue	+ 635	285	215	950[a]	250–300	3400	825[a]	
						5400	1000[a]	[131]
Na/Kr red	− 165	≈ 275		—[b]	—[b]	2900	800[a]	
Na/Xe blue	+ 835	415	320	900[a]	100–250	3000	—[d]	[53, 63]
						5400	—[d]	
Na/Xe red	− 365	600	405	—[b]		3850	—[d]	
						4350	—[d]	

[a] Estimated from figures in the references.
[b] Not measured because of overlapping bands.
[c] NO, not observed.
[d] Imprecise at the limit of the detecting system.

Downloaded At: 16:53 21 January 2011

7.1. *Alkali metals*

The spectra of MG complexes (essentially Li and Na) have been extensively studied. We have at our disposal detailed spectroscopic data for the NaNe [38, 82], NaAr [83, 84], NaKr [85] and NaXe [86] diatomic jet-cooled complexes and more limited information about Li complexes [83, 173]. As previously indicated, their ground $^2\Sigma^+_{1/2}$ states correlated to the $^2S_{1/2}$ atomic state are weakly bound while the strongly bound $^2\Pi_{1/2}$ and $^2\Pi_{3/2}$ states and the dissociative $^2\Sigma_{1/2}$ state are correlated to the first excited $^2P_{1/2,3/2}$ state of the atom.

The absorption spectra of alkali metals in rare-gas matrices have been known since the early days of the matrix technique [29, 174, 175]. In table 17 we list the available data for the main Li/G site and for two (three) types of Na/G centre. The data for K/G [46] and Rb/G [143, 176] systems are fragmentary.

The spectra consist of two (or three) 'triplets' corresponding to different sites; the intensity of the 'red' triplet absorption is strongly reduced by annealing while the 'blue' absorption is not modified [54, 131] (figure 14). In the case of Na, it has been shown that their intensity ratio depends on the deposition conditions; the 'blue' absorption is enhanced when, in the sample deposition, the laser ablation or discharge technique is used instead of effusion from the Knudsen oven. A new absorption component, a 'violet' triplet due to a third type of site, appears upon laser ablation of the metal sample. This dependence was tentatively explained by a difference in kinetic energies of alkali atoms; the high-energy atoms penetrate into well organized layers of the rare gas crystal forming stable ('blue') sites whereas the slow atoms (trapped at the surface defects) form 'red' sites [53–55, 130]. The existence of the 'violet' site is

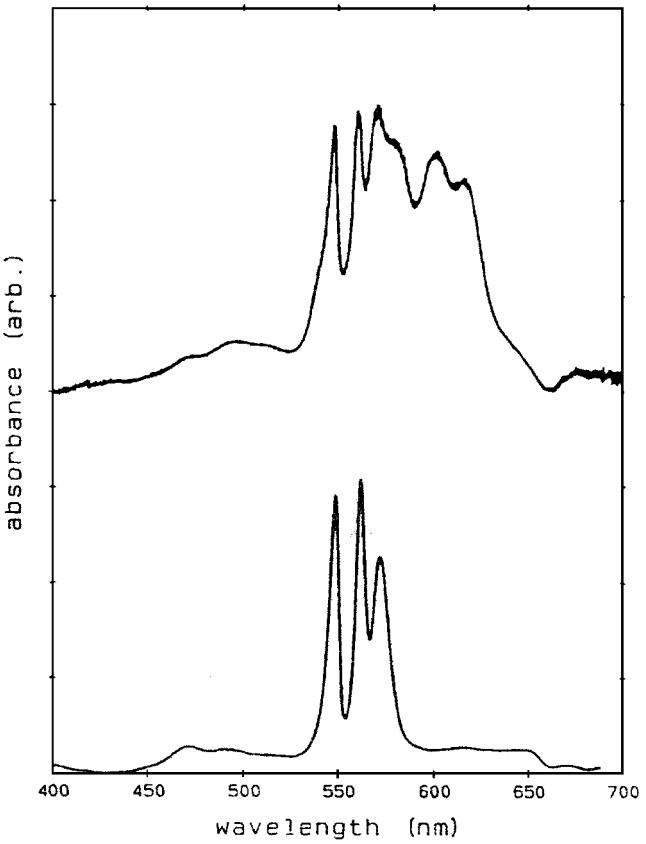

Figure 14. Dependence of the absorption spectra of Na/Xe centres (formed using laser ablation technique) on the deposition temperature $T = 10$ K (top) and 30 K (bottom). (From [54]).

Downloaded At: 16:53 21 January 2011

explained by deposition of the small Na^+ ion which occupies a 'crowded' (interstitial?) site conserved after the $Na^+ + e^-$ recombination [55].

The structures of 'red' (less stable) and 'blue' (more stable) sites cannot be unambiguously determined by experiment but some indications may be deduced from the ESR spectra; for K/Ar [46] and Rb/Ar [143] centres the HFS coupling constant A is increased with respect to the free atom ($\Delta A/A_0 \approx 0.07$) in 'blue' sites whereas in the 'red' sites $\Delta A/A_0 \approx -0.01$. Slightly smaller effects are found in the Li/Ar case [45]. Such an enhancement of the A constant indicates a contraction of the ns orbital in a 'crowded' 'blue' site (see sections 2.3.1 and 5.1.2). One can thus suppose that the 'blue' sites are one-atom substitution sites whereas the 'red' sites correspond to more extended (four-atom?) vacancies. As previously discussed, the nearly constant values of Δ_1 and Δ_2 splitting of absorption bands are surprising in view of the strong dependence of the widths $\delta\nu_{\text{part}}$ of individual triplet components on the host and site.

Many attempts have been undertaken in order to calculate the spectra of Li/G and Na/G sites [46, 113–118, 145, 146]. The most stable structures of the M/G centres were determined by the Monte Carlo or simulated annealing techniques using well known atom–atom potentials. The excited-state energies corresponding to these configurations were evaluated, the M*–G interaction being expressed either by pseudopotentials [115, 116, 145] such as those used by Baylis [88] and his followers [91, 177]

Table 18. Absorption spectra of the group IA atoms in Ar, Kr and Xe matrices

	ν (cm^{-1})								
	M = Cu			M = Ag			M = Au		
Band	Ar	Kr	Xe	Ar	Kr	Xe	Ar	Kr	Xe
A $^2P_{3/2} \leftarrow {}^2S_{1/2}$	33465	32480	31240	33440	32360	31055	43935	42790	40735
	33060	32170	30965	32895	31950	30675	43365	42300	40260
B $^2P_{1/2} \leftarrow {}^2S_{1/2}$	32570	31830	30750	31745	31055	29850	38895	38125	36645
C $^2D_{5/2} \leftarrow {}^2S_{1/2}$				30815	30440	30400			
					30720				

or by the two-body potentials deduced from the spectra of diatomics [142, 146] in a direct (the bound $^2\Pi$ state) or indirect (the dissociative $^2\Sigma$ state) way. The absorption from different ground-state energy minima were then simulated in a semiclassical Condon approximation. A quantitative agreement with experiment was not achieved but the basic properties of M/G centres were reproduced; in a recent publication [118] it was shown that the most stable Na/Ar site is the one-atom substitution site (with an energy of about 1200 cm^{-1} above that of the free Na atom and the neat Ar matrix) and that its spectrum is a triplet (owing to the removal of the degeneracy of the ^2P state) with an average blue shift of 800 cm^{-1} with respect to the free atom line (compared with the experimental value of 1400 cm^{-1} [54]). The spectrum obtained by assuming an isotropic M*–G interaction in the excited state [113] disagrees with experiment (the absorption blue shift is severely overestimated).

The fluorescence spectra of Li/G and Na/G centres show bands significantly broader than in absorption and large ('anomalous') Stokes shifts (table 17). The fluorescence spectra of Na/G obtained upon the excitation of 'red' and 'blue' bands are different what confirms their assignment to different sites. They are composed in each case of two well resolved bands corresponding probably to two energy minima at the potential energy surfaces of the excited states. Such surfaces with the energy minima strongly displaced with respect to the ground state equilibrium configuration have been obtained in simple model calculations [146].

7.2. *Metals of group IA (Cu, Ag and Au)*

The spectra of diatomic MG complexes are not known except for AgAr [65]. On the other hand, the absorption and MCD spectra [59, 64, 150] as well as fluorescence spectra [78–81, 135, 132, 162] of Cu, Ag and Au in matrices have been studied in detail. This group of atoms represents a nice example of transition from the weak spin–orbit coupling limit (Cu) through an intermediate case of Ag to the strong-coupling limit for Au and of the ^2P–^2D interaction (see section 6.4). As previously discussed (section 5.1.1), these atoms occupy single substitution sites with the O_h symmetry.

The $^2S \rightarrow {}^2P$ transition gives rise to 'triplets' in the matrix spectra. In those of Cu/Ne, Cu/Kr and Cu/Xe centres, three bands are nearly equidistant (tables 18 and 19); the spin–orbit coupling is so weak that the $^2P_{1/2}$ and $^2P_{3/2}$ states are mixed, as evidenced by identical emission spectra and lifetimes upon excitation of each of these states. In contrast, the absorption spectra of Au/G centres suggest that the $^2P_{1/2}$ and $^2P_{3/2}$ states (the latter split into two components) conserve their individual character. Unfortunately, the fluorescence spectra and lifetimes are reported only for the $^2P_{1/2}$

Downloaded At: 16:53 21 January 2011

Table 19. Fluorescence spectra of Ag atoms in Ar, Kr and Xe matrices [78, 80, 153].

		Ar			Kr			Xe		
		ν (cm^{-1})	Excitation bands[a]	τ (ns)	ν (cm^{-1})	Excitation bands[a]	τ (ns)	ν (cm^{-1})	Excitation band[a]	τ (ns)
$^2D_{5/2} \rightarrow {}^2S_{1/2}$		30 665	A, C	1800	$\approx$ 30 400	(vw)	—	—		—
$^2P \rightarrow {}^2S_{1/2}$	I	27 250	A	5	24 100	A	9	18 200	A > B	25
	II	23 650	A, B	10[b]	20 200	A, B	18	14 700	A, B	60
	III	21 900	A, B	14[b, c]	19 050	A, B	24			

[a] Presence of the A, B and C bands in the excitation spectrum.
[b] A rise time of a few nanoseconds upon excitation in the A bands.
[c] The decay contains a long ($\tau > 200$ ns) component upon excitation in the A bands.

and not for the $^2P_{3/2}$ excitation. In the case of Ag/G centres, unequal ($\Delta\nu$= 1130 and 550 cm^{-1}) energy gaps between components of the $^2S \rightarrow {}^2P$ 'triplet' suggest also that the $^2P_{1/2}$ and $^2P_{3/2}$ states are not completely mixed. This suggestion is confirmed by the difference in fluorescence spectra and decay shapes upon the selective excitation of individual absorption components.

The decay processes of excited Cu/G and Au/G centres were presented in section 6.4. We shall complete this discussion with that of the more complicated case of the Ag/Ar centre. Its emission spectrum contains a long-lived $^2D_{5/2} \rightarrow {}^2S_{1/2}$ emission and a prompt fluorescence composed of a broad band in the near ultraviolet (I) and of a double band in the visible (II and III). The intensities and decays show an unusual dependence on the excitation frequencies. The I and $^2D_{5/2} \rightarrow {}^2S_{1/2}$ emission bands are observed only upon the excitation in the A band (i.e. of the $^2P_{3/2}$ state) and show exponential decays corresponding to a direct population of emitting levels from the initial Franck–Condon state. The Stokes shift of the band I is about 6000 cm^{-1} which indicates a large difference between the initial (Franck–Condon) and final ^2P(I) configurations. The II and III emission bands appear upon excitation in the A band as well as in the B band. Their decays upon the excitation of the lower B state are also exponential and seem to correspond to two different ^2P(II) and ^2P(III) configurations showing very large (about 9000 and about 10 500 cm^{-1}) Stokes shifts. The decays of the II and III components are more complex in the case of the A-band excitation; both of them show rise times of a few nanoseconds which suggest that the ^2P(II) and ^2P(III) configurations are populated not directly but through the short-lived ^2P(I) state. Moreover, a very long component in the ^2P(III) decay indicates that a non-negligible part of its population transits through the long-lived $^2D_{5/2}$ level (figure 13). The natures of configurations I, II and III are not known. We do not see any arguments in favour of correlation between these states and the $^2P_{1/2}$ and $^2P_{3/2}$ states of the initial configuration conserving the O_h symmetry.

The rates of the relaxation processes are enhanced in Kr and Xe matrices; the $^2D_{5/2} \rightarrow {}^2S_{1/2}$ emission is very weak in Kr matrices and completely vanishes in Xe; deviations from the exponential form of ^2P fluorescence decay disappear. This difference may be due to a more rapid transfer through the $^2D_{5/2}$ state or to a direct relaxation within the ^2P state bypassing the $^2D_{5/2}$ level for energy reasons [78, 80, 135].

Fluorescence decays observed upon the excitation of higher levels (corresponding to 4d $\rightarrow$ 5p atomic transition) have complex forms and their mechanisms have not yet been completely elucidated [162, 178].

Downloaded At: 16:53 21 January 2011

7.3 *Metals of groups II and IIA*

Mg, Zn, Cd and Hg form a group for which we have at our disposal an exceptionally rich amount of information. The spectra of jet-cooled MG complexes have been reported for Mg [92, 93, 97, 98, 103, 104, 179], Ca [180, 181], Zn [30, 32, 91], Cd [33, 39, 182] and Hg [35, 36, 94–96, 100, 109, 183, 184] as well as for ionic M^+Ar complexes of Mg^+ [185] and Hg^+ [101, 186, 187]. In addition, absorption and emission spectra in rare-gas matrices have been studied for Mg [56], Zn [52, 147, 156], Cd [71] and Hg [57, 58, 138] and MCD spectra for Mg [136], Zn [149] and Hg [188].

In light atoms (Mg and Zn) the radiative singlet–triplet transitions are too weak for direct excitation of the ^3P state (and related molecular states) so that attention was focused on the lowest $^1P_1$ single state. The triplet state may be, however, attained using the techniques which prepare atoms in metastable $^3P_0$ and $^3P_2$ states, forming metastable triplet states of M*G complexes [30, 103, 181]. In the case of Hg and Cd, the oscillator strengths of the $^3P_1 \leftarrow {}^1S_0$ transitions are large enough for direct excitation of triplet states in jets and matrices.

The main parameters of the ground and excited states of MG complexes are given in table 20 whereas the characteristic features of M/G spectra may be found in table 21. In view of the large amount of data available for the whole family of group II atoms, it is interesting to make some more general remarks.

Downloaded At: 16:53 21 January 2011

Interatomic distances in the ground states of MG complexes are close to the nearest-neighbour distances in corresponding G crystals, so that all M atoms (with the possible exception of Mg) may occupy one-atom substitution sites.

The M–G bond in the ground states of complexes is weak and its enhancement upon the excitation to the C $^1\Pi_1$ ($^1P_1$) state, expressed by the ratios D_{exc}/D_g of the ground-state to excited-state dissociation energies depends strongly on the G atom. D_{exc}/D_g varies from 2 or less for Ne up to 20 for Xe complexes. However, its dependence on the M atom is less pronounced (table 20). The D_{exc}/D_g ratio is smaller here than in the case of alkali metals, this difference being due to an efficient screening of the $[X]^{2+}$ ionic core by an *n*s electron in the excited $[X]^{2+}$ $(ns)^1(np)^1$ configuration which is absent in the $[X]^+$ $(np)^1$ configuration of an alkali atom. The difference between D_{exc}/D_g ratios and R_e equilibrium distances for MG complexes in the singlet ($^1\Pi_1$) and the most stable component ($^3\Pi$–0^+) of the triplet state show that the M–G bonding is stronger in the singlet state.

The spectra of M/G centres in matrices show the same general tendencies. Their characteristic parameters, namely the gas-to-matrix frequency shift $\Delta\nu_{abs}$, its dependence on the host, $\Delta\nu_{abs}$ (Ar)–$\Delta\nu_{abs}$ (Xe), and the Stokes shift $\Delta\nu_{St}$, are very similar for the $^1P_1 \leftarrow {}^1S_0$ transitions of all M atoms. In the case of Hg, all values are reduced in the $^3P_1 \leftarrow {}^1S_0$ compared with the $^1P_1 \leftarrow {}^1S_0$ transition. Unfortunately, similar data for other M atoms are not available.

The size of the Stokes shift is obviously related to the degree of deformation of the M/G site reflecting the strength of the 'σ–π' M*–G interaction (see section 5.2). This strength may be deduced from the spectra of MG complexes. We have no information about the repulsive (σ) interaction along the axis of the *n*p orbital. However, one can assume that the attractive (π) interaction of M with the G atoms contained in the nodal plane of this orbital is closely related to the strength of the M*–G bond in the Π states of such complexes. The initial configuration prepared by the 'vertical' excitation of the ground-state configuration will thus be unstable if the M*–G equilibrium distance R_{exc} in the excited Π state is significantly shorter than the M–G distance in the ground state of the M/G centre which is supposed to be equal to the nearest-neighbour

Table 20. Equilibrium distances R_e and dissociation energies D_e of Mg, Zn, Cd and Hg complexes in their ground and valence excited states.

	Ne		Ar		Kr		Xe		
M	R_e (Å)	D_e (cm^{-1})	R_e (Å)	D_e (cm^{-1})	R_e (Å)	D_e (cm^{-1})	R_e (Å)	D_e (cm^{-1})	References
X $^1\Sigma_0^+$ ($^1S_0$)									
Mg	4.40	23	4.49	83	—	—	4.56	94	[92, 93]
Zn	4.16	27	4.18	≈ 75	4.2	115	4.38	162	[32, 91]
Cd	4.26	39	4.3	106	—	129	4.23	276	[33, 39, 189]
Hg	3.9	46	3.99	142	4.07	178	4.25	254	[94, 100]
C $^1\Pi_1$ ($^1P_1$)									
Mg	3.85	53	3.27	368	—	—	3.07	1500	[92, 93]
Zn	3.48	81	2.97	706	2.79	1466	2.86	3241	[32, 91]
Cd	3.61	89	3.28	544	3.17	993	3.04	2485	[33, 39]
Hg	3.4	89	3.28	486	2.93	1410	2.95	3463	[94–96]
a $^3\Pi$–0^- ($^3P_0$)									
Zn	—	—	3.30	330	—	—	—	—	[30]
Hg	—	—	4.33	110	—	—	—	—	[100]
A $^30^+$ ($^3P_1$)									
Cd	3.62	77	3.45	325	—	513			[39]
Hg	3.47	67	3.36	350	3.52	520	3.25	1460	[35, 100]
B ^{31} ($^3P_1$)									
Hg	4.92	13	4.70	53	4.57	96	4.47	172	[35, 100]
b ^{32} ($^3P_2$)									
Zn	—	—	3.23	487	—	—	—	—	[30]
Hg	—	—	3.31	437	—	—	—	—	[100]
MR^+ ion: $X^2\Sigma^+$									
Mg	3.30	163	—	1270	—	—	—	—	[185]
Hg	—	—	—	1630	—	3170	—	6033	[101, 186]

Downloaded At: 16:53 21 January 2011

distance R_{latt} in a pure G crystal. In table 21 we report the differences $\Delta R = R_{latt} - R_{exc}$ together with the values of the Stokes shift. A 'normal' Stokes shift, of the order of the sum of widths of the absorption and emission bands, is observed only for Hg/Ar and Hg/Kr in their $^3P_1$ states and for the Cd/Ne $^1P_1$ state for which ΔR does not exceed 0.6–0.7 Å. The 'anomalous shifts' ($\Delta\nu_{St} \gg \delta\nu_{abs}$) correspond to $\Delta R > 0.7$ Å; the only exception to this is Hg($^1P_1$)/Ar.

The Jahn–Teller splitting of absorption bands is observed for almost all systems. Its absence in the spectra of Hg/Ar and Hg/Kr centres may be explained by large widths of the overlapping component bands.

The problem of the $^1P_1 \rightsquigarrow {}^3P_J$ and $^3P_J \rightsquigarrow {}^3P_{J'}$ relaxation processes was discussed in sections 6.3 and 6.5

7.4. *Metals of group III (B, Al, Ga, In and Tl)*

The first transition in the absorption spectrum of these atoms is the $(ns)^2(np)^1\ ^2P \rightarrow (ns)^2((n+1)s)^1\ ^2S$ Rydberg transition.

The fundamental ^2P $(ns)^2(np)$ state is split into $^2P_{1/2}$ and $^2P_{3/2}$ components with the splitting increasing from 10 cm^{-1} in B to 7793 cm^{-1} in T1. In MG complexes, a further

Table 21. The gas-to-matrix shifts $\Delta\nu_{abs}$, splitting, Δ_1 and Δ_2 of the absorption bands, total absorption bandwidths $\delta\nu_{abs}$, partial absorption bandwidths $\delta\nu_{part}$, ΔR parameters, Stokes shifts $\Delta\nu_{St}$ and emission bandwidths $\delta\nu_{em}$.

M/G	$\Delta\nu_{abs}$ (cm^{-1})	Δ_1 (cm^{-1})	Δ_2 (cm^{-1})	$\delta\nu_{abs}$ (cm^{-1})	$\delta\nu_{part}$ (cm^{-1})	ΔR[a] (Å)	$\Delta\nu_{St}$ (cm^{-1})	$\delta\nu_{em}$ (cm^{-1})	References
$Mg(^1P_1)/Ne$	1365	NR[b]		815	—	—	—	—	[136]
$Mg(^1P_1)/Ar$	455	200	200	815	≈ 350	0.56	1880	485	
$Mg(^1P_1)/Kr$	210	200	215	620	≈ 250	—	1730	565	[56, 136]
$Mg(^1P_1)/Xe$	−1055	140	160	650	≈ 200	1.34	7130	1320	
$Zn(^1P_1)/Ar$	1610	400	240	1120	≈ 400	0.86	2700	1155	
							6360	1640	
$Zn(^1P_1)/Kr$	320	310	245	700	≈ 250	1.26	5330	1150	[52, 149]
							8470	1500	
$Zn(^1P_1)/Xe$	−1280	475	220	700	≈ 250	1.55	NF[c]		
$Cd(^1P_1)/Ne$	1880	420	390	1340	≈ 400	—	1570	810	[71]
$Cd(^1P_1)/Ar$	1670	365	335	1155	≈ 350	0.55	2500	880	
$Cd(^1P_1)/Kr$	450	310	155	855	≈ 250	0.88	2750	1035	
							6035	1350	
$Cd(^1P_1)/Xe$	−1135	210	220	725	NR[b]	1.37	NF[c]		
$Hg(^1P_1)/Ar$	2050	NR[b]		—	NR[b]	0.55	2900	1000	
							5250	1400	
$Hg(^1P_1)/Kr$	450	NR[b]		—	NR[b]	1.12	4200	≈ 1500	[58]
							6350	≈ 1800	
$Hg(^1P_1)/Xe$	−1600	NR[b]		—	NR[b]	1.46	NF[c]		
$Hg(^3P_1)/Ar$	1250	NR[b]		430	NR[b]	0.47	710	400	
$Hg(^3P_1)/Kr$	750			340	NR[b]	0.53	800	420	[57]
$Hg(^3P_1)/Xe$	50	80	100	330	≈ 100	1.09	2950	1200	

[a] $\Delta R = R_{latt} - R_{exc}$, where R_{exc} is the M–G equilibrium distance in the $^1\Pi$ (or $^3\Pi$) state of the MG complex and R_{latt} is the nearest-neighbour distance in the lattice of the neat G crystal.

[b] NR, non-resolved band structure.

[c] NF, non-fluorescent because of a rapid $^1P_1 \rightsquigarrow {}^3P_1$ relaxation.

splitting due to the M–G interaction is the origin for three states which may be defined at the weak spin–orbit coupling limit (Hund's case a) as X1 $^2\Pi_{1/2}$ and X2 $^2\Pi_{3/2}$ bound states and A $^2\Sigma^+_{1/2}$ repulsive state. In the strong coupling limit (Hund's case c), we have the X1 $|J=\frac{1}{2}, m_J=\frac{1}{2}\rangle$ and A $|J=\frac{3}{2}, m_J=\frac{1}{2}\rangle$ states with a mixed $\sigma\pi$ character, the X_2 $|J=\frac{3}{2}, m_J=\frac{3}{2}\rangle$ being a purely π state. In general, the degree of mixing of the X1 $^2\Pi_{1/2}$ and A $^2\Sigma^+_{1/2}$ states depends on the relation between the strength of the spin–orbit coupling and on the energy gap $\Delta E(R_{M-G})$ between the states. The observable is the ratio of bonding energies of X1 to X2 states expected to be identical in the absence of spin–orbit effects; the admixture of the repulsive σ character in the X1 state implies a decrease in its bonding energy while that of the X2 states is unaffected. In fact, they are nearly the same in the case of A1G complexes, which are close to the weak-coupling limit, while their difference is large for GaAr and GaKr and for heavier M atoms belonging to the strong-coupling limit. The A $^2\Sigma^+_{1/2}$ ($|J=\frac{3}{2}, |m_J|=\frac{1}{2}\rangle$) state remains repulsive in spite of its partial π character.

We have at hand a very limited amount of data concerning the ground states of

Downloaded At: 16:53 21 January 2011

Table 22. Splittings of $^2P_{1/2}$ and $^2P_{3/2}$ states of M atoms, bonding energies D_e and equilibrium distances R_e in M–Ar complexes of group IIIA metals in X1 $^2\Pi_{1/2}$ and X2 $^2\Pi_{3/2}$ states correlated to the ground ^2P state of M and in the B $^2\Sigma^+_{1/2}$ Rydberg state. The values in parentheses are from *ab initio* configuration interaction self-consistent field calculations [103].

	Δ	D_e (cm^{-1})			R_e (Å)			
	(cm^{-1})	X1	X2	B	X1	X2	B	References
BAr	10	?(95)	?	1100 (455)	(3.7)	—	(2.4 and 6.9)	[106]
AlAr	112	151 ± 65	183 ± 44	409 ± 65	—	—	—	[190]
GaAr	826	30 ± 20	120 ± 40	455	—	—	—	[191, 192]
InAr	2212	81 + 78 − 10	209 ± 46	319	4.13	3.77	3.28	[102, 193]
TlAr	7793	140 ± 10	310 ± 10	300 + 110–10	> 4.35	3.71	3.25	[31]

group III metals in matrices. Their ESP spectra show an important breakdown of the O_h symmetry of M/G sites due to the axial symmetry of the M atom [50]. Besides an early short report on In atoms in Kr and Xe matrices [194], more complete data are available only for the T1/G system [31, 195]. Two emission bands corresponding to B → X1 and B → X2 with the frequency difference close to that of the $^2P_{3/2}$–$^2P_{1/2}$ splitting are observed with a large but not 'anomalous', Stokes shift. The relatively strong intensity of the X2 → X1 emission corresponding in the weak-coupling limit to the strictly forbidden $^2P_{3/2} \rightarrow {}^2P_{1/2}$ transition may be explained by the $^2P_{1/2}$–$^2S_{1/2}$ mixing allowed in the D_{4h} symmetry (see table 1).

7.5. *Rydberg states*

The low-lying Rydberg ^2S $(ns)^2((n+1)s)$ states of the group III metals which may be attained by one-photon absorption have been investigated in complexes with rare gases [31, 105, 106, 190–197], in clusters [112] and in rare-gas matrices [50, 70, 194, 195]. Otherwise, beside some isolated data for alkali atoms in MG complexes [101] and Ag [81] and Cu [198] in matrices, rich material is available for the atoms of groups II and IIA but only in MG complexes [30, 100, 103, 104, 180] and not in clusters or matrices.

A characteristic feature of the Rydberg state spectroscopy is a drastic difference between the spectra of M/G centres and of M–G complexes which may be illustrated by the case of T1 atom [31, 70, 195]. The Rydberg B $^2\Sigma^+_{1/2}$ states of T1G complexes are more strongly bound than their ground states (table 22) so that the frequencies of 'vertical' transitions (those of the strongest bands in the excitation spectra) are red shifted with respect to the free atom spectral line. In contrast, the absorption maximum in the matrix of the same rare gas is strongly blue shifted (table 23). Nearly identical shifts are observed for other metals of group III (table 24).

This difference may be explained following the suggestions of Bondybey [160]. The large bonding energy of M*G complexes in the Rydberg state is due to the penetration of the G atom within the extended ($(n+1)s$) Rydberg orbital of M* across a barrier at a distance corresponding to the maximum overlap of M* and G orbitals (see section 4.1.4). In the best-known E $^3\Sigma^+$ state of the HgAr complex [100], a deep (D_e = 1430 cm^{-1}) minimum at R_{M-G} = 2.8 Å is separated from the secondary shallow

Downloaded At: 16:53 21 January 2011

minimum at $R_{M-G} = 6.95$ Å by an approximately 120 cm^{-1} barrier at about 5 Å. This configuration is very far from that of the ground state of the Hg/Ar centre where the Hg–Ar distance is 3.76 Å for the 12 equivalent nearest neighbours. The 'vertical' optical excitation gives the system a geometry in which all Hg*–Ar distances are close to that of the energy barrier. If the additivity of M–G interactions is assumed, the sum of repulsive terms due to 12 neighbours will be of the order of $12 \times 120 \approx 1500$ cm^{-1}. The data for Hg/Ar are not available, but this rough estimation amounts to 50% of the blue shifts observed for atoms of the group III in Ar matrices.

The fluorescence spectra of T1/Ne, T1/Ar and T1/Kr centres show large but not excessively large Stokes shifts of 2000–2700 cm^{-1}, the emission frequency being close to that of the free atom (table 23). The Stokes shift $\Delta\nu_{St} = 4100$ cm^{-1} and gas-to-matrix shift of the emission frequency are much more pronounced in Xe matrices. It is difficult to say whether or not this shift is due to the penetration of one (or more than one) G atom within the M*Rydberg orbital.

To our knowledge, transitions to higher Rydberg states ($n = 4$–10) involving the s, d and f states of the metal atom have been studied for AlAr and AlKr complexes [99]. They show significant and interesting deviations from the simple picture of a series of states monotonically converging to the $AlAr^+$ or $AlKr^+$ ions. In fact in AlAr the values of D_0 increase monotonically with increasing n in all series but the vibrational frequencies $\omega_e(n)$ of the ns ($n = 4$–7) states vary in an irregular way. Similar irregularities are observed for AlKr [199]; the increase of the bonding energy from the B(4s) to the H(5s) state (from 1000 to 1262 cm^{-1}) seems to contradict the increase in the equilibrium distance from 3.03 to 3.10 Å. Several discrepancies may be explained by avoided crossing with repulsive valence states [199]. On the other hand, assignment of observed transitions to different Rydberg series is not always evident.

The spectra of high ($n = 8$ to 10) $Hg(^3S_1)$ Rydberg states of HgNe and HgAr complexes [200] may be described well in terms of the ionic Hg^+–G potential modified by the terms describing the n-dependent repulsion between the Rydberg electron of Hg and the electron shell of the rare gas atom.

In matrices, higher Rydberg states for which the Rydberg electron radius is significantly larger than the interatomic distance usually show no (or little) correlation with isolated atom states and are treated in terms of Wannier excitons [17, 201].

The spectroscopy of Rydberg states of MG_n clusters seems to be the best way to follow the transition from the MG to the M/G structure. Unfortunately, the structures of MG_n clusters with the metal atom inside the cluster (intermediates between MG diatomics and M/G centres in matrices) are unstable. For this reason, we shall turn to the systems involving two different rare-gas atoms instead of a metal atom: a heavy atom in the Rydberg state G* (e.g. Xe*) and one or more lighter atoms G´ (Ne or Ar). The Rydberg state is here the lowest excited state of G. The experimental data are available for mixed dimers (hetero-excimers) G*G´ [73, 202–206], mass selected $G^*G'_n$ clusters [157, 158, 207–209] and G*G´ matrices [17, 210].

The bonding energy of the mixed XeAr dimer is slightly increased upon the $5p \rightarrow 6s$ excitation of the Xe atom (table 25). This bond is weaker than that of the Xe^+Ar ion in its ground or $A^2\Pi_J$ states. Obviously, the screening of the Xe ionic core is not significantly reduced by promotion of one the six 5p electrons to the Rydberg 6 s orbital.

In matrices the lowest Rydberg states of G/G´ centres show blue shifts with respect to the gas phase of the order of 5000–7000 cm^{-1} (about 6500 cm^{-1} for Xe/Ar [17, 20])

Downloaded At: 16:53 21 January 2011

Table 23. Displacements of absorption maxima (in cm^{-1}) of the $^2P_{1/2} \rightarrow {}^2S_{1/2}$ transitions in TlG complexes and of absorption and emission bands in Tl/G matrices with respect to the free Tl atom [31, 70, 195].

		G = Ar	G = Kr	G = Xe
Tl-G complex		+ 120	~ 0	− 180
Tl/G matrix,	absorption	+ 4120	+ 1840	+ 1400
	emission	+ 200	− 300	− 2650

Table 24. Gas-to-matrix shifts of the absorption bands in matrices.

	$\Delta\nu_{abs}$ (cm^{-1})				
	Ne	Ar	Kr	Xe	References
Al	5900	4120	1820	1640	[50]
Ga	5740	4360	1860	520	[50]
Tl	5900	4120	1840	1400	[31]

Table 25. Bonding energies of XeAr and $XeAr^+$ in the ground and excited states [77, 204, 205].

	Bonding energy (cm^{-1})	
XeAr	$X\ ^1\Sigma^+$	130
	$\ldots(6p)_{5/2}$	227
	$\ldots(6p)_{3/2}$	160 or 200
$XeAr^+$	$X\ ^2\Sigma^+$	1445
	$A1\ ^2\Pi_{3/2}$	548
	$A1\ ^2\Pi_{1/2}$	875

Downloaded At: 16:53 21 January 2011

equal to or even larger than those observed for metal atoms. The Stokes shifts are not very large; they amount in the case of Xe/Ar centres to about 3000 cm^{-1} [20].

A supplementary piece of information may be deduced from experimental and theoretical studies of mixed clusters such as $XeAr_n$ studied in a wide range of cluster sizes ($\langle n \rangle$ = 10–150 000 in experiments [207–209] and n = 12–200 in molecular dynamics simulations [157, 158]). The fluorescence excitation spectra of large $XeAr_n$ clusters consist of three broad absorption bands with blue shifts with respect to the free atom: $\Delta\nu_{abs} \approx 1900$ cm^{-1} (band I), $\Delta\nu_{abs} \approx 5000$ cm^{-1} (band II) and $\Delta\nu_{abs} \approx 6900$ cm^{-1} (band III is quasi-identical with the absorption of the Xe/Ar centre in matrices). They are assigned to Xe atoms close to the cluster surface, in its peripheral layers and in the centre of the cluster respectively. Their intensity ratios depend on the cluster size, the spectrum of the largest clusters ($n > 10\,000$) being nearly the same as that of the Xe/Ar matrix. The assignment is confirmed by the fluorescence spectra observed upon a selective pumping of individual transitions. The 68 100 cm^{-1} emission ($\Delta\nu_{em} \approx 0$; $\Delta\nu_{St} = 1900$ cm^{-1}) upon excitation in band I is assigned to Xe atoms ejected from the cluster or weakly bound to its surface. A complex spectrum observed upon the excitation in band III in the medium-sized clusters is composed of four bands with intensities dependent on the cluster size and Stokes shifts of 3600, 4150, 5600 and 6800 cm^{-1}. The first of these is nearly the same as in the Xe/Ar matrix whereas the second corresponds to a more important modification of the emitting centre. The third and fourth emission components are also observed upon the excitation in band II.

They correspond to Xe atoms in the 'soft' structure in the vicinity of the surface. The last, with the frequency close to that of the free Xe atom, cannot be assigned to the atoms rejected from the cluster and seems to be due to the formation of a 'bubble' around Xe* resulting from the repulsion of the host atoms. Such a 'bubble' model was already proposed many years ago for the Rydberg ($A\ ^2\Sigma^+$) state of NO in rare gas matrices [211] (see also [18, 19]). We do not have available any experimental data (time-resolved emission spectra) which could indicate whether different emission components are due to parallel or sequential relaxation paths.

The relaxation of excited $G^*G_n^!$ states was simulated using the molecular dynamics method and the exp–6 Xe*–Ar potential. Such simulations show that the bubble formation is a sequential process occurring on the 50 fs to 10 ps time scale [158].

Further development of experiment and simulation will be important for a better understanding of the dynamics of the G^*G_n and M^*G_n excited states of clusters with a cautious extrapolation to G/G´ and M/G matrices.

8. Final remarks

A large amount of data collected for diatomic MG (metal–rare gas) complexes allows the establishment of some general rules concerning the bonding, structure and dynamics of this class of molecular systems. Among the 'holes' in our knowledge, the most striking is a very limited information concerning the radiative properties of MG systems (breakdown of atomic selection rules, effect of the M–G interaction on the oscillator strengths of transitions localized at the M atom, etc.).

We have tried to show that a detailed knowledge of MG spectra is a necessary condition for good understanding of the properties of M/G centres in rare-gas matrices. The case of the rare-gas complexes and matrices of the group II and IIA metals is a good example of such a correlation. From this point of view, the absence of experimental data for rare-gas complexes of the group IA atoms (except for AgAr) is a handicap for the analysis of interesting results obtained for these systems in matrices (see section 7.2).

The experimental data for matrices obtained by optical spectroscopy (including MCD spectra) are abundant but have not been sufficiently analysed. We mentioned in previous sections (section 5.2) that large changes in the widths of component bands of the Jahn–Teller 'triplets' and their nearly constant splitting are surprising and not really correlated with the strengths of M–G interaction.

The analysis of optical spectra is uncertain as long as the symmetry and structure of the M/G centres are not determined. Important and interesting information may be deduced from ESR spectra but application of this technique to metal atoms in matrices seems to have been out of fashion for the last 20 years. It is surprising that we have at our disposal only one report on the ESR of M/G centres involving non-spherical atoms in the ^2P ground state. It is also surprising that ESR spectroscopy was never applied to excited states of M/G centres with non-zero orbital or spin moments. Other techniques able to probe the environment of an atom, such as EXAFS or resonance Raman spectroscopy have not been seriously employed.

The gap between diatomics and matrices can be, in principle, filled by a study of MG_n clusters. The attempts to follow this course were discouraged in view of the weakness of the M–G interaction in the ground states of M atoms. Since the G–G bonding energy is larger than that of M–G bonds, stable configurations of clusters correspond to the M atom at the surface of a G_n cluster. Are there any exceptions to

Downloaded At: 16:53 21 January 2011

this rule? If there are, spectroscopic studies of small clusters with the M atom inside the volume would be of great interest; such systems would be finite analogues of the infinite MG_∞ cluster, that is an M/G centre in the matrix. In any case, the studies of small ($n = 3$ or 4) MG_n clusters, for which the structures with the M atom at the top of a triangular or square pyramid is expected, would produce a large amount of information about the potential energy surfaces of many-body systems in their ground and excited states. Such projects are realistic as shown by a few published results [112, 123]. Time-resolved fluorescence spectra of mass-selected clusters would be extremely valuable for better understanding of 'anomalously large' Stokes shifts in matrices.

The *ab initio* and semiempirical calculations carried out for small clusters (mainly $NaAr_n$) predict their structures and spectra but could not be compared with experimental data. A further development of such calculations in parallel with experimental studies is needed. To our knowledge, no attempt to predict the equilibrium configuration of a cluster involving an M atom in the ^{2S+1}P ground state has been reported.

This review is limited to metal atoms interacting with rare-gas atoms. There is already a non-negligible number of publications devoted to complexes with simple molecules and to metal atoms in molecular hosts. We referred previously to the results obtained for HgN_2 complexes and Hg atoms in N_2 (or N_2-containing) matrices, important for understanding the mechanisms of non-radiative transitions between electronic states (section 6.5). Similar studies have been performed for metal complexes with methane ($Cd.CH_4$ [212] and $Hg.CH_4$ [213]) and for metal atoms in methane matrices ($Mg.CH_4$ [214] and $Hg.CH_4$ [155, 215, 216]). Some of these are photoreactive and a parallel studies of their spectra, relaxation paths and reactivity seem to be really promising.

Downloaded At: 16:53 21 January 2011

Acknowledgements

The authors are highly indebted to Bill Breckenridge, Andrew Mayne, John McCaffrey, Benoit Soep and Anne Zehnacker-Rentien, for critical reading of this manuscript, interesting remarks and suggestions.

References

[1] Breckenridge, W. H., Jouvet, C., and Soep, B., 1995, *Adv. Metal Semicond. Clusters* **3**, 1.
[2] Crépin, C., Legay, F., Legay-Sommaire, N., and Tramer, A., 1999, *Trends in chem. Phys.* (in the press).
[3] Breckenridge, W. H., and Umemoto, H., 1982, *The Dynamics of the Excited State*, Advances in Chemical Physics, Vol 50, edited by K. Lawley (Chichester: Wiley).
[4] Breckenridge, W. H., 1996, *J. Phys. Chem.*, **100**, 14840.
[5] Callear, A. B., and Wood, P. M., 1972, *J. chem., Soc., Faraday Trans. II*, **68**, 302.
[6] Breckenridge, W. H., Jouvet, C., and Soep, B., 1986, *J. chem. Phys.*, **84**, 1443.
[7] Legay-Sommaire, N., and Legay, F., 1993, *Chem. Phys. Lett.* **207**, 123.
[8a] Legay-Sommaire, N., and Legay, F., 1995, *J. phys. Chem.*, **99**, 16945.
[8b] McCaffrey, M. G., Parnis, J. M., Breckenridge, W. H., and Ozin, G. A., 1985, *J. phys. Chem.*, **89**, 4945.
[9] Whittle, E., Dows, D. A., and Pimentel, G. C., 1954, *J. chem. Phys.*, **22**, 1943.
[10] Smalley, R. E., Wharton, L., and Levy, D. H., 1978, *J. chem. Phys.*, **68**, 671, and references therein.
[11] Leutwyler, S., 1984, *Chem. Phys. Lett.*, **107**, 284, and references therein.
[12] Longuet-Higgins, H. C., 1961, *Adv. Spectroscopy*, **2**, 429.
[13] Sturge, M. D., 1967, *Solid St. Phys.* **20**, 91.
[14] Bersuker, L. B., 1984, *The Jahn–Teller Effect and Vibronic Interactions in Modern Chemistry* (New York: Plenum).

[15] Personov, R. I., Alshitz, E. I., Bykovskaya, L. A. and Kharlamov, B. M. 1973, *Zh. eksp. teor. Fiz.*, **65**, 1825.
[16] Personov, R. I., 1983, *Spectroscopy and Dynamics of Condensed Molecular Systems*, edited by V. M. Agranovich and R. M. Hochstrasser (Amsterdam: North-Holland) p. 137.
[17] Schwentner, N., Koch, E. E., and Jortner, J., 1985, *Electronic Excitations in Condensed Rare Gases* (Berlin: Springer).
[18] Chergui, M., Schriever, R., and Schwentner, N. 1988, *J. chem. Phys.*, **89**, 7083.
[19] Chergui, M., and Schwentner, N., 1988, *J. chem. Phys.*, **91**, 5993.
[20] Baldini, G., 1964, *Phys. Rev.* **136**, A248; 1965, *ibid.*, **137**, A508.
[21] Moran, P. R., 1965, *Phys. Rev.*, **137**, A1016.
[22] O'Brien, M. C. M., 1971, *J. Phys.* C, **4**, 2524.
[23] Henry, C. H., Schnatterly, S. E., and Slichter, C. P., 1965, *Phys. Rev.*, **137**, A583.
[24] Stephens, P. J., 1976, *Adv. chem. Phys.*, **35**, 197, and references therein.
[25] Roubin, P., Varin, S., Crépin, C., Gauthier-Roy, B., Flank, A. M., Delaunay, R., Pompa, M., and Tremblay, B., 1998, *J. chem. Phys.*, **109**, 7945, and references therein.
[26] Kageyama, K., Kawasaki, S., Mibulley, K., Yoshimura, K., and Kosuge, K., 1997, *Phys. Rev. Lett.*, **79**, 3258, and references therein.
[27] Legay, F., Legay-Sommaire, N., and Chandrasekharan, V., 1990, *J. phys. Chem.*, **94**, 8548.
[28] Legay, F., and Legay-Sommaire, N., 1995, *J. phys. Chem.*, **99**, 5277.
[29] McCarty, M., Jr., and Robinson, G. W., 1959, *Mol. Phys.*, **2,** 415.
[30] Bennett, R. R., and Breckenridge, W. H., 1990, *J. chem. Phys.*, **92**, 1588.
[31] Stangassinger, A., Scheuchenpflug, J., Prinz, T., and Bondybey, V. E., 1993, *Chem. Phys.*, **178**, 533.
[32] Wallace, I., Kaup, J. G., and Breckenridge, W. H., 1991, *J. phys. Chem.*, **95**, 8060.
[33] Funk, D. J., Kvaran, A., and Breckenridge, W. H., 1989, *J. chem. Phys.*, **90**, 2915.
[34] Dietz, T. G., Duncan, M. A., Liverman, M. G., and Smalley, R. E., 1980, *J. chem. Phys.*, **73**, 4816.
[35] Duval, M. C., Soep, B., and Breckenridge, W. H., 1991, *J. phys. Chem.*, **95**, 7145.
[36] Jouvet, C., 1985, Thesis, Orsay.
[37] Yamanouchi, K., Duval, M. C., Jouvet, C., Benoist d'Azy, O., and Soep, B., 1988, *J. chem. Phys.*, **89**, 2975, and references therein.
[38] Tellinghuisen, J., Ragone, A., Kim, M. S., Auerbach, D. J., Smalley, R. E., Wharton, L., Levy, D. H., 1979, *J. chem. Phys.*, **71**, 1283.
[39] Funk, D. J., and Breckenridge, W. H., 1989, *J. chem. Phys.*, **90**, 2927.
[40] Biligh, S., Gutowski, M., Simons, J., and Breckenridge, W. H., 1993, *J. chem. Phy.*, **99**, 3815.
[41] Ben-Horin, N., Bahatt, D., Even, U., and Jortner, J., 1992, *J. chem. Phys.*, **97**, 6011, and references therein.
[42] Schmidt, M., Le Calvé, J., and Mons, M., 1993, *J. chem. Phys.*, **98**, 6102, and references therein.
[43] Troxler, T., and Leutwyler, S., 1991, *J. chem. Phys.*, **95**, 4110, and references therein.
[44] McGlynn, S. P., Azumi, T., and Kinoshita, M., 1969, *Molecular Spectroscopy of the Triplet State* (Englewood Cliffs, New Jersey: Prentice-Hall).
[45] Schrimpf, A., Rosendal, R., Bornemann, T., Stöckmann, H. J., Faller, F., and Manceron, L., 1992, *J. chem. Phys.*, **96**, 7992.
[46] Schrimpf, A., Sulzer, G., Stöckmann, H. J. and Ackerman, H., 1987, *Z. Phys.* B, **67**, 531.
[47] Adrian, F. J., 1960, *J. chem. Phys.*, **32**, 972.
[48] Smith, D. Y., 1963, *Phys. Rev.*, **131,** 2056; 1964, *ibid.*, **133**, A1087.
[49] Kasai, P. H., and McLeod, D., 1971, *J. chem. Phys.*, **55**, 1566.
[50] Ammeter, J. H., and Schlossnagle, D. C., 1973, *J. chem. Phys.*, **59**, 4784.
[51] Kottis, P., and Lefebvre, R., 1964, *J. chem. Phys.*, **39**, 393; *ibid.*, **41**, 379.
[52] Bracken, V. A., Gürtler, P., and McCaffrey, J. G., 1997, *J. chem. Phys.*, **107**, 5290.
[53] Fajardo, M. E., Carrick, P. G., and Kenney, III., J. W., 1991, *J. chem. Phys.*, **94**, 5812.
[54] Tam, S., and Fajardo, M. E., 1993, *J. chem. Phys.*, **99**, 854.
[55] Silverman, D. C., and Fajardo, M. E., 1997, *J. chem. Phys.*, **106**, 8964.
[56] McCaffrey, J. G., and Ozin, G. A., 1994, *J. chem. Phys.*, **101**, 10354.

Downloaded At: 16:53 21 January 2011

[57] CRÉPIN, C., and TRAMER, A., 1992, *J. chem. Phys.*, **97**, 4772.
[58] CRÉPIN, C., CHERGUI, M., HERBERT, T., KÖNIG, L., MARTIN, P. and TRAMER, A., 1994, *J. phys. Chem.*, **98**, 3280.
[59] STEPHENS, P. J., 1970, *J. chem. Phys.*, **52**, 3489.
[60] ROSE, D., PELLOW, R., EYRING, M., VALA, M., LIGNIÈRES, J., and RIVOAL, J. C., 1992, *Chem. Phys.*, **166**, 393.
[61] OSBORNE, G. A., and STEPHENS, P. J., 1972, *J. chem. Phys.*, **56**, 609.
[62] LUND, P. A., SMITH, D., JACOBS, S. M., and SCHATZ, P. N., 1984, *J. phys. Chem.* **88**, 31.
[63] ROSE, J., SMITH, D., WILLIAMSON, B. E., SCHATZ, P. N., and O'BRIEN, M. C. M., 1986, *J. phys. Chem.*, **90**, 2608.
[64] ZERINGUE, K. J., SHAKHS EMAMPOUR, J., RIVOAL, J. C. and VALA, M., 1983, *J. chem. Phys.*, **78**, 2231.
[65] JOUVET, C., LARDEUX-DEDONDER, C., MARTRENCHARD, S., and SOLGADI, D., 1991, *J. chem. Phys.*, **94**, 1759.
[66] COHEN-TANNOUDJI, C., DIU, B., and LALOË, F., 1973, *Mécanique Quantique* (Paris: Hermann).
[67] HERZBERG, G., 1950, *Spectra of Diatomic Molecules* (New York: Van Nostrand).
[68] LEFEBVRE-BRION, H., and FIELD, R. W., 1986, *Perturbations in the Spectra of Diatomic Molecules* (Orlando, Florida: Academic Press).
[69] SAMET, C., ROSE, J. L., SCHATZ, P. N., and O'BRIEN, M. C. M., 1989, *Chem. Phys. Lett.*, **159**, 567.
[70] WURFEL, B. E., THOMA, A., SCHALLMOSER, G., LAMMERS, A., and BONDYBEY, V. E., 1994, *J. chem. Phys.* **100**, 8003.
[71] HEALY, B., and MCCAFFREY, J. G., 1999, *J. chem. Phys.*, **110,** 3903.
[72] KASHA, M., 1949, *J. chem. Phys.*, **17**, 71.
[73] PELLOW, R., and VALA, M., *J. chem. Phys.*, **90**, 5612.
[74] SUBBARAM, K. V., COXON, J. A., and JONES, W. E., 1976, *Can. J. Phys.*, **54**, 1535.
[75] LIAO, C. L., and NG, C. Y., 1986, *J. chem. Phys.*, **84**, 1142.
[76] KLINGBEIL, R., 1972, *J. chem. Phys.*, **57**, 1066.
[77] HUXLEY, P., KNOWLES, D., MURRELL, J. N., and WATTS, J. D., 1984, *J. chem. Soc., Faraday Trans. II*, **80**, 1349.
[78] WIGGENHAUSER, W., SCHRÖDER, W., and KOLB, D. M., 1988, *J. chem. Phys.*, **88**, 3434.
[79] WIGGENHAUSER, H., KOLB, D. M., ROTERMUND, H. H., SCHRITTENLACHER, W., and SCHRÖDER, W., 1985, *Chem. Phys. Lett.*, **122**, 71.
[80] LEUTLOFF, D., and KOLB, D. M., 1979, *Ber. Bunsenges. phys. Chem.*, **83**, 666.
[81] SCHRITTENLACHER, W., and KOLB, D. M., 1984, *Ber. Bunsenges. phys. Chem.*, **88**, 492.
[82] LAPATOVICH, W. P., AHMAD-BITAR, R., MOSKOVITZ, P. E., RENHORN, I., GOTTSCHO, R. A., and PRITCHARD, D. E., 1980, *J. chem. Phys.*, **73**, 5419.
[83] GOTTSCHO, R. A., AHMAD-BITAR, R., LAPATOVICH, W. P., RENHORN, I., and PRITCHARD, D. E., 1980, *J. chem. Phys.*, **73**, 5419.
[84] SMALLEY, R. E., AUERBACH, D. J., FITCH, P. S. H., LEVY, D. H., and WHARTON, L., 1977, *J. chem. Phys.*, **66**, 3778.
[85] BRÜHL, R., KAPETANAKIS, J., and ZIMMERMANN, D., 1991, *J. chem. Phys.*, **94**, 5865.
[86] BAUMANN, P., ZIMMERMANN, D., and BRÜHL, R., 1992, *J. Molec. Spectrosc.*, **155**, 277.
[87] DUVAL, M. C., 1988, Thesis, Orsay.
[88] BAYLIS, W. E., 1969, *J. chem. Phys.*, **51**, 2665.
[89] MASNOU-SEEUWS, F., PHILLIPPE, M., and VALIRON, P., 1978, *Phys. Rev. Lett.*, **41**, 395.
[90] SAXON, R. P., OLSON, R. E., and LIU, B., 1977, *J. chem. Phys.*, **67**, 2692.
[91] WALLACE, I., BENNETT, R. B., and BRECKENRIDGE, W. H., 1988, *Chem. Phys. Lett.*, **153**, 127.
[92] BENNETT, R. R., MCCAFFREY, J. G., WALLACE, I., FUNK, D. J., KOWALSKI, A., and BRECKENRIDGE, W. H., 1989, *J. chem. Phys.*, **90**, 2139.
[93] MCCAFFREY, J. G., FUNK, D. J., and BRECKENRIDGE, W. H., 1993, *J. chem. Phys.*, **99**, 9472.
[94] TSUCHIZAWA, T., YAMANOUCHI, K., and TSUCHIYA, S., 1988, *J. chem. Phys.*, **89**, 4646.
[95] PULLINS, S. H., SCURLOCK, C. T., REDDIC, J. E., and DUNCAN, M. A., 1996, *J. chem. Phys.*, **104**, 7518.
[96] REDDIC, J. E., and DUNCAN, M. A., 1999, *J. chem. Phys.*, **110**, 9948.

Downloaded At: 16:53 21 January 2011

[97] Leung, A. W. K., Robertson, M., Simons, J., and Breckenridge, W. H., 1996, *Chem. Phys. Lett.*, **259**, 199.
[98] Massick, S., and Breckenridge, W. H., 1996, *J. chem. Phys.*, **104**, 7784.
[99] Heidecke, S. A., Fu, Z., Colt, J. R., and Morse, M. D., 1992, *J. chem. Phys.*, **97**, 1692.
[100] Duval, M. C., Benoist d'Azy, O., Breckenridge, W. H., Jouvet, C., and Soep, B., 1986, *J. chem. Phys.*, **85**, 6324.
[101] Linn, S. H., Brom, Jr., J. M., Tzeng, W. B., and Ng, C. Y., 1985, *J. chem. Phys.*, **82**, 648.
[102] Lee, C. J., and Havey, M. D., 1991, *Phys. Rev.* A **43**, 6066.
[103] Bennett, R. R., McCaffrey, J. G. and Breckenridge, W. H., 1990, *J. chem. Phys.*, **92**, 2740.
[104] Bennett, R. R., and Breckenridge, W. H., 1992, *J. chem. Phys.*, **96**, 882.
[105] Hackett, P. A., Balfour, W., James, A. M., Fawzy, W. M., Shetty, B. J., and Simard, B., 1993, *J. chem. Phys.*, **99**, 4300.
[106] Hwang, E., Huang, Y. L., Dagdigian, P. J., and Alexander, M. H., 1993, *J. chem. Phys.*, **98**, 8484.
[107] Park, S. J., Kim, M. C., Lee, Y. S., and Jeung, G. H., 1997, *J. chem. Phys.*, **107**, 2481.
[108] Schreiner, E. W. S., 1996, Thesis, Tehnische Universität München.
[109] Breckenridge, W. H., Duval, M. C., Jouvet, C., and Soep, B., 1985, *Chem. Phys. Lett.*, **119**, 317.
[110] Aziz, R. A., and Slaman, M. J., 1986, *Molec. Phys.*, **58**, 679.
[111] Visticot, J. P., Berlande, J., Cuveillier, J., Lallement, A., Mestdagh, J. M., Meynardier, P., de Pujo, P., and Sublemontier, O., 1992, *Chem. Phys. Lett.*, **191**, 107.
[112] Whetten, R. L., Schriver, K. E., Persson, J. L., and Hahn, M. Y., 1990, *J. chem. Soc., Faraday Trans.*, **86**, 2375.
[113] Gross, M., and Spiegelman, F., 1998, *J. chem. Phys.*, **108**, 4148.
[114] Dawson, J. F., and Balling, L. C., 1979, *J. chem. Phys.*, **71**, 836.
[115] Ossicini, S., and Forstmann, F., 1981, *J. chem. Phys.*, **75**, 2076.
[116] Tsoo, C., Estrin, D. A., and Singer, S. J., 1990, *J. chem. Phys.*, **93**, 7187.
[117] Tsoo, C., Estrin, D. A., and Singer, S. J., 1992, *J. chem. Phys.*, **96**, 7977.
[118] Boatz, J. A., and Fajardo, M. E., 1994, *J. chem. Phys.*, **101**, 3472.
[119] Martyna, G., Cheng, C., and Klein, M. L., 1991, *J. chem. Phys.*, **95**, 1318.
[120] Visticot, J. P., de Pujo, P., Mestdagh, J. M., Lallement, A., Berlande, J., Sublemontier, O., Meynardier, P., and Cuveillier, J., 1994, *J. chem. Phys.*, **100**, 158.
[121] Roncero, O., Beswick, J. A., Halberstadt, N., and Soep, B., 1990, *Dynamics of Polyatomic van der Waals Complexes*, edited by N. Halberstadt and K. C. Janda (London: Plenum) p. 471.
[122] Zuniga, J., Bastida, A., Requena, A., Halberstadt, N., and Beswick, J. A., 1993, *J. Chem. Phys.*, **98**, 1007.
[123] Martrenchard-Barra, S., Jouvet, C., Lardeux-Dedonder, C., and Solgadi, D., 1993, *J. chem. Phys.*, **98**, 5281.
[124] Martrenchard-Barra, S., 1993, *Thesis*, Orsay.
[125] Kaup, J. G., and Breckenridge, W. H., 1995, *J. phys. Chem.*, **99**, 13701.
[126] Breckenridge, W. H., Morse, M. D., and McCaffrey, J. G., 1998, *J. chem. Phys.*, **109**, 3137.
[127] Schrittenlacher, W., Rotermund, H. H., and Kolb, D. M., 1985, *J. chem. Phys.*, **83**, 6145.
[128] Karplus, M., and Porter, R. N., 1970, *Atoms and Molecules* (New York: Benjamin).
[129] Badenhoop, J. K., and Weinhold, F., 1997, *J. chem. Phys.*, **107**, 5422.
[130] Fajardo, M. E., 1993, *J. chem. Phys.*, **98**, 110.
[131] Balling, L. C., Havey, M. D., and Dawson, J. F., 1978, *J. chem. Phys.*, **69**, 1970.
[132] Hormes, J., Grinter, R., Breithaupt, B., and Kolb, D. M., 1963, *J. chem. Phys.*, **78**, 158.
[133] Moskovits, M., and Hulse, J. E., 1997, *J. chem. Phys.*, **67**, 4271.
[134] Brewer, L., and King, B., 1970, *J. chem. Phys.*, **53**, 3981.
[135] Mitchell, S. A., Farell, J., Kenney-Wallace, G. A., and Ozin, G. A., 1980, *J. Am. chem. Soc.*, **102**, 7702.
[136] Mowery, R. L., Miller, J. C., Krauts, E. R., States, P. N., Jacobs, S. M., and Andrews, L., 1979, *J. Chem. Phys.*, **70**, 3920.

Downloaded At: 16:53 21 January 2011

[137] CHERGUI, M., CRÉPIN, C., HEBERT, T., and TRAMER, A., *Chem. Phys. Lett.*, **197,** 467.
[138] BREWER, L., MEYER, B., and BRABSON, G. D., 1965, *J. chem. Phys.*, **43**, 3973.
[139] SCHRITTENLACHER, W., SCHRÖDER, W., ROTERMUND, H. H., and KOLB, D. M., 1984, *Chem. Phys. Lett.* **109**, 7.
[140] SCHRÖDER, W., GRINTER, R., SCHRITTENLACHER, W., ROTERMUND, H. H., and KOLB, D. M., 1985, *J. chem. Phys.*, **82**, 1623.
[141] RASANEN, M., HEIMBROOK, L. A., and BONDYBEY, V. E., 1987, *J. molec. Struct.*, **157**, 129.
[142] JEN, C. K., BOWERS, V. A., COCHRAN, E. L., and FONER, S. N., 1962, *Phys. Rev.*, **126**, 1749.
[143] KUPFERMANN, S. L., and PIPKIN, F. M., 1968, *Phys. Rev.*, **166**, 207.
[144] FAJARDO, M. E., 1993, *J. chem. Phys.*, **98**, 119.
[145] BALLING, L. C., and WRIGHT, J. J., 1983, *J. chem. Phys.*, **79**, 941.
[146] BALLING, L. C., and WRIGHT, J. J., 1984, *J. chem. Phys.*, **81**, 675.
[147] KERINS, P. N., and MCCAFFREY, J. G., 1998, *J. chem. Phys.*, **109**, 3131.
[148] HOFFMANN-MILLACK, B., KLEIN, A., LAGIER, H., MAID, B., and HORMES, J., 1989, *Chem. Phys.*, **136**, 453.
[149] HAM, F. S., 1965, *Phys. Rev.*, **138**, A1727.
[150] VALA, M., ZERINGUE, K., SHAKHS EMAMPOUR, J., RIVOAL, J. C., and PYZALSKI, R., 1984, *J. chem. Phys.* **80**, 2401.
[151] STEPANOV, B. I., 1957, *Soviet Phys. Dokl.* **2**, 81.
[152] JEONG, G. H., and KLABUNDE, K. J., 1989, *J. chem. Phys.*, **91**, 1958.
[153] MEHRETEAB, A., ANDREWS, J. R., SMITH, III., A. B., and HOCHSTRASSER, R. M., 1982, *J. phys., Chem.*, **86**, 888.
[154] BRACKEN, V. A., KERINS, P. N., GÜRTLER, P., and MCCAFFREY, J. G., 1997, *J. chem. Phys.*, **107**, 5300.
[155] CRÉPIN, C., and TRAMER, A., 1994, *J. chem. Phys.*, **100**, 5459.
[156] MCCAFFREY, J. G., and KERINS, P. N., 1997, *J. chem. Phys.*, **106**, 7885.
[157] GOLDBERG, A., HEIDENREICH, A., and JORTNER, J., 1995, *J. phys. Chem.*, **99**, 2662.
[158] GOLDBERG, A., and JORTNER, J., 1997, *J. chem. Phys.*, **107**, 8894.
[159] SIEBRAND, W., 1967, *J. chem. Phys.*, **46**, 440.
[160] BONDYBEY, V. E., 1978, *J. chem. Phys.*, **68**, 1308.
[161] JOUVET, C., and BESWICK, J. A., 1987, *J. chem. Phys.*, **86**, 5500.
[162] HEBERT, T., WIGGENHAUSER, H., SCHRIEVER, U., and KOLB, D. M., 1990, *J. chem. Phys.* **92**, 1575.
[163] JOUVET, C., and SOEP, B., 1984, *J. chem. Phys.*, **80**, 2229.
[164] CONNERADE, J. P., and BAIG, M. A., 1979, *Proc. R. Soc.* A, **365**, 253.
[165] BRECKENRIDGE, W. H., and MALMIN, O. K., 1981, *J. chem. Phys.*, **74**, 3307.
[166] DUVAL, M. C., and SOEP, B., 1991, *J. phys. Chem.*, **95**, 9075.
[167] CRÉPIN, C., and TRAMER, A., 1997, *J. chem. Phys.*, **107**, 2205.
[168] CRÉPIN, C., LEGAY, F., LEGAY-SOMMAIRE, N., and TRAMER, A., 1987, *Chem. Phys.*, **111**, 169.
[169] CRÉPIN, C., LEGAY, F., LEGAY-SOMMAIRE, N., and TRAMER, A., 1987, *Chem. Phys.*, **111**, 183.
[170] CRÉPIN, C., and MILLIÉ, P., 1989, *Chem. Phys.*, **133**, 377.
[171] CRÉPIN, C., LEGAY, F., LEGAY-SOMMAIRE, N., and TRAMER, A., 1989, *Chem. Phys.*, **136**, 1.
[172] CRÉPIN, C., and TRAMER, A., 1994, *J. chem. Phys.*, **100**, 5475.
[173] SCHEPS, R., OTTINGER, CH., YORK, G., and GALLAGHER, A., 1975, *J. chem. Phys.*, **63**, 2581.
[174] WEYHMAN, W., and PIPKIN, F. M., 1965, *Phys. Rev.* A, **137**, 490.
[175] MEYER, B., 1965, *J. chem. Phys.*, **43**, 2986.
[176] BALLING, L. C., and WRIGHT, J. J., 1983, *J. chem. Phys.*, **78**, 592.
[177] PASCALE, J., and VANDENPLANQUE, J., 1974, *J. chem. Phys.*, **60**, 2278.
[178] HORMES, J., and HAPPEL, G., 1983, *J. chem. Phys.*, **78**, 1758.
[179] MCCAFFREY, J. G., FUNK, D. J., and BRECKENRIDGE, W. H., 1994, *J. chem. Phys.*, **100**, 955.
[180] KAUP, J. G., and BRECKENRIDGE, W. H., 1997, *J. chem. Phys.*, **107**, 5283.
[181] KOWALSKI, A., FUNK, D. J., and BRECKENRIDGE, W. H., 1986, *Chem. Phys. Lett.*, **132**, 263.

Downloaded At: 16:53 21 January 2011

[182] CZAJKOWSKI, M., and KOPERSKI, J., 1998, *Proceedings of the Jablonski Centennial Conference*, Torun, 1998 Book of Abstracts (Torun: Wydawnicturo Uniwersyteta), p. 154.
[183] AMANO, K., OHMORI, K., KUROSAWA, T., CHIBA, H., OKUNISHI, M., UEDA, K., SATO, Y., DEVDARIANI, A. Z., and NIKITIN, E. E., 1998, *J. chem. Phys.*, **108**, 8110.
[184] HISHIKAWA, A., SATO, H., and YAMANOUCHI, K., *J. chem. Phys.*, **108**, 9202.
[185] PILGRIM, J. S., YEH, C. S., and DUNCAN, M. A., 1993, *Chem. Phys. Lett.*, **210**, 322.
[186] BRIDGE, N. J., 1972, *J. molec. Spectrosc.* **42**, 370.
[187] HOUGEN, J. T., 1972, *J. molec. Spectrosc.*, **42**, 381.
[188] VANCOTT, T. C., 1984, Ph.D Thesis, University of Virginia.
[189] WALLACE, I., RITTER, J., and BRECKENRIDGE, W. H., 1992, *J. chem. Phys.*, **96**, 136.
[190] CALLENDER, C. L., MITCHELL, S. A., and HACKETT, P. A., 1989, *J. chem. Phys.*, **90**, 5252.
[191] STANGASSINGER, A., KNIGHT, A. M., and DUNCAN, A. M., 1998, *J. chem. Phys.*, **108**, 5733.
[192] STANGASSINGER, A., SCHEUCHENPFLUG, J., PRINZ, T., and BONDYBEY, V. E., 1993, *Chem. Phys. Lett.*, **209**, 372.
[193] FAWZY, W. M., LEROY, R. J., SIMARD, B., NIKI, H., and HACKETT, P. A., 1993, *J. chem. Phys.*, **98**, 140.
[194] BALLING, L. C., and WRIGHT, J. J., 1981, *J. chem. Phys.*, **74**, 6554.
[195] MITCHENKO, N. S., PREDTECHENSKI, Y. B., and SHCHERBA, L. D., 1976, *Opt. Spectrosc.* **41**, 521.
[196] CALLENDER, C. L., MITCHELL, S. A., and HACKETT, P. A., 1989, *J. chem. Phys.*, **90**, 2535.
[197] STANGASSINGER, A., MANE, I., and BONDYBEY, V. E., 1995, *Chem. Phys.*, **201**, 227.
[198] HORMES, J., GRINTER, R., BREITHAUPT, B., and KOLB, D. M., 1983, *J. chem. Phys.*, **78**, 158.
[199] FU, Z., MASSICK, S., KAUP, J. G., BENOIST D'AZY, O., and BRECKENRIDGE, W. H., 1992, *J. chem. Phys.*, **97**, 1683.
[200a] OKUNISHI, M., YAMANOUCHI, K., ONDA, K., and TSUCHIYA, S., 1993, *J. chem. Phys.*, **95**, 2675.
[200b] ONDA, K., YAMANOUCHI, K., OKUNISHI, M., and TSUCHIYA, S., 1994, *J. chem. Phys.*, **101**, 7290.
[200c] ONDA, K., and YAMANOUCHI, K., 1995, *J. chem. Phys.* **102,** 1129.
[201] KATZ, B., BRITH, M., SHARF, B., and JORTNER, J., 1969, *J. chem. Phys.* **50**, 5195, and references therein.
[202] BALAKRISHNAN, A., JONES, W. J., MAHAJAN, C. G. and STOICHEFF, B. P., 1989, *Chem. Phys. Lett.*, **155,** 43.
[203] DU, N. Y., and GREENE, C. H., 1989, *J. chem. Phys.* **90**, 6347.
[204] PRATT, S. T., DEHMER, P. M., and DEHMER, J. L., 1985, *J. chem. Phys.*, **83**, 5380.
[205] HUBER, K. P., and LIPSON, R. H., 1986, *J. molec. Spectrosc.* **119**, 433.
[206] DEHMER, P. M., and PRATT, S. T., 1982, *J. chem. Phys.*, **77**, 4804.
[207] LENGEN, M., JOPPIEN, M., VON PIETROWSKI, R., and MÖLLER, T., 1994, *Chem. Phys. Lett.*, **229**, 362.
[208] LENGEN, M., JOPPIEN, M., WÖRMER, J., and MÖLLER, T., 1994, *Phys. Rev. Lett.*, **68**, 2362.
[209] VON PIETROWSKI, R., LENGEN, M., MOUSSAVIZADEH, L., MUSEUR, L., KANAEV, A. V., CASTEX, M. C., and MÖLLER, T., 1997, **108**, 175.
[210] GEDANKEN, A., RAZ, B., and JORTNER, J., 1973, *J. chem. Phys.*, **59**, 5471.
[211] GOODMAN, J., and BRUS, L. E., 1978, *J. chem. Phys.*, **69**, 4083.
[212] WALLACE, I., and BRECKENRIDGE, W. H., 1992, *J. chem. Phys.*, **97**, 2318.
[213] DUVAL, M. C., and SOEP, B., 1987, *Chem. Phys. Lett.*, **141**, 225.
[214] MCCAFFREY, J. G., and OZIN, G. A., 1988, *J. chem. Phys.*, **89**, 1839, 1844, 1858.
[215] LEGAY-SOMMAIRE, N., and LEGAY, F., 1994, *Chem. Phys. Lett.*, **217**, 97.
[216] LEGAY-SOMMAIRE, N., and LEGAY, F., 1996, *Chem. Phys.*, **211**, 367.

Downloaded At: 16:53 21 January 2011